PROCESSING AND CHARACTERIZATION OF CARBON NANOPARTICLE/ FIBER-REINFORCED POLYMER COMPOSITES

A Dissertation by

Alejandro Jose Rodriguez

Master of Science, University of South Alabama, USA, 2005

Mechanical Engineer, Universidad Tecnológica del Centro, Venezuela, 2002

Submitted to the Department of Mechanical Engineering
and the faculty of the Graduate School of
Wichita State University
in partial fulfillment of
the requirements for the degree of
Doctor of Philosophy

August 2010

PROCESSING AND CHARACTERIZATION OF CARBON NANOPARTICLE/
FIBER-REINFORCED POLYMER COMPOSITES

The following faculty members have examined the final copy of this dissertation for form and content, and recommend that it be accepted in partial fulfillment of the requirement for the degree of Doctor of Philosophy with a major in Mechanical Engineering.

Bob Minaie, Committee Chair

Hamid Lankarani, Committee Member

Ramazan Asmatulu, Committee Member

Klaus Hoffmann, Committee Member

William Stevenson, Committee Member

Accepted for the College of Engineering

Zulma Toro-Ramos, Dean

Accepted for the Graduate School

J. David McDonald, Dean

DEDICATION

To my wife, my parents, my siblings, and everyone else who made it possible

ACKNOWLEDGEMENTS

I would like to express my gratitude and appreciation to my advisor, Professor Bob Minaie, who provided me with the confidence, support, and guidance to complete this research. I am especially thankful to him for giving me many opportunities to actively participate in endeavors that led to the advancement of my professional skills. I would also like to thank the other members of my committee, Dr. William Stevenson, Dr. Hamid Lankarani, Dr. Ramazan Asmatulu, and Dr. Klaus Hoffmann for their valuable comments and suggestions.

I wish to give special thanks to my dear colleagues Mauricio Guzman and Chee-Sern Lim for their friendship, academic support, and assistance in conducting experiments during the course of this investigation. Their support was essential to the success of this work. Thanks are also due to them and Joey Schaefer for their efforts in reviewing this manuscript in detail and making helpful comments and suggestions. I would like to express my sincere gratitude to my other colleagues from Professor Minaie's research group, Behrouz Tavakol, Seyed Soltani, Ronald Joven, Hoda Koushiar, Rony Das, and Ashraf Ahmed for their friendship and support. They have certainly made this work better and more enjoyable.

I gratefully acknowledge the financial support from the Office of Naval Research (ONR), National Aeronautics and Space Administration (NASA), Kansas Technology Enterprise Corporation (KTEC), and Wichita State University (WSU). Without the support of these organizations, this work would not have been possible.

Finally, I am mostly indebted to my beautiful wife and family who have given me all the necessary support to complete this task. Words are not enough to express my deepest love and appreciation. I am especially thankful to them for believing in me and my dreams . . . and also for helping me to make my dreams happen.

ABSTRACT

Carbon nanotubes (CNTs) and carbon nanofibers (CNFs) have an exceptional combination of properties that make them ideal materials for use as reinforcing particles in advanced composites. This investigation was aimed at obtaining fundamental understanding of the processing and properties of carbon nanoparticle/fiber-reinforced polymer composites —defined as multiscale-reinforced polymer composites (MRPCs)— manufactured through a practical and scalable process. Such process consists of two stages. The first stage involves the synthesis of multiscale-reinforcement fabrics (MRFs) by electrophoretic deposition of carboxylic acid- or amine-functionalized CNTs and CNFs onto the surface of carbon fiber layers in aqueous medium; while the second stage proceeds with the stacking of the MRFs and infusion of the resulting preforms with an epoxy-amine resin system to obtain the MRPC.

MRPCs manufactured following the described approach were tested for mechanical and electrical properties. Mechanical test results showed an increase in interlaminar shear strength (ILSS), shear stiffness, and compressive strength of all panels manufactured. Panels containing amine-functionalized carbon nanoparticles had the highest increase in properties: 13% in ILSS, 2.5-4 fold in shear stiffness, and up to 15% in compressive strength. On the other hand, it was found that through-plane electrical conductivity of MRPCs increased by 100% when using unsized MRFs. Investigation into the enhancement mechanism of mechanical and electrical properties was also performed. Discussion of these mechanisms are presented with emphasis placed on the fiber/matrix interface and the load transfer mechanisms between matrix, carbon nanoparticles, and carbon fiber.

TABLE OF CONTENTS

TABLE OF CONTENTS (continued)

LIST OF TABLES

LIST OF FIGURES

LIST OF FIGURES (continued)

LIST OF FIGURES (continued)

Figure Page

LIST OF FIGURES (continued)

Figure Page

LIST OF ABBREVIATIONS/NOMENCLATURE

A-CNF	Amidized-Carbon Nanofiber
A-CNT	Amidized-Carbon Nanotube
A-MWCNT	Amine-Functionalized Multi-Walled Carbon Nanotube
AR-CNF	As-Received Carbon Nanofiber
AR-CNT	As-Received Carbon Nanotube
AR-MWCNT	As-Received Multi-Walled Carbon Nanotube
ATR	Attenuated Total Reflection
CF	Carbon Fiber
CNF	Carbon Nanofiber
CNT	Carbon Nanotube
COV	Coefficient of Variation
CVD	Chemical Vapor Deposition
DMF	Dimethylformamide
EM	Electrophoretic Mobility
EPD	Electrophoretic Deposition
FRPC	Fiber-Reinforced Polymer Composite
FRPN	Fiber-Reinforced Polymer Nanocomposite
FTIR	Fourier-Transform Infrared Spectrometry
Hi-res	High Resolution
ILSS	Interlaminar Shear Strength
MRF	Multiscale-Reinforcement Fabric
MRPC	Multiscale-Reinforced Polymer Composite

MWCNT	Multi-Walled Carbon Nanotube
O-CNF	Oxidized Carbon Nanofiber
O-CNT	Oxidized Carbon Nanotube
OM	Optical Microscopy
O-MWCNT	Oxidized Multi-Walled Carbon Nanotube
PAN	Polyacrylonitrile
SBS	Short-Beam Shear
SEM	Scanning Electron Microscopy
SWCNT	Single-Walled Carbon Nanotube
TEM	Transmission Electron Microscopy
TGA	Thermo-Gravimetric Analyzer
VARTM	Vacuum-Assisted Resin Transfer Molding
VGCF	Vapor-Grown Carbon Fiber
VGCNF	Vapor-Grown Carbon Nanofiber
XPS	X-Ray Photoelectron Spectroscopy

LIST OF SYMBOLS

Å	Angstrom
°	Degree
Δ	Heat
μ	Micron
V	Volt
ζ	Zeta

CHAPTER 1

INTRODUCTION

1.1 Motivation

Advanced polymer composites provide excellent tensile strength-to-weight and stiffness-to-weight ratios which are dominated by the mechanical properties of the fibers and the ability of the matrix to transfer load to the fibers. Conversely, typical advanced polymer composites have poor out-of-plane and in-plane compressive properties such as interlaminar shear strength (ILSS) and stiffness, and compressive strength. The out-of-plane behavior is explained by the dependence of these properties on the weaker polymeric resin system and the strength of the fiber/matrix interaction while compressive behavior is explained by the matrix playing a fundamental role in preventing the fibers from micro-buckling and kinking [1].

Carbon nanotubes (CNTs) and carbon nanofibers (CNFs) have an exceptional combination of mechanical, electrical, and physical properties that make them ideal materials as reinforcing nanoparticles in advanced polymer composites [2-4]. Their unique traits such as high modulus, strength, and electrical conductivity along with low density have motivated the research community to develop manufacturing technologies that seek the creation of a new class of nano-enhanced multiscale-reinforced polymer composites (MRPCs) with improved and controlled properties. If these unique nanoparticles can be successfully incorporated into advanced polymer composites, a new generation of high-performance, light-weight, nano-enhanced advanced polymer composites can be created.

In order to properly incorporate CNTs/CNFs into advanced composites, three major manufacturing challenges must be overcome: (1) dispersion of CNTs/CNFs into the matrix system, (2) uniform impregnation of the preform by the CNTs/CNFs, and (3) bonding and

compatibility between the CNTs/CNFs, matrix, and micro-sized reinforcement fibers. The usual approach to manufacturing MRPCs is through liquid composite molding. This process consists of four steps: (1) dispersion and mixing of the CNT/CNF in a polymer resin, (2) infusion of the CNT/CNF resin mixture into a mold containing dry preforms, (3) curing of the part, and (4) extraction of the part from the mold. Ideally, this manufacturing approach should produce MRPCs with enhanced mechanical and electrical properties. However, due to the major manufacturing challenges, enhanced and consistent mechanical and electrical properties are not always achieved. These manufacturing challenges along with the traditional method to manufacture MRPCs are schematically shown in Figure 1 and explained in detail below.

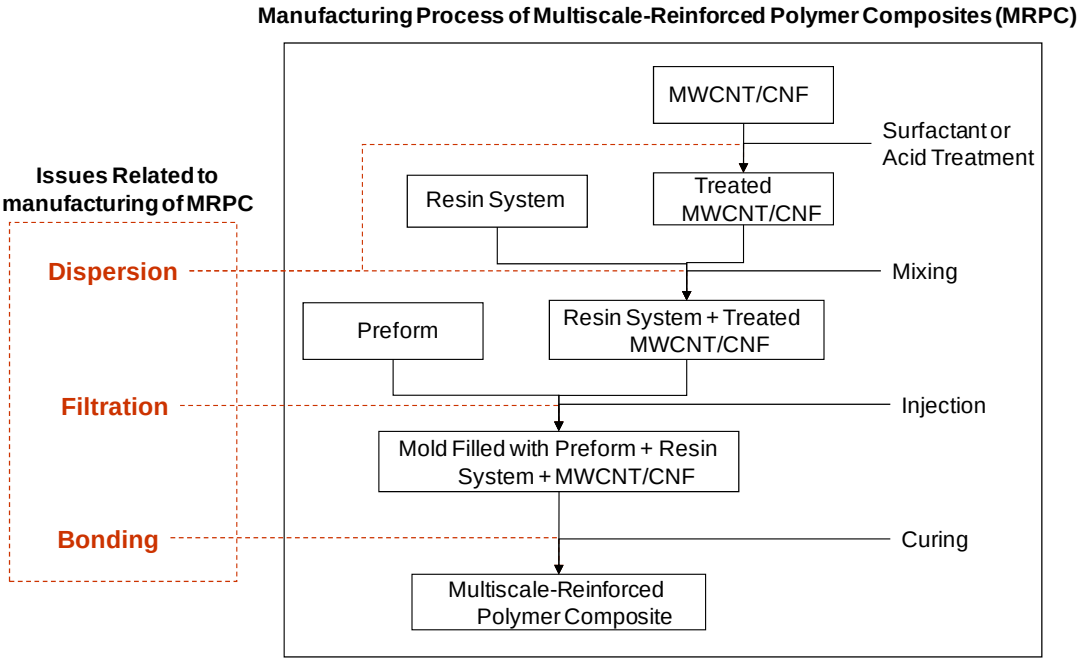

Figure 1. Issues related to manufacturing of fiber-reinforced polymer nanocomposites.

1. ***Dispersion of CNTs/CNFs into matrix system*** [5-12]. Due to their high surface area and high aspect ratio (> 1,000) along with weak van der Waals forces, CNTs/CNFs in their pristine state tend to agglomerate and form clusters and bundles of ropes that are difficult to disrupt or disentangle [13]. If these agglomerates are not broken apart before

incorporating the CNTs/CNFs into advanced composites, then the nanomaterials cannot be effectively dispersed in the resin, which results in lower interaction among the CNTs/CNFs, resin, and microfibers [14]. As a result, the ineffective load transfer between matrix and CNTs/CNFs will not be enough to attain reinforcement at the macro-scale level and will lead to lower overall properties of the composite. Scanning electron microscopy (SEM) images of CNT and CNF agglomerates are shown in Figure 2. Current CNT/CNF dispersion methods used in polymer resin systems, including chemical and physical mixing/processing methods along with mechanical shear mixing [2, 15-18], have achieved some level of success. However, these methodologies are not enough to ensure the desired dispersion level and other MRPC manufacturing techniques are required.

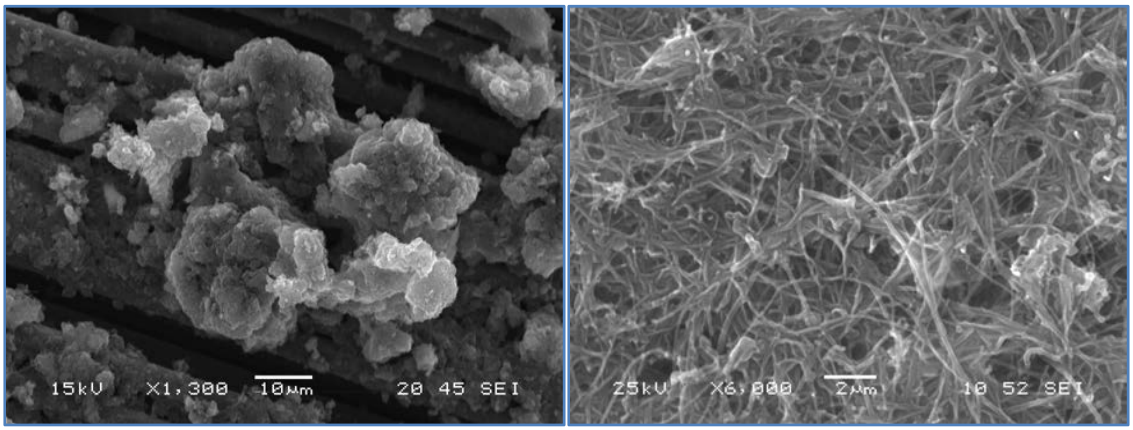

Figure 2. Left: SEM image CNT agglomerates. Right: SEM image of CNF agglomerates.

2. ***Uniform impregnation of preform by CNTs/CNFs*** [4, 6]. Traditionally, manufacturing of MRPCs is achieved through liquid injection molding where initially the CNTs/CNFs are added to the resin, mixed, and subsequently injected into the preform. The size of CNTs/CNFs is small compared to the space between the microfiber layers that comprise the preform of an MRPC. During injection of the CNT/CNF-resin mixture, the

nanoparticles should penetrate the preform without any hindrance; however, if the agglomerates/bundled ropes are large due to poor dispersion and/or the resin contains a high loading of CNTs/CNFs, the microfibers may act as a filter when injecting the CNT/CNF resin into the preform preventing the flow of agglomerates inside the part. This "filtering" phenomenon creates two types of regions inside the part: (1) regions with excess CNT/CNF where ineffective load transfer from the matrix to the nanomaterial causes a decrease in the properties of the part, and (2) regions of low CNT/CNF concentration where the amount of nanomaterial may not be enough for the part to attain reinforcement. An additional challenge associated with MRPC liquid injection molding techniques is that higher loading of CNTs/CNFs in the matrix causes the viscosity of the mixture to increase significantly due to the high aspect ratio of the CNTs/CNFs. If the increase in viscosity is too high, then it becomes extremely difficult —if not impossible— to impregnate the preform with the mixture of CNT/CNF resin. This limits the processability of the MRPCs, especially at high CNT/CNF concentrations [6]. Under these circumstances, void formation also becomes a concern [19].

3. ***Bonding and compatibility between CNTs/CNFs, matrix, and micro-sized reinforcement fibers*** [20-24]. In fiber and particle-reinforced systems, it is essential that all constituents interact effectively to achieve the material's full potential by exploiting the properties of all phases. Therefore, high surface interaction among the CNTs/CNFs, matrix, and fibers is crucial in harnessing the properties of the nanomaterials. Different resins have different chemical compositions; therefore, the surface interaction between the CNTs/CNFs and the resin and micro-sized fibers may change depending on their surface chemistry [25, 26]. If the interaction forces are low, then overall material

properties will also be low due to inefficient load transfer between phases. In this case, chemical modification to the surface of the nanomaterials and fibers is necessary to ensure good compatibility and load transfer between phases.

1.2 Research Objectives

To manufacture MRPCs with improved and consistent mechanical properties, the three aforementioned manufacturing challenges must be addressed and resolved. As such, it is necessary to develop and study novel processes to manufacture MRPCs that can exploit the unique properties of CNT and CNF in order to render high-performance materials.

In this work, a methodology to manufacture multiscale-reinforced polymer composites containing functionalized CNTs and CNFs was developed and studied. This methodology addresses current MRPC manufacturing issues by placing either carboxylic acid- or amine-functionalized MWCNTs/-CNFs directly into the dry carbon fiber layers prior to infusion of the matrix system. The methodology for manufacturing MRPCs is divided into two stages. In the first stage, multiscale-reinforcement fabrics (MRFs) were manufactured by depositing carboxylic acid- or amine-functionalized CNTs and CNFs on the surface of carbon fiber layers by electrophoretic deposition. In the second stage, preforms containing the MRFs were assembled and infused with an epoxy-amine resin system by resin infusion to manufacture the final MRPCs. The resulting MRPCS were then tested for mechanical and electrical properties.

This research work is aimed at obtaining a fundamental understanding of the processing and properties of MRPCs that are manufactured following the aforementioned process. These findings are intended to be used to further knowledge in the manufacturing of MRPCs in order to aid in the creation of the next generation of high-performance polymer composites.

Based on the motivation of this project, the dissertation research objectives are as follows:

- To develop a process to synthesize multiscale-reinforcement fabrics (MRFs) containing functionalized CNTs/CNFs with the aim of enhancing the properties of multiscale-reinforced polymer composites manufactured with such layers.
- To study the effectiveness of the multiscale-reinforcement fabrics on the mechanical and electrical properties of multiscale-reinforced polymer composites manufactured with the synthesized multiscale fabrics.

Chapter 1 provides an introduction to the subject where the main issues related to manufacturing of MRPC are discussed and the research objectives are presented. Chapter 2 presents a review of the research related to CNT/CNF technology, where the synthesis, morphology, and properties of CNT/CNF are studied along with MRPC processing techniques and characterization. In Chapter 3, a process to synthesize multiscale-reinforcement fabrics (MRFs) containing functionalized CNT-/CNF is described and studied. To assess the effect of the hierarchical structures of MRFs described in Chapter 3, Chapter 4 shows the processing and characterization of MRPCs manufactured with such layers. Finally, Chapter 5 presents the conclusions of the work with emphasis placed on understanding the reinforcement mechanism of MRFs.

CHAPTER 2

LITERATURE REVIEW

2.1 Morphology, Properties, and Synthesis of Carbon Nanotubes and Carbon Nanofibers

2.1.1 Carbon Nanotubes

Although carbon nanotubes are believed to have been initially observed by Oberlin et al. [27] and other authors [28] in the 1970's (although not claimed by them to be CNTs), they were first unambiguously observed and reported by Iijima in 1991 [29]. These allotropes of carbon were “needle-like” tubes comprised of 2 to 50 coaxial sheets of graphitic carbon forming a tube-like wall with a diameter ranging in the tens of nanometers (electron micrographs of this discovery are provided in Figure 3). These carbon forms were later named multi-walled carbon nanotubes (MWCNTs). In 1993, two separate and independent reports by Iijima and Ichihashi [30] and Bethune et al. [31] described the structure of a newly discovered form of carbon exhibiting a single wall of carbon. Both publications reported single-shell carbon structures made by an electric arc discharge using iron and cobalt catalysts, respectively. The single-shell nanotubes, named single-walled carbon nanotubes (SWCNTs), were reported to have diameters of approximately 1 nm for iron and 1.2 nm for cobalt catalysts. An electron diffraction pattern and micrograph of the SWCNT reported by Iijima and Ichihashi are shown in Figure 4.

2.1.1.1 Morphology and Properties of Carbon Nanotubes

CNTs' manufacturing and characterization techniques have evolved since their discovery. To date, CNTs are generally classified into two types: (i) multi-walled carbon nanotubes and (ii) single-walled carbon nanotubes. MWCNTs have diameters of 3-80 nm depending on the number of carbon shells while SWCNTs have a diameter of 1-2 nm. Both types of CNTs have been

observed to have a typical length from hundreds of nanometers to hundreds of microns. A schematic of the morphology of a SWCNT and a MWCNT is provided in Figure 5.

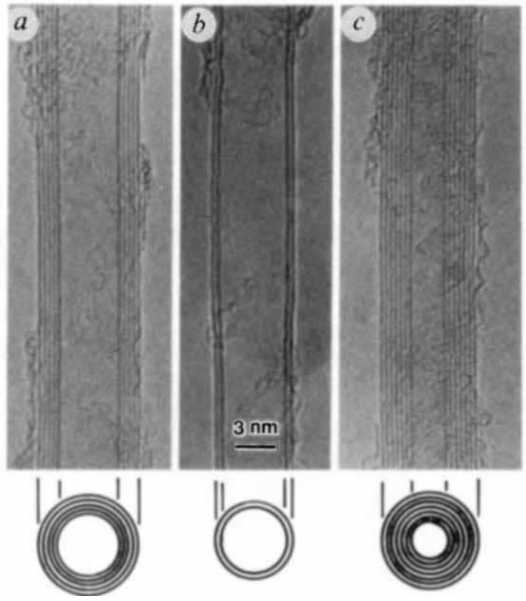

Figure 3. Electron micrographs of microtubules of graphitic carbon: (a) tube consisting of five graphitic sheets, diameter 6.7 nm, (b) two-sheet tube, diameter 5.5 nm, (c) seven-sheet tube, diameter 6.5 nm, which has the smallest hollow diameter (2.2 nm) [29].

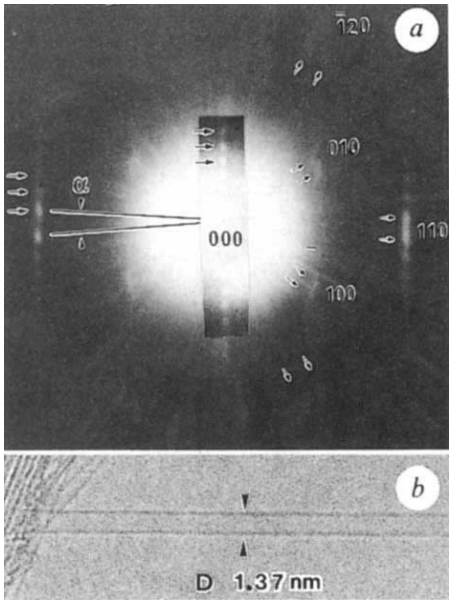

Figure 4. (a) Electron diffraction pattern taken from a single-shell nanotubule of diameter 1.37 nm. (b) Electron micrograph of same tubule [30].

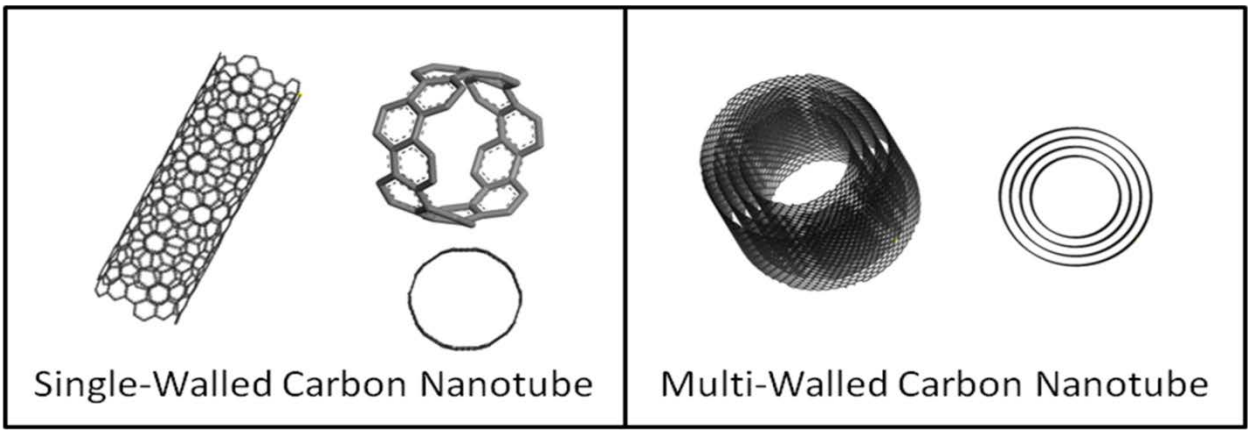

Figure 5. Schematic of morphology of SWCNT and MWCNT.

CNTs have an extraordinary combination of mechanical, electrical, and physical properties. CNT Young's modulus can range from 590 to 1,105 GPa, its strength can range from 35 to 110 GPa [32], and its axial electrical conductivity has been estimated to be ~10^6 and ~10^8 S/m depending on the type of CNT, SWCNT and MWCNT, respectively [33]. With one-sixth of the density of steel, CNTs are about 100 times stronger and have the ability to sustain high strain (10%–30%) without breaking.

A CNT can be visualized as a hexagonal graphene sheet rolled to form a tube-like carbon arrangement. This arrangement makes carbon atoms sp^2 hybridized in a helical manner (graphene sheet lattice configuration). The diameter and properties of CNTs depend on how the graphene sheets are "rolled." This difference in configuration is described in terms of helicity, which is mathematically described in terms of a chiral vector, $\vec{C}_h$, and chiral angle, θ. The chiral vector describes the direction to which the graphene sheet is rolled over and is defined by two integers, *n* and *m*, and two unit vectors, $\vec{a}_1$ and $\vec{a}_2$, related by the following equation: $\vec{C}_h = m\vec{a}_1 + n\vec{a}_2$. The integers describe the lattice atom that will be superimposed with the reference carbon atom, as indicated in Figure 6.

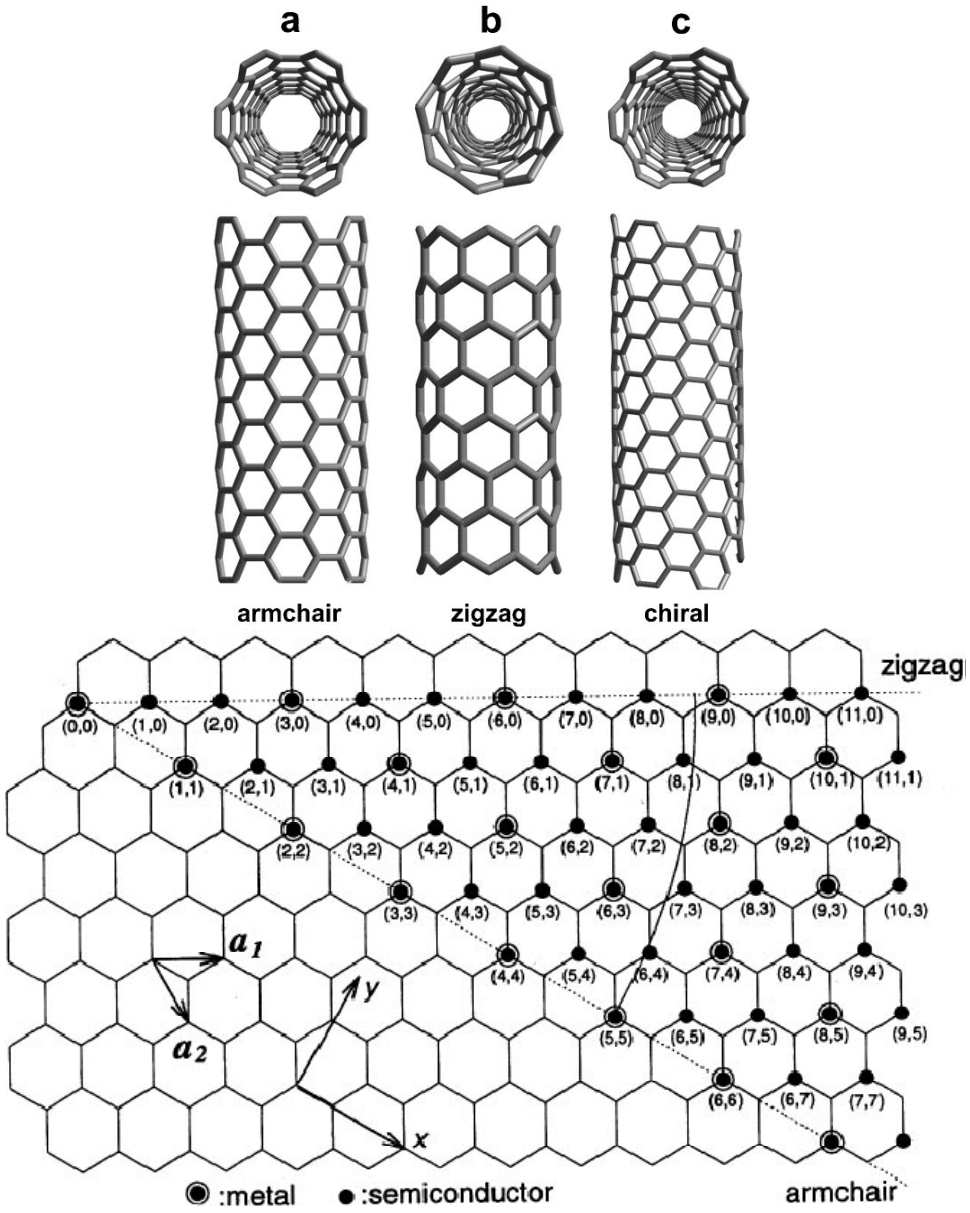

Figure 6. Top: Molecular models of SWCNTs with different chiralities: (a) armchair, (b) zig-zag, (c) chiral. Bottom: Schematic diagram of chiral vector and chiral angle of graphene lattice [33].

The chiral angle is defined by the aperture between the chiral vector and the zig-zag structure of the graphene sheet [33]. The two limiting cases for the helicity or "twist" of CNTs is when the chiral angle is either 0° or 30°; these configurations are referred to as armchair and zig-zag, respectively. In the former case (*n*, *n*), some of the carbon-carbon bonds (C-C) lie along the circumference of the CNTs whereas in the latter case (*n*, 0), the C-C bonds lie in the crosswise

direction with respect to the chiral vector [34]. All other configurations of the CNTs lie within these limiting cases and are referred to as chiral nanotubes (*m*, *n*). The difference in configuration between the aforementioned CNTs is schematically shown in Figure 6. Based on the chiral angle and vector, the diameter of the CNTs can be defined by $d = \frac{a\sqrt{m^2 + mn + n^2}}{\pi}$ where $a = 1.42 \times \sqrt{3}$ Å and represents the lattice constant in the graphene sheet. Note that the inter-atomic distance is 1.42 Å.

Several researchers have investigated the effect of chirality on the mechanical and electrical properties of CNTs. Vaccarini et al. [35] studied the effects of tube chirality on the axial stiffness, bending, and torsion of CNTs. They found that chiral CNTs exhibit asymmetrical torsional behavior with respect to right or left twist, which was not present in armchair and zig-zag nanotubes. They also reported no significant tensile modulus change due to chirality. Yakobson et al. [36] also studied the effect of chirality on the mechanical properties of CNTs. Here, the morphological behavior of CNTs was examined using molecular dynamic simulations when CNTs were subjected to compression, tension, or bending. The authors found that chirality had negligible influence on the elastic properties of CNTs and that high deformation of nanotubes caused sudden changes in the morphological patterns. These changes were mainly attributed to the Stone-Wales transformation which is a reversible configuration of atoms where the lattice configuration is rearranged to form a structure of two heptagons and two pentagons, as shown in Figure 7. In terms of electrical conductivity, CNTs can be either metallic or semi-conducting depending on chirality [37]. Armchair CNTs as well as zig-zag nanotubes with values of *m*, *n* related by multiples of three have been predicted to be metallic whereas all other types have been termed semi-conducting.

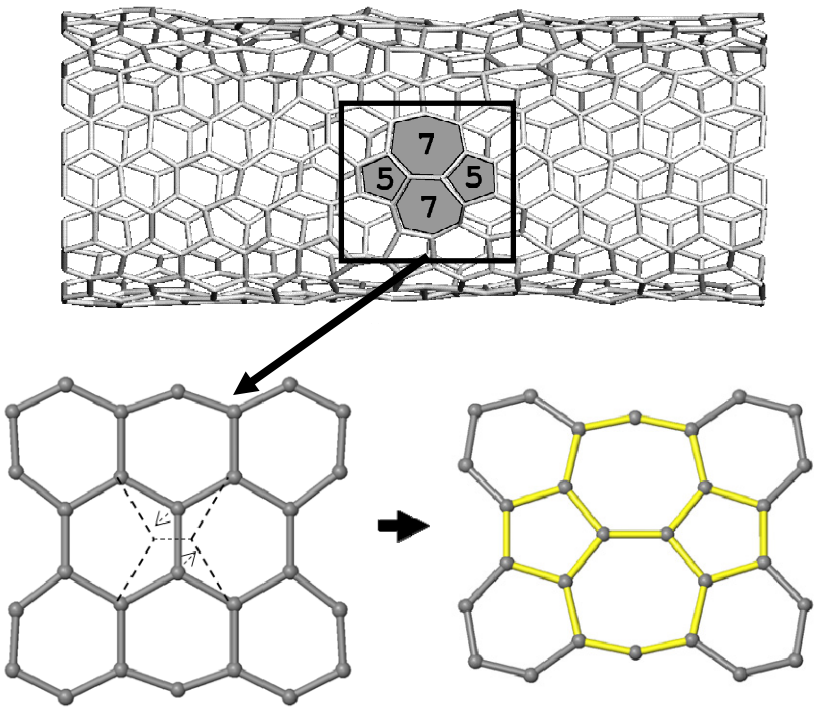

Figure 7. Top: Formation of Stone-Wales defect at T = 2000 K and 10% strain [38]. Bottom: Stone-Wales diatomic interchange in nanotube hexagonal wall [39].

2.1.1.2 Synthesis of Carbon Nanotubes

Several techniques exist to manufacture carbon nanotubes: electric arc-discharge [29-31, 33, 40, 41], laser ablation [42-44], gas-phase catalytic growth [45], chemical vapor deposition (CVD) [46-49], and electrochemical growth in condensed phase [50].

Arc-discharge and laser ablation techniques consist of the condensation of carbon atoms after being evaporated from high-purity carbon electrodes under inert atmosphere (usually helium). In the arc-discharge method, a direct-current is used to evaporate carbon from the solid carbon sources, whereas in laser ablation, a laser aimed at the carbon sources vaporizes the material. To date, both techniques are able to produce a high yield of CNTs. However, the downside of these processes is the cost associated with manufacturing due to limited source of carbon during the production process. In addition, formation of by-products, such as

encapsulated metal particles and amorphous carbon, and lack of control in the final dimensions of the nanotubes are also concerns.

Gas-phase catalytic growth and chemical vapor deposition techniques are more promising methods of producing low-defect cost-effective CNTs due to their capability of being scaled-up and also the ability to control many parameters in the process. Both processes employ continuous injection of a hydrocarbon gas in a reactor as source of carbon, thus, the cost of production is substantially lower than in the previous two methods. In the gas-phase growth, CNT's catalysts are formed in-situ by decomposition of iron when heated in the presence of a flow of carbon monoxide at 1–10 atm and 800°C –1,200°C. In CVD, the CNTs grow in the presence of a metal catalyst (although Steiner et al. have recently reported the use of ceramic particles as catalyst [51]) when carbon decomposes from gases of high carbon content at elevated temperatures — typically between 700°C and 1,000°C.

Electrochemical growth is a new method to grow CNTs in liquid phase. In this process, CNTs are formed when graphite electrolytes are immersed in LiCl under inert atmosphere and DC electric field. When the current passes through the system, the carbon dissolves in the molten salt, thus forming Li_2Cl_2. The carbon atoms then become isolated in an ordered hexagonal array resulting in the formation of CNTs. The drawback from this process is the lack of controllability due to the complexity of the chemical reactions.

2.1.2 Carbon Nanofibers

Early in the 1970s and 1980s, research efforts were focused on combining polyacronitrile (PAN)- and pitch-based carbon fibers with polymers to manufacture advanced composites with outstanding properties. Due to the their high-cost, research focused on developing methodologies to manufacture vapor grown carbon fibers (VGCFs) ―from hydrocarbons― with similar

properties than those of previous generations but at a lower cost [52]. Careful examination of fibers manufactured following newly developed methods revealed that they had two types of textures that resulted from two different growth processes: core regions with long and straight carbon layers formed by catalytic effect, and external regions that consisted of deposited carbon that occurred during the thickening process [27]. From these fibers, small “cementite crystals” of about 10 nm were identified at the tip of the central tube of the fibers. Further studies of VGCF production revealed that growing the predecessor of carbon filaments was very effective and that nanometer sized filaments were being “grown” very efficiently inside the reactor. Afterwards, these carbon filaments were being deposited onto some of the larger carbon filaments to make the macroscopic thickened carbon fibers [53]. From these findings, researchers started manipulating the processing techniques to continuously produce the more efficient submicron-sized filaments, named vapor grown carbon nanofibers (VGCNFs) and later called simply carbon nanofibers (CNFs). A review by Tibbetts et al. [54] and Lake et al. [55] discusses in depth the main manufacturing and property aspects of VGCFs and VGCNFs.

2.1.2.1 Morphology and Properties of Carbon Nanofibers

Morphologically, pristine CNFs are comprised of two layers of different carbon arrangements. The interior layer resembles a hollow tube surrounded by cone-shaped graphitic sheets cup-stacked at ~25° with respect to the longitudinal axis; the outer layer is a turbostratic layer of graphene sheets stacked surrounding the inner layer and aligned in the longitudinal direction of the fiber [54]. Depending on the stacking arrangement of the graphene planes, CNFs can have different configurations such as cup-stacked [56], bamboo-like [57], and parallel [58]. Miyagawa et al. [59] reported that the spacing between planes is 3.4 Å which corresponds to the

spacing between the walls of MWCNTs. Transmission electron microscopy (TEM) images of a CNF with one and two layers are provided in Figure 8 [54, 58].

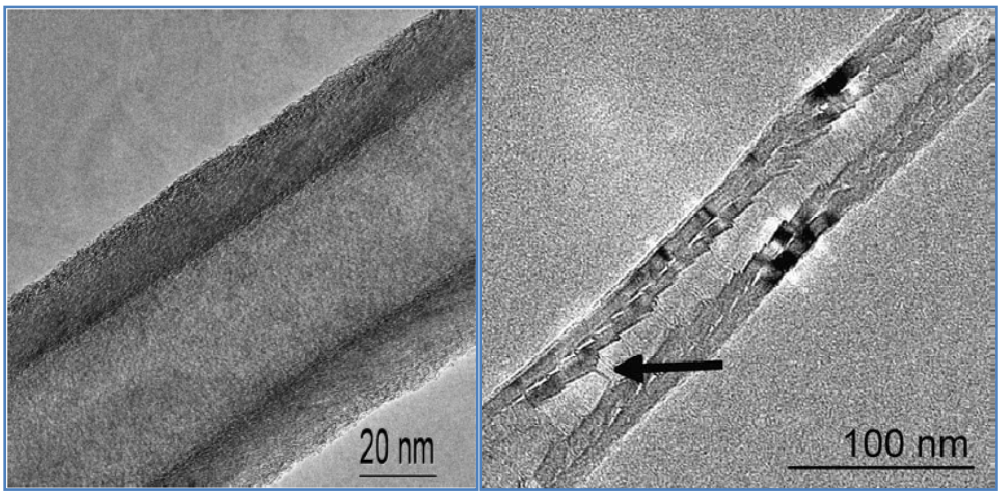

Figure 8. Left: TEM showing the structure of a CNF with one layer (cylindrical hollow core at center) [54]. Right: TEM showing structure of a CNF with cylindrical hollow and turbostratic layer [58].

Although their mechanical properties are lower than carbon nanotubes, CNFs strength and modulus is still high and have been experimentally determined to be 2.90 ± 1.4 GPa and 180 ± 60 GPa, respectively [60]. CNF's electrical conductivity and density have been estimated to be 10^6 S/m and 1.95 g/cm^3, respectively [61]. A summary of the mechanical, electrical, and physical properties of CNFs, SWCNTs, and MWCNTs along with other materials of interest are compared in Table 1.

2.1.2.2 Synthesis of Carbon Nanofibers

CNFs are nano-sized fibrils that are manufactured by chemical vapor deposition. This process involves growing CNFs by feeding a flow of hydrocarbon ―natural gas, benzene, ethylene, and acetylene among others― through a reactor maintained at 500°C to 1,500°C in the presence of metal catalysts such as iron, nickel, cobalt or a metal alloy. To date, this process is the most widely used for manufacturing CNFs due to its efficiency and high yield. Further

treatment of CNFs includes graphitization of the exterior plane or recrystallization of nested graphite planes. The former treatment yields CNFs with higher mechanical and electrical properties due to alignment of the outer layer in the fiber direction while the latter treatment results in lower physical properties due to the formation of discontinuous conical crystallites [54]. Ideal heat treatment for CNFs was investigated and reported by Tibbetts et al. [62] who found that the optimal performance for mechanical or electrical properties can be achieved by treating the CNFs at 1,500°C and 1,300°C, respectively.

TABLE 1

MECHANICAL, ELECTRICAL, AND PHYSICAL PROPERTIES OF VARIOUS MATERIALS

Material	Strength [GPa]	Young's Modulus [GPa]	Electrical Conductivity [S/m]	Density [g/cm^3]	Specific Strength [MPa·m^3/Kg]
CNF	2.90 ± 1.4 [60]	180 ± 60 [60]	10^6 [61]	1.95 [61]	1.49
MWCNT	35-82 [32]	590-932 [32]	10^6 [33]	1.3-2.25 [63]	15.5-63.08
SWCNT	97-110 [32]	990-1,105 [32]	10^4 [33]	1.33-1.4 [63]	69.29-82.71
Carbon Fiber (PAN-Based Precursor) [64]	4.65-6.35	285	6.66×10^4	1.78	2.61-3.57
Aluminum 7075-T6 [64]	0.572	71	1.91×10^7	2.80	0.204
Steel 316 (cold drawn and annealed) [64]	0.620	193	1.5×10^6	8.00	0.075

2.2 Processing of Carbon Nanotubes and Carbon Nanofibers

Due to the their surface area and van der Waals forces, pristine CNTs and CNFs tend to agglomerate and form bundles that are difficult to disrupt. In order to enhance the mechanical properties of materials using CNTs/CNFs, these agglomerates must be broken apart so that

effective load transfer from the matrix to the nanomaterials can occur. To break these agglomerates and improve dispersion of the CNTs/CNFs within the matrix (or other media), several CNT/CNF treatments have been investigated by various researchers. These techniques include chemical functionalization of the surface of the nanomaterials to increase the surface energy [65, 66], ultrasonic dispersion [11, 67-69], surfactant treatment of nanoparticles [70], high mechanical shear mixing [71-74], in-situ polymerization [75, 76], and various combinations of these [77]. Of these methods, chemical functionalization has proven to be one of the most promising ways to tailor the surface of nanoparticles to obtain proper dispersion and bonding with different matrices. As a result, higher mechanical and electrical properties have been achieved.

Several chemical functionalization strategies have been investigated to disperse CNTs/CNFs in different media. These functionalization methods involve the introduction of moieties on the walls of nanomaterials to obtain higher surface energy. In terms of dispersion, this higher surface energy makes the functionalized CNTs/CNFs repel each other and exfoliate in the medium. In regards to bonding, researchers have investigated the use of matrix compatible functional groups to obtain higher load transfer between material phases [78-81]. To this end, several functional groups have been grafted onto the CNTs/CNFs with varying levels of success [8, 82]. The most commonly utilized functional groups are as follows: carboxylic acid [83, 84], hydroxyl [85], amine [86], epoxy [87], and different types of polymers [88-90]. Lachman and Wagner [78] proved that using MWCNTs functionalized with carboxylic acid and amine functional groups to reinforce an epoxy resin system can increase the toughness of the nanocomposite. They attributed these results to an increase in dispersion quality and in interfacial adhesion. Seyhan et al. [91] studied the fracture toughness of an epoxy-based resin

reinforced with carboxylic acid and polymer functionalized CNFs. Results showed that the addition of both types of functionalized CNFs also increased the fracture toughness of the nanocomposites. In a later study by Kathi et al. [92], nanocomposites with oxidized and silanized MWCNTs were prepared by cast molding. Results from this work showed that the addition of functionalized MWCNTs improved the flexural strength and modulus by adding MWCNTs up to 0.2wt.%. Prolongo et al. [12] studied the effects of adding amine-functionalized CNFs on the dispersion of CNFs and final properties of epoxy nanocomposites. Results showed that the nanocomposites containing well dispersed CNFs exhibited a higher storage modulus and no porosity. The authors of this work concluded that to obtain well-dispersed CNFs in epoxy matrix, chemical functionalization coupled with ultrasonic and high-shear mixing is needed. In a study by Peng Cheng et al. [93], investigation into the effect of CNT silane functionalization on the mechanical and thermal properties of epoxy-based nanocomposites was examined. Results from this work concluded that nanocomposites with silane-CNTs exhibited higher flexural modulus and strength along with better thermal stability. This was attributed to an improved interfacial interaction between the functional group and the matrix system.

From the latter results, it is clear that treatment of the nanoparticles is an imperative step towards the realization of higher properties of CNT/CNF-polymer systems. These conclusions are crucial to the study of processing techniques in other hierarchical structures such as multiscale-reinforced composites, which is the subject of this dissertation.

2.3 Manufacturing Methodologies of Multiscale-Reinforced Polymer Composites

Multiscale-reinforced polymer composites (MRPCs) are defined as structures having material reinforcement on at least two different scales. In this dissertation: nano-scale and micro-scale. Several researchers have worked on the development of processes that allow incorporation

of CNTs/CNFs (nano-scale reinforcement) into advanced polymer composites (micro-scale reinforcement) to enhance the properties of such materials with different levels of success. To date, four main approaches exists to incorporate CNTs/CNFs into advanced polymer composites: (1) infusion of a CNT/CNF mixture into the preform, (2) growth of CNTs/CNFs onto different substrates through chemical vapor deposition, (3) direct placement of CNTs/CNFs between layers of the preform, and (4) deposition of carbon nanoparticles onto fabric layers. These methodologies are discussed in detail in the following subsections.

2.3.1 Infusion of CNT/CNF Mixture into Preform

In preform infusion, CNTs/CNFs are initially dispersed in the resin to form a CNT/CNF resin mixture. This mixture is then infused into the preform by liquid injection molding and subsequently cured to manufacture the final MRPC part. This method is the most widely used in manufacturing MRPCs because of its practicality and scalability. In addition, the carbon nanomaterials used can be functionalized with the desired moiety to be more compatible with the resin system.

Qiu et al. [4] manufactured MRPCs by infusing a mixture of MWCNTs and polymer resin into a glass-fiber preform via vacuum-assisted resin transfer molding (VARTM). The mixture was prepared by sonicating the MWCNTs in the curing agent and then in an epoxy-based matrix. Mechanical test results showed a moderate increase of 5% and 8% for shear strength and short-beam shear (SBS) modulus, respectively, without compromising the in-plane properties. Sadeghian et al. [6] prepared MRPCs by infusing mixtures of surfactant-aided dispersed CNFs in polyester resin into a glass preform. Results showed an increase in the energy for delamination (G_{IC}) initiation of ~100% when 1wt.% of CNFs was dispersed in the resin. Although significant improvement was obtained in the MRPC, the authors pointed out

difficulties in manufacturing the MRPCs due to an increase in viscosity of the resin ―due to CNF loading― and void formation. Morales et al. [94] prepared glass-reinforced plastic composites with non-functionalized CNF-loaded polyester resin by light resin transfer molding. Results showed an increase in flexural and tensile strengths with an addition of 0.5wt.%.

The limitations of this approach are that dispersion and filtration issues are not usually resolved, especially at CNT/CNF loadings higher than 1wt.%. In addition, an excessive increase in the viscosity of CNT-/CNF-resin mixture and also void formation pose major manufacturing difficulties [95].

2.3.2 Growth of CNTs/CNFs on Fibers by Chemical Vapor Deposition

In this method, chemical vapor deposition is used to grow CNTs and CNFs directly on the surface of micro-scale fiber reinforcement. This multiscale structure is then used to assemble the preform that is later injected by the polymer resin. The methodology has several advantages, the most important of which are the ability to control the uniformity and alignment of nanoparticles.

Previous researchers have achieved the growth of CNTs in alumina blocks [96], woven alumina cloth [97], silica fibers [98], quartz fibers [99], single carbon fibers [100-105], and carbon fiber layers [106, 107]. In addition, growth of CNFs in single carbon fibers [108] and activated carbon fiber layers [109] has also been reported. Qian et al. [103] performed fiber pull-out tests after growing CNTs on a carbon fiber surface. Results showed that interfacial shear strength between the hybrid CNT-carbon fibers and the matrix increased by ~57%. Thostenson et al. [100] reported that the interfacial load transfer between matrix and fiber increased by 15% when using carbon fibers with MWCNTs grown on their surface. Sager et al. [101] reported that carbon fibers with CNT grown on their surface had up to 71% increase in interfacial shear

strength over untreated unsized fibers. Although higher fiber/matrix interfacial properties were attained, authors of the latter studies reported that growth of CNTs on carbon fibers could decrease the tensile strength of the fiber by up to 37%. Properties of MRPCs manufactured with CNT-grafted carbon fiber layers was investigated by Kepple et al. [106] and Mathur et al. [110]. The authors of the former study reported that fracture toughness of the MRPCs had an increase of approximately 50% when tested under Mode I, while the authors of the latter study reported an increase in flexural strength and modulus for MRPCs with carbon fiber cloth and carbon fiber felt.

Less research has been devoted to the growth of CNFs on any type of fiber. Growth of CNFs on the surface of carbon fibers and glass fibers was reported by Duan et al. [108]; although no properties of MRPCs were reported, it was found that CNFs could be successful grown by CVD and that the morphology of the CNFs could be controlled by the feedstock gas (ethanol) pretreatment.

Results from the aforementioned research are promising in terms of dispersion, controlled growth of the nanoparticles, and final properties of the MRPCs. However, the method's lack of practicality due to the limitations in growing CNTs/CNFs in large size and within complicated layers in the presence of catalysts limits its application. In addition, difficulties arise when functionalizing CNTs/CNFs grown in fibers with functional groups that are compatible with the matrix system. Furthermore, degradation of the fibers due to the extreme conditions required by CVD to grow nanoparticles is also of concern [101].

2.3.3 Direct Placement of CNTs/CNFs between Layers of Preform

Due to the difficulties associated with manufacturing MRPCs following the aforementioned two methodologies, researchers have investigated direct placement of the

nanomaterials on the preform. In this process, CNTs/CNFs are placed between the layers of the preform before consolidating the part and curing the polymer resin. In this way, the challenges of dispersing the particles in the matrix and impregnating the preform with the nanomaterial can be better addressed and, in some cases, alignment of the nanoparticles inside the part can be controlled.

Several researchers have used this technique to manufacture MRPCs yielding interesting results [111, 112]. Garcia et al. [113] added aligned CNT arrays, referred to as CNT forests by the authors, directly between the layers of the preform after growing the CNTs on Si substrate using chemical vapor deposition. Results from this work showed that the fracture toughness of MRPCs increased 1.5 to 2.5 times in Mode I delamination, and 3 times in Mode II testing. In a similar approach by Wicks et al. [114], it was found that the interlaminar fracture toughness of MRPCs could be increased by using radially-aligned CNTs between the layers of the composite, leading to a modest increase in tension-bearing stiffness and strength. In a study by Rojas et al. [115], CNTs and CNFs were sprayed onto the carbon fiber layers before assembly of the preform and infusion of the matrix. The authors concluded that even though a significant increase in interlaminar shear strength was not attained, the change in mode of failure from delamination to tensile fracture was evidence of reinforcement in the sample's mid-plane. The drawback from this approach is the impracticality due to size limitations in growing CNT in Si substrate. In a study by Li et al. [116], a similar approach was followed to manufacture MRPCs, where the powder of CNFs was manually introduced at the mid-plane of the composite. Results showed a modest improvement in the mode-I delamination and bending strength and modulus of the samples. The downside to this approach was the increase in thickness caused by the additional layer of CNFs. Warrier et al. [24] studied the effect of adding CNTs to the sizing of glass fibers,

the matrix, or both on the properties of MRPCs. Results showed a reduction of ~31% in the coefficient of thermal expansion and an increase in the resistance to crack initiation of ~10%, although the crack propagation toughness decreased by 53%.

2.3.4 Deposition of Carbon Nanoparticles onto Fabric Layers

Deposition of functionalized CNTs/CNFs onto fabric layers show the highest advantages in terms of practicality, scalability, and cost-effectiveness. In this process, the particles are initially charged by attaching the desired functional group to the wall of the nanomaterial. Then the CNTs/CNFs are dispersed in a liquid medium, and upon application of an electric field, the particles move and deposit onto a conductive substrate.

Electrophoretic deposition (EPD) has proven to be an effective technique for manipulating and depositing large amounts of nanosized particles on different substrates [117-122]. Cho et al. [121] and Du et al. [120, 123] used this process to fabricate form coatings of functionalized CNTs. The authors of the former research reported that they were able to accurately control the thickness and also manufacture coatings with uniform homogeneity, showing that EPD is a convenient method to produce uniform coatings. The authors of the latter research reported that the microstructure of the nanotube films of CNT was strictly dependent of the solvent used. Yu Jun et al. [124] successfully deposited CNFs on the surface of indium tin oxide electrodes using dimethylformamide (DMF) as dispersive medium. They concluded that the density of the deposition of CNF was greatly influenced by the electric field and concentration of CNFs. Schausten et al. [125] also used EPD to deposit bioglass and MWCNTs on stainless steel substrates to fabricate bioactive nanostructured composite layers. In this research, the EPD parameters such as voltage and time were varied to obtain the optimal experimental parameters. The authors reported that co-deposition of the particles resulted in

homogeneous and dense coatings, which highlights the usefulness of this process. Another interesting study of MWCNTs was performed by Wu et al. [126]. Here, MWCNT/polyimide composite films were manufactured by deposition of MWCNT-polyamic acid colloidal suspension. Under the electric field, both charged particles migrated to the anode simultaneously and were converted to MWCNT/polyimide composite films. The authors also reported the ability to control the thickness of the film by varying the deposition time and anode conductivity. The underlying result of the research is that EPD represented a convenient approach to fabricate composite films with tailored thickness and electrical conductivity.

Recently, Zhang et al. [127] deposited functionalized MWCNTs onto electrically insulating glass fiber through electrophoretic deposition. Results showed that the interfacial shear strength increased significantly compared to that of conventional glass fiber composite. In addition, the semi-conductive glass/MWCNT interphase electrical conductivity was extremely sensitive to the tensile strain of single-glass fiber model composites, thus making this system a viable structure for monitoring damage in MRPCs via resistance. Theodore et al. [128] also deposited functionalized MWCNTs dissolved in DMF onto carbon fiber layers with the aim of improving fiber thermal conductivity. Results showed that MWCNT/carbon fiber structures exhibit an increase of one fold in the nanocomposite thermal conductivity. Bekyarova et al. [129] utilized EPD to deposit carboxylic acid-functionalized CNTs onto the surface of carbon fiber layers that were then used to manufacture MRPCs. Results indicated an increase in interlaminar shear strength of ~27% and through-plane electrical conductivity of ~30%. An important conclusion from this work is that EPD of carboxylated CNT onto the surface of carbon fiber layers did not negatively affect the in-plane tensile strength of the MRPCs. As previously mentioned, other methods for fabric reinforcement, such as in-situ growth of CNTs on the

surface of carbon fibers by thermal chemical vapor deposition, have been shown to reduce the tensile strength of carbon fibers, which is detrimental to the in-plane mechanical properties of MRPCs [101]. The authors of this work reported the deposition of only carboxylated CNT on the reinforced composite, but no other particles with alternate functional groups were studied.

2.4 Summary

In this chapter, the morphology, properties, and synthesis of CNTs and CNFs have been reviewed. Special emphasis was placed on the mechanical and electrical properties of these materials due to the promise they hold as reinforcing particles for enhancing the macro-scale properties of MRPCs. In addition, processing requirements to effectively incorporate CNTs and CNFs into polymer based matrices have been addressed and discussed.

Current techniques for manufacturing MRPCs have been introduced and reviewed in this chapter. Several researchers have worked on the development of processes that allow incorporation of CNTs/CNFs into conventional advanced polymer composites to enhance the properties of such materials with different levels of success. To date, four different approaches to incorporate CNTs/CNFs into advanced polymer composites exist: (1) infusion of CNT/CNF mixture into the preform, (2) growth of CNTs/CNFs on different substrates through chemical vapor deposition, (3) direct placement of CNTs/CNFs between the layers of the preform, and (4) deposition of carbon nanoparticles onto fabric layers.

CHAPTER 3

SYNTHESIS OF MULTISCALE-REINFORCEMENT FABRICS BY ELECTROPHORETIC DEPOSITION OF FUNCTIONALIZED CARBON NANOMATERIALS ONTO CARBON FIBER LAYERS

3.1 Introduction

Due to their unique combination of properties, MWCNTs/CNFs are regarded as ideal materials to enhance the properties of advanced composite parts. However, challenges arise when traditional MRPC manufacturing techniques are followed to produce MWCNT-/CNF-reinforced composites: (1) dispersion of MWCNTs/CNFs into the matrix system, (2) uniform impregnation of the preform by MWCNTs/CNFs, and (3) bonding and compatibility between the MWCNTs/CNFs, matrix, and micro-sized reinforcement fibers (i.e., carbon fibers, glass fibers, etc.).

This chapter describes a process to synthesize multiscale-reinforcement fabrics (MRF) by directly depositing functionalized MWCNTs/CNFs onto the surface of carbon fiber layers through electrophoretic deposition (EPD) using water as dispersive medium. This process aims at placing the CNFs/CNTs directly on the dry carbon fiber plies prior to infusion of the matrix system to enhance dispersion of MWCNTs/CNFs in the resin and avoid filtration of the MWCNTs/CNFs by the preform. In addition, to address the bonding and compatibility issue, functionalized MWCNTs/CNFs having functional groups compatible with the polymer matrix system were used as the reinforcing particles.

EPD is a process in which charged particles suspended in a liquid medium move and deposit onto the counter electrode upon application of a DC electric field. EPD is a cost-effective and scalable technique that has proven to be an effective method for manipulating and depositing large amounts of nano-sized particles on different substrates with complex shapes [117-119, 122,

123]. EPD has been used to deposit CNTs and CNFs onto various substrates with the purpose of making thin film electrodes [130], composite sheets [120], coatings [121, 124, 125, 131], hybrid fabrics [127-129], and field emission arrays [132-134].

A schematic of the process for depositing MWCNTs/CNFs onto the surface of dry carbon fiber layers for synthesis of the MRFs using EPD is shown in Figure 9 (although this schematic is for functionalized CNFs, the same process applies for MWCNTs). In order to deposit the MWCNT/CNF, the as-received nanoparticles were functionalized to introduce charges on them and make them more compatible with the resin system. Then, EPD was employed to deposit the charged particles onto the surface of the carbon fiber layers to synthesize the MRFs. These MRFs were used to manufacture MRPCs which will be described and shown in Chapter 4.

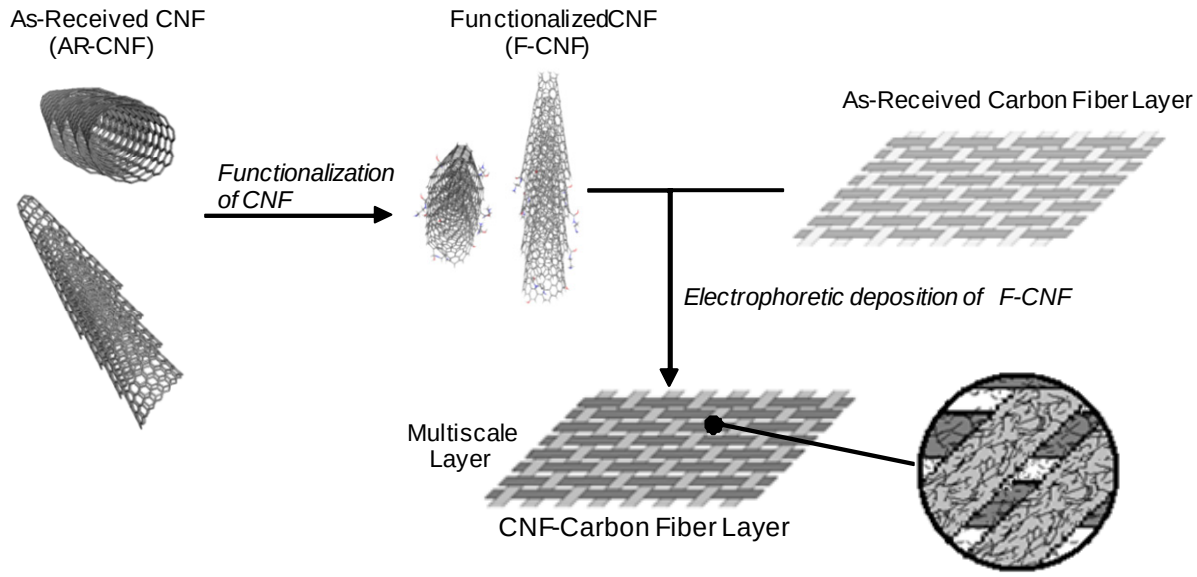

Figure 9. Schematic of manufacturing process of multiscale-reinforcement fabric.

Due to the fact that pristine CNTs/CNFs have low surface charge, the nanoparticles were initially modified by functionalizing the walls with organic groups; this modification allowed for the disruption of the CNFs/CNTs bundles by repulsion forces exerted by the functional groups

and also forced the CNFs/CNTs to travel towards a counter electrode when an electric field was applied.

In this study, two types of functional groups were grafted onto the surface of MWCNTs and CNFs in order to be used to synthesize the MRFs: carboxylic acid and amine. Previous research has shown that CNTs with carboxyl groups can exert enough repulsion energy (zeta potential les than -30mV) to appropriately disperse in water provided that the pH range is between 2 and 10 [135]. This means that, depending on the amount of COOH grafted onto the surface of the CNFs/CNTs, the carboxylated carbon nanoparticles will also have sufficient surface charge to travel towards a positive counter electrode upon application of a DC electric field.

Synthesis of MRFs with carboxylated MWCNTs/CNFs will produce layers in which the nanomaterials can impregnate the fabric. However, carboxylated MWCNTs/CNFs do not provide strong interaction among the nanomaterial, the epoxy-amine polymer matrix system, and the sizing of the carbon fiber. Since bonding is an issue when reinforcing polymer composites using MWCNTs/CNFs, a higher level of reinforcement can be achieved if a functional group compatible with the resin system is used. This can be accomplished by grafting organic groups to the CNTs/CNFs that can have high interaction with the matrix system. For this reason, amine functional group was chosen. A schematic of the functionalization of MWCNTs and CNFs with carboxylic acid and amine functional groups is shown in Figure 10.

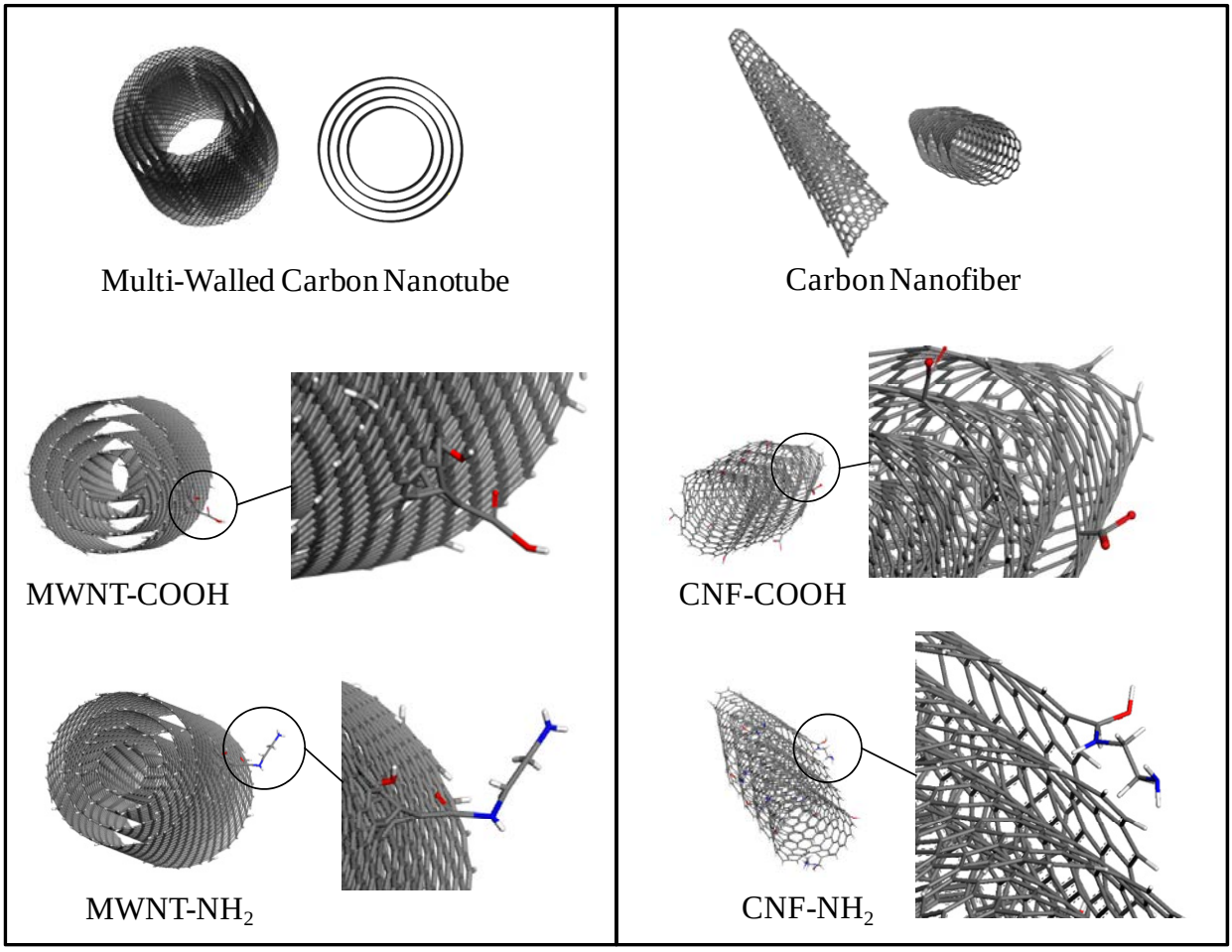

Figure 10. Schematic of functionalization method for multi-walled carbon nanotubes and carbon nanofibers.

In summary, an electrophoretic process to deposit carboxylic acid-functionalized as well as amine-functionalized MWCNTs and CNFs onto the surface of carbon fiber layers using water as the dispersive medium is described and studied. This methodology was used to synthesize MRFs that promote uniform distribution of the nanomaterials on the surface of carbon fiber layers and deposition in hard-to-reach areas such as intra-tow regions. This configuration gives the multiscale layers the potential to enhance the mechanical properties of advanced composites by means of fiber bridging when the hybrid layers are used to manufacture parts. Furthermore,

since water is a more abundant, cost-effective, and environmentally friendly solvent than organic solvents, the process can be scaled-up to fabricate larger parts.

3.2 Experimental Section

3.2.1 Materials

MWCNTs manufactured by chemical vapor deposition were used in this study. They had a diameter of 20–30 nm, length of 10–30 μm, purity of more than 95 wt.%, ash content less than 1.5 wt.%, and electrical conductivity of 10^{-2} S/cm, as provided by the vendor (Cheaptubes Inc.). A TEM image of the as-received MWCNTs is shown in Figure 11 [136].

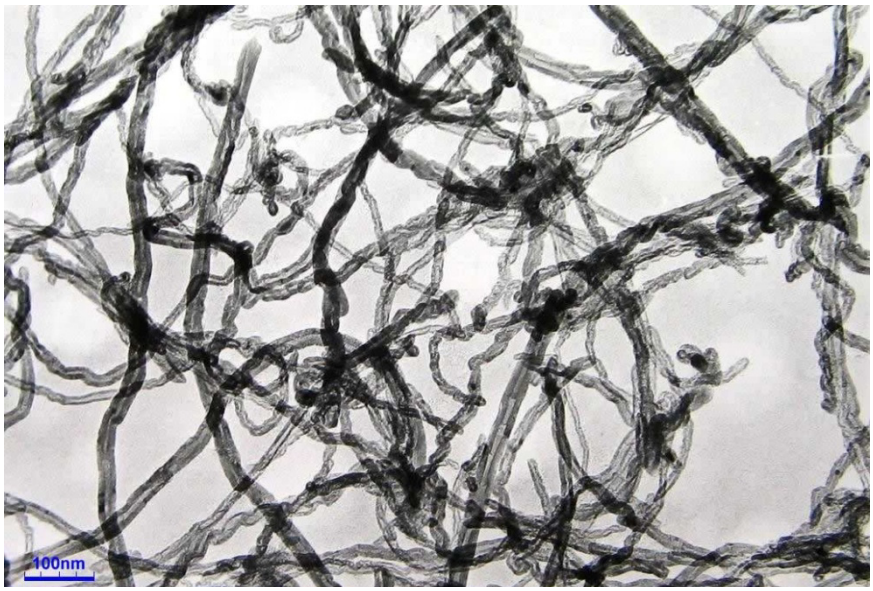

Figure 11. TEM image of as-received MWCNTs [136].

The CNFs used in this study were Pyrograf PR 24-XT-PS (Applied Sciences Inc.) with an average diameter and length in the range of 60–150 nm and 30–100 μm, respectively. The average of the specific surface area of the CNFs is 42 m^2/g, with moisture and iron contents of less than 5% and 14,000 ppm, respectively, as provided by the vendor. SEM images of the as-received CNFs are shown in Figure 12.

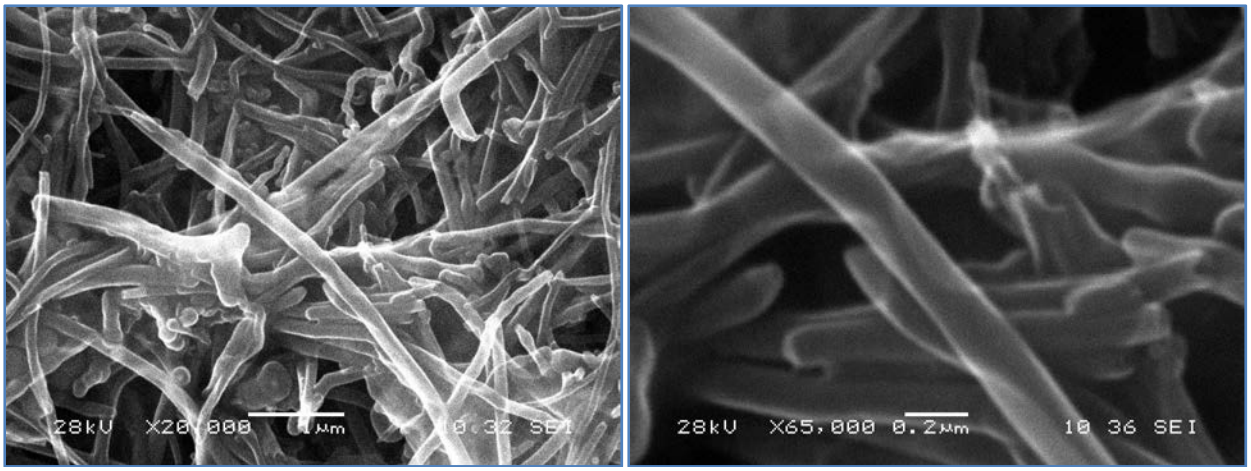

Figure 12. SEM images of as-received CNFs.

Aerospace grade plain woven carbon fiber layers with an epoxy-based sizing were used in this work as the deposition target for MWCNTs/CNFs. These layers were comprised of PAN-based IM7 6K carbon fibers with a nominal diameter of 5.2 μm, density of 1.78 g/cm^3, and tensile strength and modulus of 5.48 GPa and 276 GPa, respectively, also as provided by the vendor. Figure 13 shows optical and SEM images of as-received carbon fiber layers and an individual fiber, respectively. All other chemicals used in this study were obtained from Fisher Scientific and used as-received.

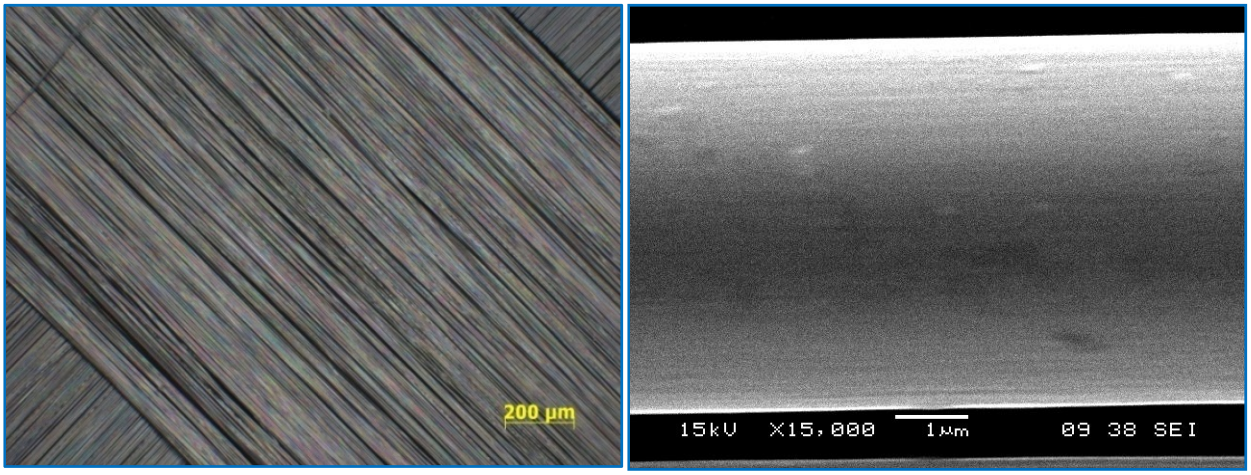

Figure 13. Left: Optical image of as-received carbon fiber layer. Right: SEM image of as-received carbon fiber.

3.2.2 Functionalization of Carbon Nanomaterials

For this study, it was desired that the MWCNTs and CNFs were functionalized to the extent of having charges with the following characteristics: (i) could overcome the attractive van der Waals forces and allow them to form a stable solution in aqueous medium, (ii) could allow the MWCNTs/CNFs to move upon application of a DC electric field when dispersed in water, and (iii) did not modify significantly the structure of the nano-scale materials so that they would be able to attain higher properties. Previous research has reported that acid functionalization shortens the length of MWCNTs [137, 138]. Therefore, the methodology required a balance between refluxing time and temperature to achieve the incorporation of moieties with minimum structural damage to the particles.

3.2.2.1 Multi-Walled Carbon Nanotubes

The methodology to functionalize MWCNTs with carboxylic acid groups consisted of three major steps: (i) purification [139], (ii) air oxidation [22, 139], and (iii) acid oxidation [140]. For the first step, 2 g of MWCNTs were initially mixed with 400 ml of nitric acid (67%–70%) by sonication (150W for 30 min). After sonication, the mixture was refluxed (120.5°C for 120 min), cooled to room temperature, diluted with 1,500 ml of ultrapure water, filtered (with millipore 0.1 μm pore size filter), and washed with ultrapure water until the filtrate was neutral. Then, the MWCNTs were vacuum-dried overnight (100°C) and placed in a desiccator until further use. For the second step, air oxidation, the MWCNTs obtained from the first step were heated to 550°C in air (30 min) to oxidize the nanotubes and eliminate the carbonaceous impurities [22]. After heating, the MWCNTs were allowed to cool to room temperature. For the third step, the MWCNTs obtained from the previous step were mixed with a 3:1 v/v mixture of sulfuric acid (F.W. 98.08) and nitric acid (F.W. 63.012) via sonication (20 min at 105W) and subsequently

refluxed (60°C for 240 min). After refluxing, the mixture was allowed to cool to room temperature, and then filtered and washed until the pH of the filtrate was neutral. The oxidized MWCNTs, herein referred to as O-MWCNTs, were dried in a vacuum oven (60°C) overnight and place in a desiccator until further processing.

Amine group functionalization of MWCNTs was achieved through a two-step process: acylation and amidation. For the acylation step, 5 g of O-MWCNT were mixed with 80 ml of thionyl chloride ($SOCl_2$) and 4 ml of dimethylformamide (DMF) by water bath sonication (80W for 20 min). The mixture was then heated to 65°C for 24 hours to achieve substitution of the hydroxyl group of the carboxylic acid with one of the chlorine atoms of the $SOCl_2$. After substitution, the liquid was distilled, and the remaining MWCNTs were immediately mixed with 100 ml of ethylenediamine and 5 ml of DMF followed by heating and stirring (100°C for 48 hours). The mixture was allowed to cool to room temperature, diluted in ultrapure water, filtered (millipore 0.1 µm pore size), and vacuum-dried overnight (60°C). After drying, the amine-functionalized MWCNTs, herein referred to as A-MWCNTs, were placed in a desiccator until further use. In this study, ethylenediamine was used so that the A-MWCNT could be more soluble in water. Amine-containing molecules with higher carbon contents have a lower solubility in water. The overall functionalization scheme for multi-walled carbon nanotubes is shown in Figure 14.

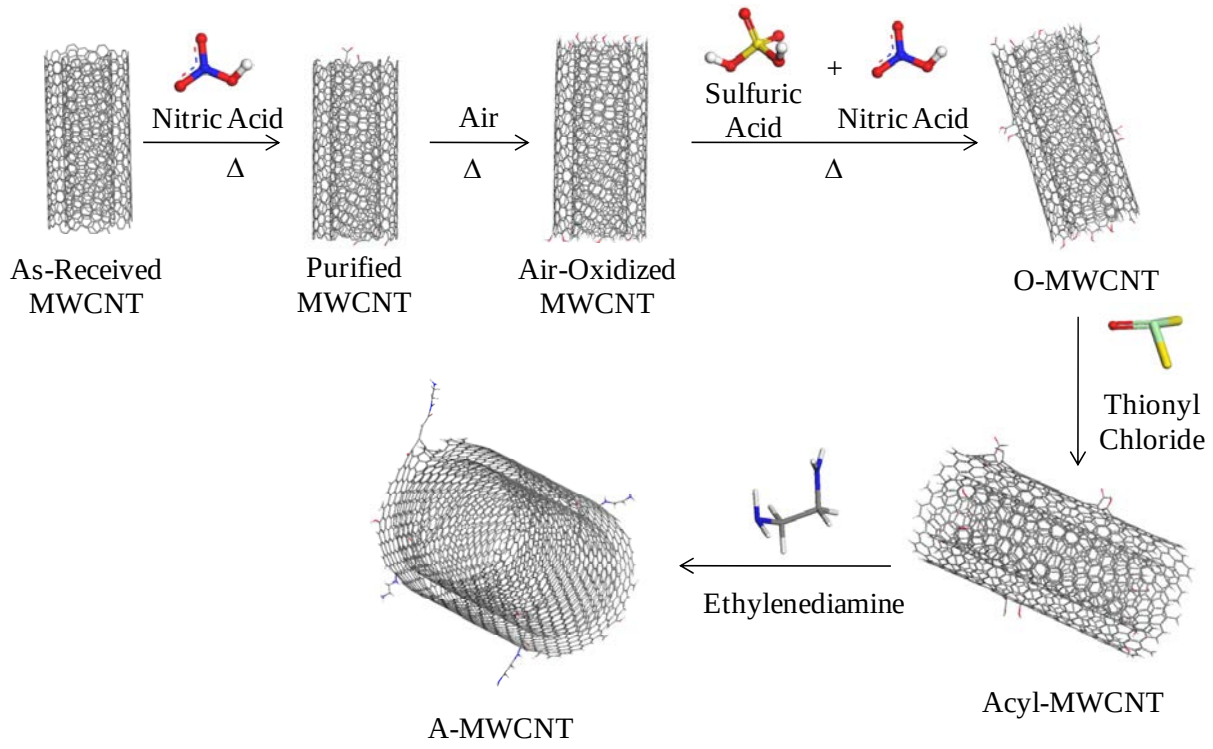

Figure 14. Functionalization scheme for multi-walled carbon nanotubes.

3.2.2.2 Carbon Nanofibers

CNF functionalization with carboxylic acid groups consisted of one major step: acid oxidation. For this purpose, 2.5 g of as-received CNFs (AR-CNFs) were initially mixed with 500 ml of nitric acid (67%–70%) by sonication in a water bath (150W for 20 min) and refluxed (120.5°C for 240 min) in an oil bath. After refluxing, the mixture was carefully diluted in 1,500 ml of ultrapure water, filtered (millipore 0.45 µm pore size filter), and washed until the filtrate was neutral. The oxidized CNFs, herein referred to as O-CNFs, were collected, vacuum-dried overnight (100°C), and placed in a desiccator until further use.

Amidation of CNFs was achieved following the same process as for MWCNTs. In this document, the amidized CNFs will be referred to as A-CNFs. The functionalization scheme for carbon nanofibers is shown in Figure 15.

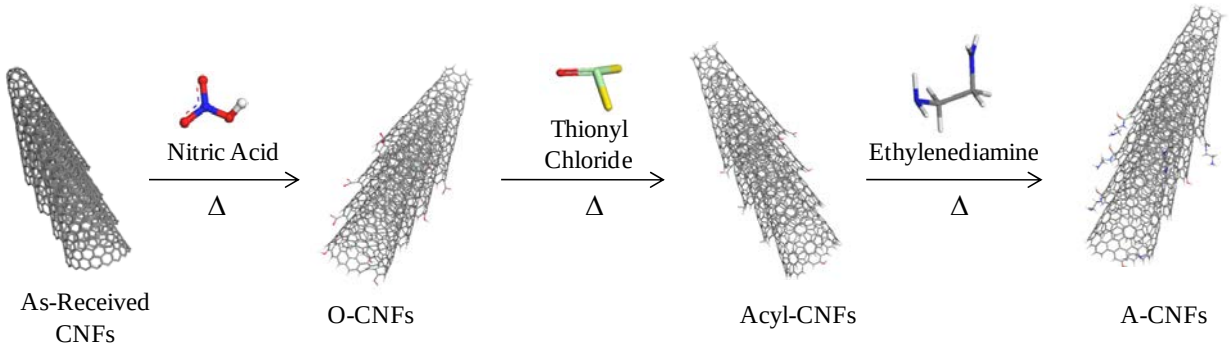

Figure 15. Functionalization scheme for carbon nanofibers.

3.2.3 Electrophoretic Deposition of Functionalized Carbon Nanotubes and Carbon Nanofibers onto Carbon Fiber Layers

3.2.3.1 Experimental Setup

In a typical EPD process, charged particles are mixed with a solvent and poured into an electrophoresis tank. An electric field is then applied between two counter electrodes, and depending on the surface charge of the particle, the particles travel towards the cathode or the anode and are deposited on its surface. For the purpose of synthesizing MRFs as intended herein, the typical EPD setup had to be modified. A schematic of the EPD deposition setup is shown in Figure 16. The most important feature of the EPD setup design is that it had to be able to accommodate a carbon fiber layer in the middle of the tank so that deposition of the functionalized MWCNTs/CNFs would take place onto both sides of the layer. Another important feature of the design is that the field generated by the power supply had to be perpendicular and uniform throughout the carbon fiber layer in order to guarantee constant processing parameters.

To make the EPD experimental setup, an electroblotting system was modified to fit the design requirements. The final configuration of the setup consisted of seven parts: (1) DC power supply, (2) electrophoretic tank (3,800 ml), (3) tank cover with wire leads, (4) cables, (5) counter electrodes, (6) metal frames, and (7) carbon fiber layer. These parts are depicted in Figure 17.

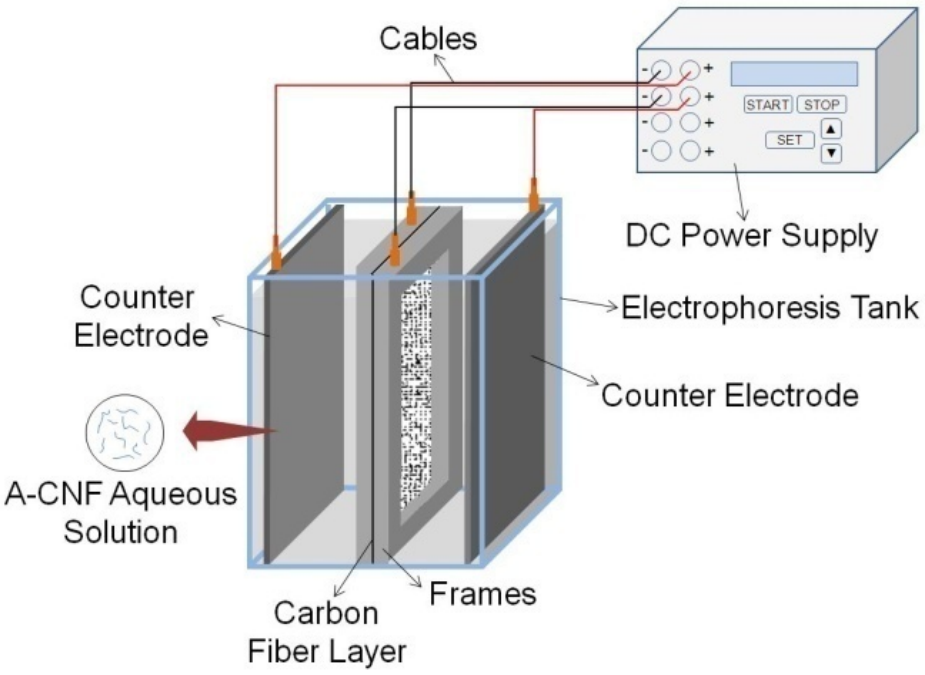

Figure 16. Schematic of designed electrophoretic deposition setup.

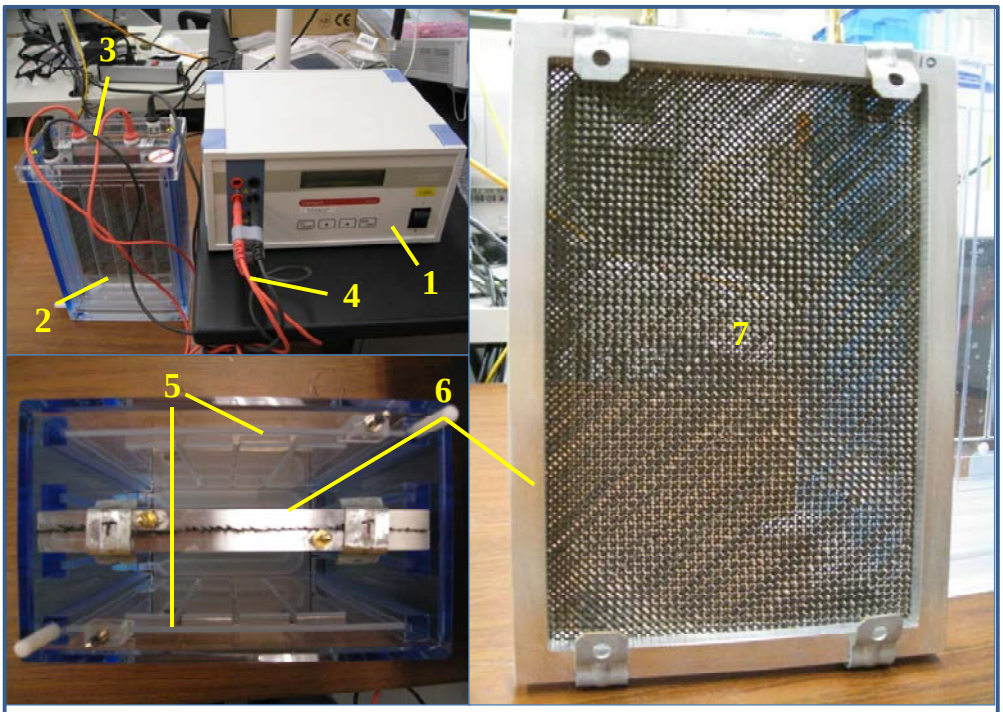

(1) DC Power Supply
(2) Electrophoretic Tank
(3) Tank Cover with Wire Leads
(4) Cables
(5) Counter Electrodes
(6) Metal Frames
(7) Carbon Fiber Layer

Figure 17. Experimental setup for electrophoretic deposition.

3.2.3.2 Electrophoretic Deposition Process

3.2.3.2.1 EPD of Carboxylic Acid-Functionalized MWCNTs/CNFs

For deposition of O-MWCNTs/O-CNFs, 190 mg of the nanoparticles were initially dispersed in 100 ml of water via sonication (150W for 10 min). After sonication, the mixture was transferred to the electrophoretic tank and mixed by mechanical stirring with 3,700 ml of water already contained in the tank. This amount of nanomaterials in the water resulted in a MWCNT/CNF concentration of 0.05 mg/ml. At this point, the pH and electrical conductivity of the solution was measured to assure proper conditions for the EPD process (i.e., low electrical conductivity of the solution and high electrophoretic mobility of the particles [141]). Then, a 25 x 17 cm^2 epoxy-sized carbon fiber layer was clamped between two metal frames and inserted in the middle of the tank halfway between the metal counter electrodes, as depicted in Figure 16. After securing the tank cover of the EPD tank and connecting all cables to the electrodes and power supply, a 30V electric potential was applied for 30 minutes between the metal counter electrodes (negative) and the frame connected to the carbon fiber layer (positive). Separation between the counter electrodes and the carbon fiber layer was 4.5 cm. This combination of deposition time and electric field were chosen since a higher electric field and longer deposition time lead to stiffening of the carbon fiber layer. After 30 minutes of deposition, the electric field was stopped and the carbon fiber layers and metal frames were removed from the tank and dried in vacuum (60°C for 30 min).

3.2.3.2.2 EPD of Amine-Functionalized MWCNTs/CNFs

For EPD of the A-MWCNT/A-CNF, a similar process to that of O-MWCNT/O-CNF was followed. For this deposition process, 190 mg of A-MWCNT/A-CNF were mixed via sonication with 100 ml of ultrapure water (150W for 20 min). Then, the mixture was added to the

electrophoretic deposition tank containing 3,700 ml of ultrapure water and mixed by mechanical stirring. At this point, the pH and the electrical conductivity of the solution were measured. The carbon fiber layer was then clamped between the metal frames and inserted in the middle of the tank halfway between the metal counter electrodes. The EPD tank was covered, and all cables were connected to the power supply and the electrodes of the system. In the first stage of this deposition process, a 30V DC electric potential was applied by connecting the positive pole to the carbon fiber layer and the negative pole to the metal counter electrodes. This electric field was kept for 40 minutes. In the second stage, the polarity of the DC electric field was inverted and the same potential was applied for another 40 minutes so that the A-MWCNT/A-CNF would travel towards the carbon fiber layer. Once the second stage was completed, the resulting MRF was removed from the EPD tank and vacuum-dried (45°C for 30 min).

3.2.4 Characterization Methods

3.2.4.1 Nanomaterial Characterization

Characterization of MWCNTs and CNFs was performed using the following methods: Fourier-transform infrared spectrometry (FTIR), thermo-gravimetric analysis (TGA), X-ray photoelectron spectroscopy (XPS), and laser Doppler velocimetry.

FTIR spectra were obtained using an attenuated total reflection (ATR) accessory. Typical samples used for FTIR characterization consisted of approximately 5 mg of nanomaterial which were compressed between the ATR tower and a Germanium crystal to obtain the spectra. IR spectra were collected from 400 cm^{-1} to 3,600 cm^{-1}.

Further characterization of functionalized MWCNTs/CNFs was performed through TGA. To prepare the samples, approximately 3.5 mg of MWCNTs/CNFs were weighed and placed inside a high-temperature platinum pan and then inserted into the TGA instrument furnace. Tests

were carried out in nitrogen atmosphere from 25°C to 600°C following a temperature ramp rate of 10°C/min.

XPS was also used to characterize the surface of functionalized-MWCNTs/CNFs. Samples were measured at a 90 degree take-off-angle, which yields a sample depth of ~10 nm. The analysis area was ~500 µm in diameter. Studies were performed with a monochromatic Al k· x-ray source powered at 15 kV and 15 mA. Charge neutralization of the sample surface was achieved with the use of a low-energy electron flood gun. Energy scales of the spectra were referenced to the C 1s C-C/C-H signal at 284.5 eV. High-energy resolution (hi-res) XPS analyses of the C 1s , N 1s, and O 1s regions were also performed on the samples. XPS hi-res analysis provides information on the bonding state of the element in question. In order to obtain information about the species, the hi-res data curve was fitted as follows. The background was an integrated Shirley with the pass energy for the hi-res data acquisition of 40 eV (as compared to 160 eV for the survey data). The line shape used for the fitting was a convolution of 30% Lorentzian with Gaussian (Voigt-type convolution), and a Marquardt-Levenberg least-squares algorithm was used to determine the best fit of the peaks placed under the curve given the constraints imposed. Line widths used were in the range of 0.85 eV to 1.5 eV.

O-MWCNTs/O-CNFs and A-MWCNTs/A-CNFs were also characterized using laser Doppler velocimetry coupled with phase analysis to obtain electrophoretic mobility (EM) values. The purpose of measuring EM is to determine the charge and speed of the nanoparticles in an aqueous medium when subjected to a DC electric field. Higher EM will result in faster deposition time, which in turn shortens the processing time. It also gives a comparative measurement of the surface charge of all different types of particles used in this study. For sample preparation, 5 mg of the nanoparticles were mixed with 100 ml of ultrapure water via

water bath sonication (150W for 10 min). After sonication, the samples were injected into a capillary cell and at least 10 EM measurements were made for each sample. Electrophoretic mobility of the nanoparticles was measured from pH 2 to 10 to capture the effect of ionization of functional groups grafted on the wall of the MWCNTs/CNFs on the speed of the particles. The pH of the aqueous samples was adjusted to the desired values using 6N NaOH or 6N HCl solutions. Note that for this study, the salt concentration was kept to a minimum to avoid high ionic electrical conductivity in the system, which is a prerequisite for effective EPD of particles [141]. The average values and the standard deviation for the EM values was computed and reported as a function of pH.

3.2.4.2 Multiscale-Reinforcement Fabric

3.2.4.2.1 Qualitative Dispersion

Dispersion of the functionalized MWCNTs/CNFs on the surface of the carbon fiber layers was qualitatively characterized through SEM and optical microscopy (OM). SEM was used for characterization of as-received carbon fiber layers and MRFs containing both MWCNTs and CNFs, while OM was only utilized to characterize as-received and CNF-deposited MRFs.

3.2.4.2.2 Quantitative Characterization of Deposition through Light Absorption

One of the most important parameters in EPD of MWCNTs/CNFs on any type of surface is to quantify the amount of material deposited after the process has been completed. Since scanning electron and optical microscopy can only be used to qualitatively characterize the deposition of MWNT/CNF, another method that can quantitatively estimate the deposition must be employed. From experiments performed in the laboratory, it was observed that light transmission through the dispersive medium changed as a function of time during the EPD process. At the beginning of the process, just after mixing the MWCNTs/CNFs with the

ultrapure water, the aqueous solution in the electrophoretic tank was extremely dark and opaque. Conversely, after the EPD process ended, the aqueous solution became more translucent, and light could clearly pass through the solution. Based on this observation, it was envisioned that by measuring the amount of light through the aqueous samples, the concentration of the nanoparticles in the aqueous media could be estimated. For this task, using light transmission, the deposition of functionalized MWCNTs/CNFs was estimated by determining the concentration of the nanoparticles in the aqueous solution in the electrophoresis tank before and after EPD. By subtracting the final concentration of MWCNT/CNF in the aqueous solution from the initial known concentration and multiplying it by the volume of water, the amount of nanomaterial on the surface of the carbon fiber layer could be estimated. Equation 1 shows this relation as,

$$p_f = (c_i - c_f)V_t \tag{1}$$

where p_f represents the amount of nanomaterial deposited on the surface of the carbon fiber layer, c_i and c_f are the initial and final concentrations of MWCNTs/CNFs in the tank, and V_f is the volume of the water contained in the electrophoresis tank.

For determining the initial and final concentrations of MWCNTs/CNFs, the following procedure was employed. First, the absorbance spectra of different known concentrations of MWCNTs/CNFs in aqueous media were obtained using an ultraviolet-visible spectrometry instrument. Then, using the data obtained, a linear correlation between the absorbance and the known MWCNT/CNF concentrations was determined for three different wavelengths: 400 nm, 500 nm, and 600 nm. From these three calibration curves, the curve with the best linear fit (as determined by the R^2 values) was selected as the reference curve. To obtain the concentration of MWCNTs/CNFs in the aqueous medium after EPD, the absorbance of a sample taken from the

tank was determined in the same manner as for the absorbance values of the calibration curve. Then, the equation obtained using the linear regression fit was used to estimate the concentration of MWCNTs/CNFs in aqueous medium after EPD. With this concentration value and using equation 1, the amount of nanomaterial deposited on the surface of the carbon fiber layer was estimated.

3.3 Results and Discussion

3.3.1 Characterization of Functionalized Carbon Nanotubes and Carbon Nanofibers

3.3.1.1 Fourier-Transform Infrared Spectrometry

In order to confirm functionalization of the MWCNTs with carboxylic acid and amine functional groups, IR spectra for as-received MWCNTs (AR-MWCNTs), oxidized-MWCNTs (O-MWCNTs), and amidized-MWCNTs (A-MWCNTs) were obtained (Figure 18). Spectrum (a) of Figure 18, AR-MWCNT, shows a featureless plot characteristic of MWCNT with no organic groups grafted on its surface. Conversely, plots (b) and (c) corresponding to O-MWCNTs and A-MWCNTs, respectively, show peaks that confirm carboxylic acid and amine functionalization of the nanoparticles, respectively. Carboxylic acid functionalization is confirmed by the presence of peaks at ~1,738 cm^{-1}, ~1,216 cm^{-1}, and ~3,000 cm^{-1}, corresponding to the vibration frequencies of C=O, C-O, and O-H bonded to the COOH group, respectively [142, 143]. Spectrum (c), corresponding to A-MWCNT, confirms the presence of amine with a peak at ~3,294 cm^{-1} assigned to the presence of N-H of the amine group, and a shift in the peak of the C=O of the carboxylic acid to ~1,649 cm^{-1}, which confirms the presence of the carbonyl group of the amide linkage [144]. The reduction of the intensity of the peak at ~1,216 cm^{-1} going from O-MWCNT to A-MWNCT is attributed to the substitution of the C-O bond with the C-N bond of the amide group [145].

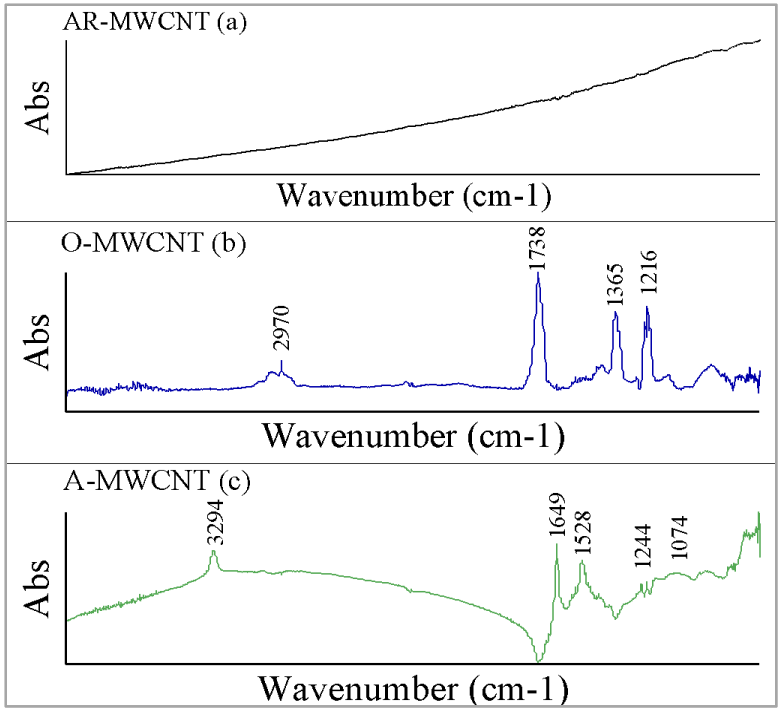

Figure 18. FTIR spectra of (a) as-received (AR-MWCNT), (b) oxidized- (O-MWCNT), and (c) amidized- (A-MWCNT) multi-walled carbon nanotubes.

FTIR spectra of AR-CNFs, O-CNFs, and A-CNFs were also obtained to assure CNF functionalization (see Figure 19). As for the case of AR-MWCNTs, the AR-CNFs spectrum shows no peaks, which is also characteristic of this type of pristine nanoparticle. In contrast, spectrum (b) confirms the presence of carboxylic acid groups on the surface of CNFs with peaks at ~1,738 cm^{-1}, ~1,216 cm^{-1}, and ~3,000 cm^{-1}, corresponding to the vibration frequencies of C=O, C-O, and O-H of the COOH, respectively. Spectrum (c) verifies the presence of amine functional groups on the surface of CNF by showing a peak centered at ~3,257 cm^{-1} assigned to the presence of amine. The peak at 1,659 cm^{-1} suggests the presence of the carbonyl group of the amide linkage that appears as a result of a shift from the peak at 1,738 cm^{-1} (carbonyl group of the carboxylic acid) after substitution of the hydroxyl group by the amine group. In addition, the reduction of the peak at 1,216 cm^{-1} suggests the substitution of the C-O bond of the carboxylic acid by the C-N bond of the amide linkage.

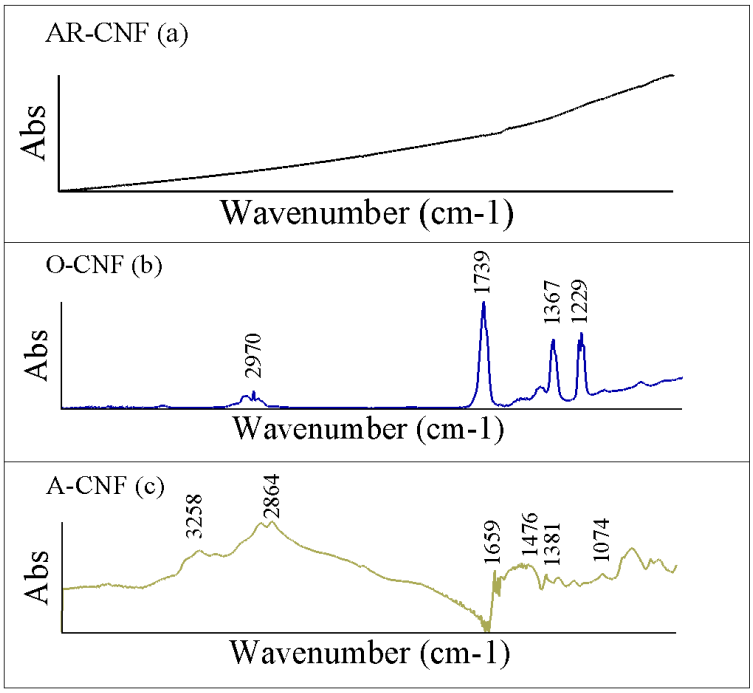

Figure 19. FTIR spectra of (a) as-received (AR-CNF), (b) oxidized- (O-CNF), and (c) amidized- (A-CNF) carbon nanofibers.

3.3.1.2 Thermo-Gravimetric Analysis

Confirmation of functionalization of MWCNTs and CNFs with carboxylic acid and amine functional groups can also be inferred from TGA analyses. This analysis shows that AR-MWCNT and AR-CNF had a negligible weight loss from room temperature to 600°C, which is characteristic of untreated carbon nanoparticles. On the contrary, O-MWCNTs/O-CNFs and A-MWCNTs/CNFs showed a significant decrease in weight for the same temperature range. These plots can be seen in Figure 20 for MWCNTs and Figure 21 for CNFs. The initial weight loss between room temperature to ~100°C for both types of functionalized nanoparticles is attributed to evaporation of water absorbed on the surface of the particles. An inflection point at around 200°C is seen for both O-MWCNTs and A-MWCNTs with a total weight loss of approximately 8.26% and 10.02% between the temperatures of 100°C and 400°C, respectively, which has been associated with the loss of carboxylic acid groups [146]. These results confirm that since the A-

MWNCTs have higher molecular weight groups attached to their surfaces than O-MWCNTs, A-MWCNTs would lose more weight when being decomposed and the organic groups are depleted from the MWCNT wall upon heating [26]. TGA plots for AR-CNFs, O-CNFs, and A-CNFs show a similar trend as for MWCNTs. The AR-CNFs show no significant weight loss for the entire temperature range while O-CNFs and A-CNFs show evidence of functionalization with a total weight loss of 3.64% and 5.43%, respectively, for the temperature range between 100°C and 400°C.

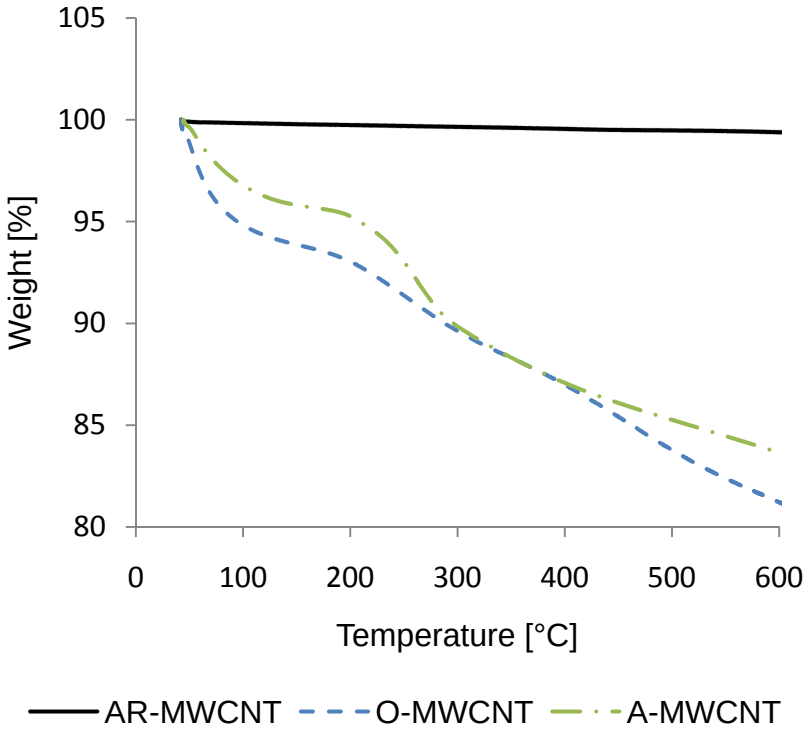

Figure 20. TGA plots for as-received (AR-MWCNT), oxidized- (O-MWCNT), and amidized- (A-MWCNT) multi-walled carbon nanotubes.

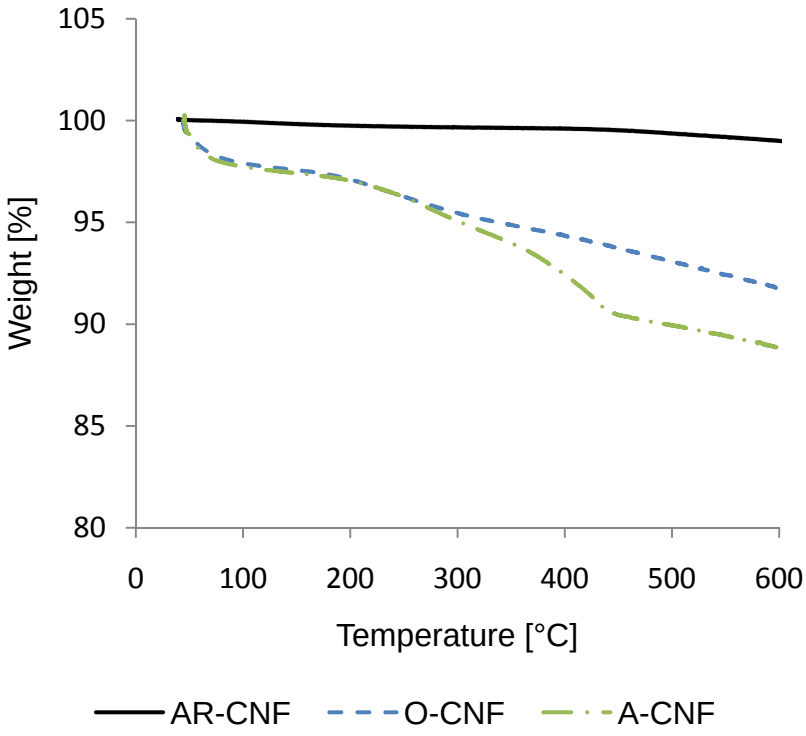

Figure 21. TGA plots for as-received (AR-CNF), oxidized- (O-CNF), and amidized- (A-CNF) carbon nanofibers.

3.3.1.3 X-Ray Photoelectron Spectroscopy

3.3.1.3.1 Functionalized Multi-Walled Carbon Nanotubes

Elemental analysis tests were performed for functionalized MWCNTs. Elemental survey results show that O-MWCNTs have a carbon and oxygen surface content of 85 and 15 atom%, respectively, with a small trace of nitrogen and silicon (less than 0.2 atom%). The elemental composition of the O-MWCNT is shown in Figure 22 and Table 2. To obtain more information regarding the bonding state, high-energy resolution (hi-res) analysis was also performed for the C 1s and O 1s regions. From the carbon hi-res analysis, it can be observed that the O-C=C represents approximately 5.3 atom% of the surface, whereas the C-C and C-H represents 54.9 atom% (Table 3). The rest is attributed to other types of oxygen functionalities such as carbonyl, ether, and hydroxyl groups. Hi-res of the O 1s region also revealed that the O-C and O=C

represented 50.5 and 49.5 atom%, respectively (Table 4). These results show that the surface chemistry of functionalized MWCNTs is complex with different types of oxygen groups interacting. This results in an increase in the surface energy of the carbon nanomaterial, which is one of the main goals of surface functionalization.

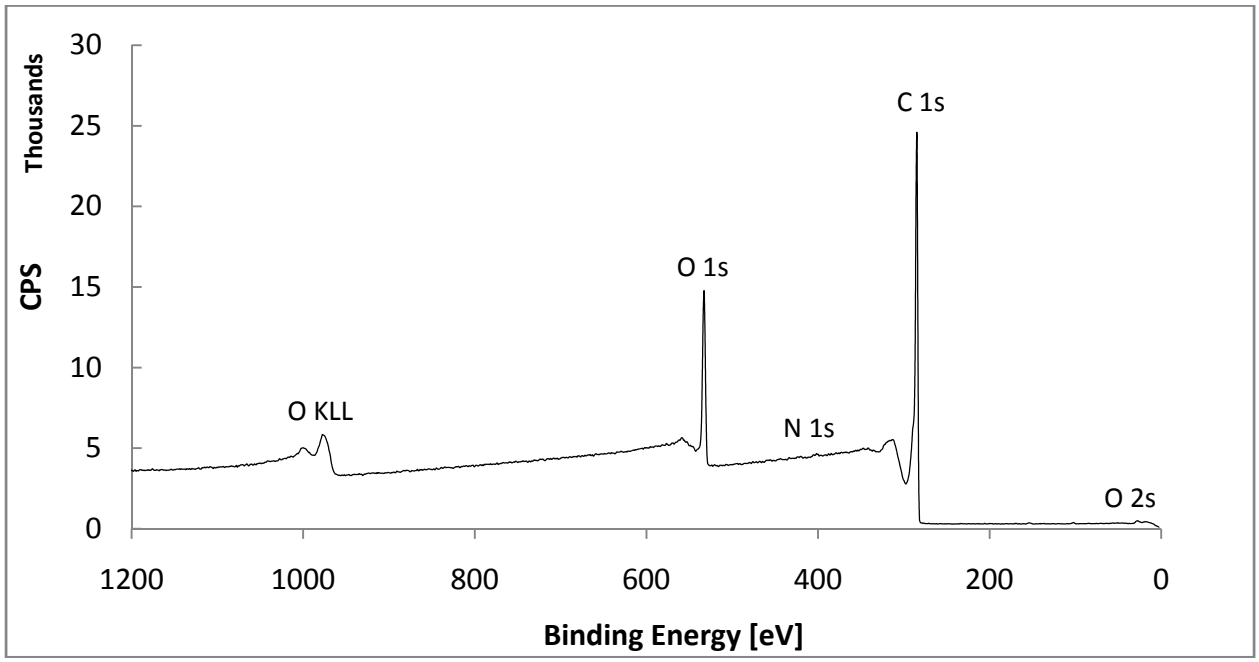

Figure 22. XPS elemental survey of oxidized-MWCNTs.

TABLE 2

RELATIVE ELEMENTAL COMPOSITION OF O-MWCNT AS DETERMINED BY XPS

Name	Position	Area	At%
C 1s	284.7	10570.9	84.9
N 1s	401.7	43.7	0.2
O 1s	532.7	5143.1	14.7
Si 2p	102.7	31.7	0.2

Surface chemistry characterization was also performed for A-MWCNTs. Elemental analysis shows a carbon, oxygen, and nitrogen content of 83.4, 8.7, and 6.9 atom%, respectively, with some traces of S, Si, and Cl (Figure 23 and Table 3). Sulfur and chlorine contents are attributed to residuals of thionyl chloride from the amidation process. A comparison of the O-

MWCNT and A-MWCNT elemental surveys shows that carbon content stays at ~84 atom%, oxygen relative content decreases from 14.7 to 8.7 atom%, and nitrogen increases from 0.2 to 6.9 atom%. Reduction in the oxygen content is attributed to the substitution of the OH group of the carboxylic acid with the ethylenediamine, which is also in agreement with the increase in nitrogen content. Hi-res analyses of the carbon, oxygen, and nitrogen peaks (Appendix A) show a reduction in carboxyl species due to amidation, which is in agreement with the reduction in C-O; also, all nitrogen species are either amine or amide and no other nitrogen groups are left after amidation of MWCNTs (Table 5 and Table 6).

TABLE 3

RELATIVE ELEMENTAL COMPOSITION OF A-MWCNT AS DETERMINED BY XPS

Name	Position	Area	Atom%
C 1s	285.0	9931.7	83.4
N 1s	400.0	1413.3	6.9
O 1s	532.0	2898.0	8.7
Si 2p	169.0	9.6	0.1
S 2p	169.0	239.4	0.8
Cl 2p	201.0	19.9	0.1

TABLE 4

RELATIVE COMPOSITION AND PEAK ASSIGNMENT FOR CARBON SPECIES FOR O-MWCNT AND A-MWCNT, C 1S REGION

Peak Assignment	O-MWCNT [Atom %]	A-MWCNT [Atom %]
C-C, C-H	54.6	59.2
C-O, C-N	31.2	16.5
C=O	8.9	19.0
O-C=O/*N-C=O	5.3	*5.3

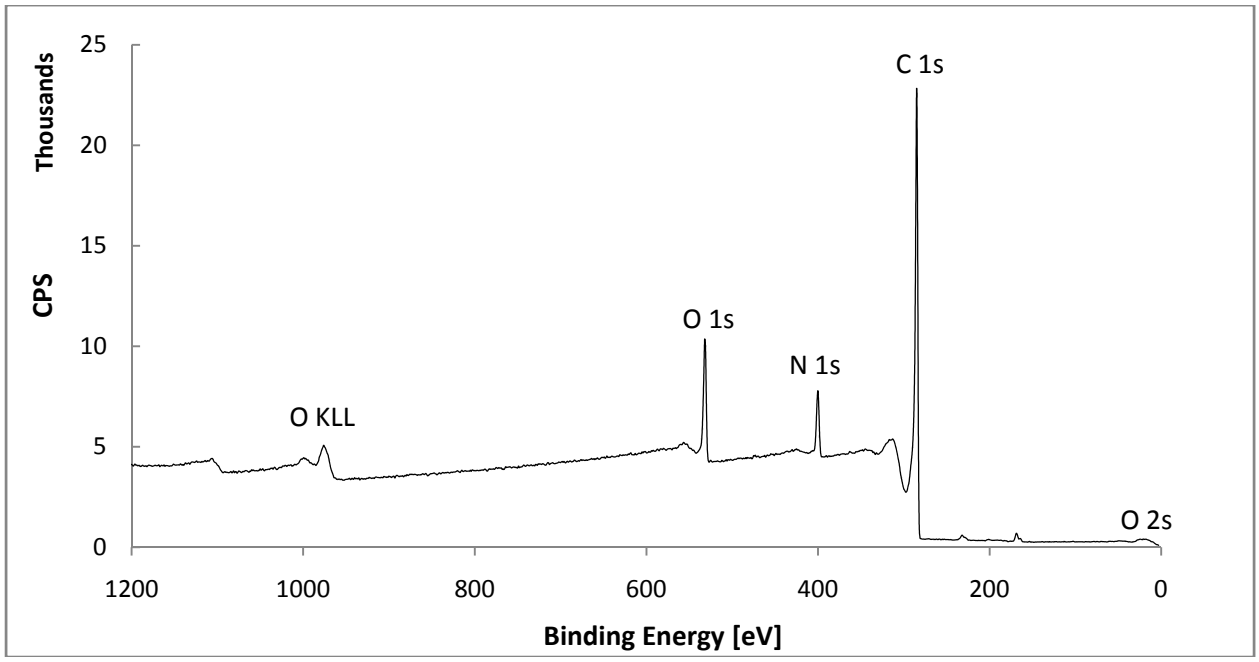

Figure 23. XPS elemental survey of amidized-MWCNTs.

TABLE 5

RELATIVE COMPOSITION AND PEAK ASSIGNMENT FOR NITROGEN SPECIES FOR O-MWCNT AND A-MWCNT, N 1S REGION

Peak Assignment	O-MWCNT [Atom %]	A-MWCNT [Atom %]
Amine, Amide	-	100
Nitrite	-	0

TABLE 6

RELATIVE COMPOSITION AND PEAK ASSIGNMENT FOR OXYGEN SPECIES FOR O-MWCNT AND A-MWCNT, O 1S REGION

Peak Assignment	O-CNF [Atom %]	A-CNF [Atom %]
O=C	50.5	77.7
O-C	49.5	22.3

3.3.1.3.2 Functionalized Carbon Nanofibers

Elemental analysis was also performed on functionalized CNFs, and results are shown in Figure 24. XPS results confirm functionalization of O-CNFs with carbon, oxygen, and nitrogen contents of 82.6, 16.5, and 1.0 atom%, respectively, as shown in Table 7. From high-energy

resolution XPS analyses of the C 1s , N 1s, and O 1s regions, it is noticeable that the O-C=O species represented 8.4 atom% with respect to the overall count (Table 8). Another important observation is that, as in the case of O-MWCNTs, O-CNFs also have other oxygen species such as carbonyl, ethers, and hydroxyl groups (see Table 9). Hi-res analysis of the O 1s region shows that O=C and O-C species have a relative elemental composition of 54 and 46 atom%, respectively, which contributes to the surface charge and in turn the electrophoretic mobility of the particles upon application of a DC electric field in aqueous media. Hi-res data of the N 1s region reveals that the presence of nitrogen is due to nitrites and amine/amides, which are attributed to side products in the oxidation of CNFs, as shown in Table 10 and Table 11.

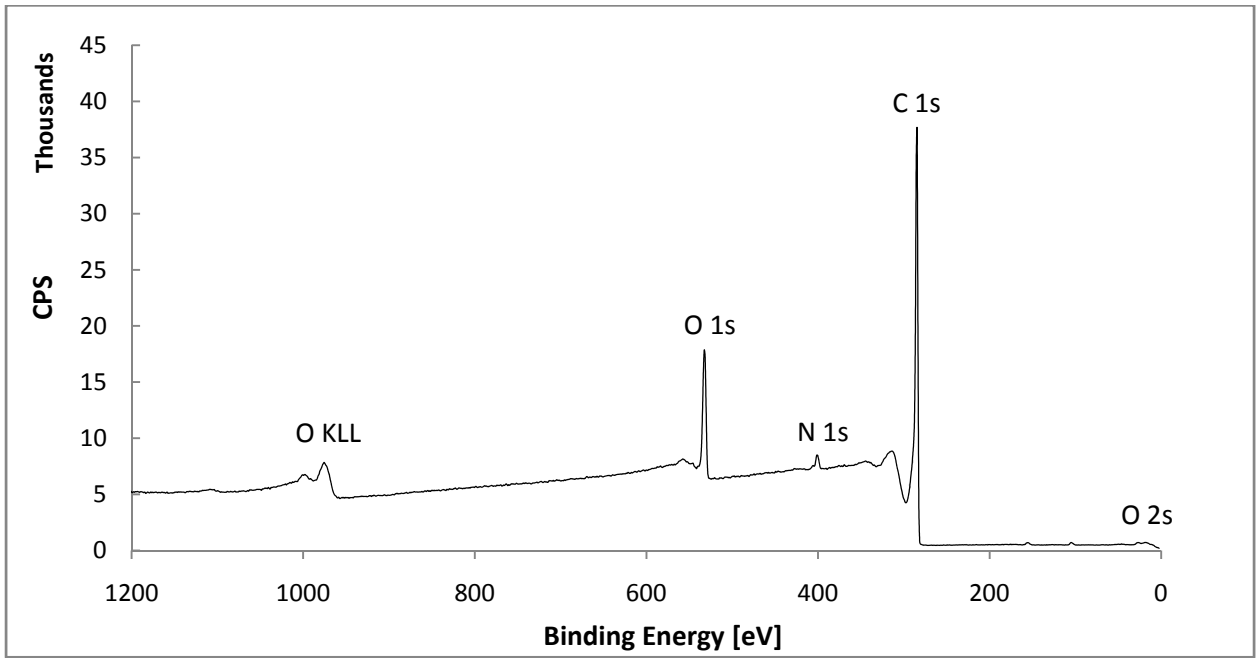

Figure 24. XPS elemental survey of oxidized-CNFs.

TABLE 7

RELATIVE ELEMENTAL COMPOSITION OF O-CNF AS DETERMINED BY XPS

Name	Position	Area	Atom%
C 1s	285.2	11561.8	82.6
N 1s	406.2	230.7	1.0
O 1s	532.2	6469.2	16.5

TABLE 8

RELATIVE ELEMENTAL COMPOSITION OF A-CNF AS DETERMINED BY XPS

Name	Position	Area	At%
C 1s	285.2	11561.8	83.8
N 1s	400.0	2189.8	8.8
O 1s	532.2	3371.7	7.7
S 2p	168.0	101.4	0.3
Cl 2p	202.0	32.8	0.1

Results for XPS elemental analysis characterization of A-CNFs are shown in Figure 25. It is clear that amidation resulted in an increase in nitrogen content as compared to carbon and oxygen. In this sample, carbon, oxygen, and nitrogen content corresponded to 83.8, 7.7, and 8.8 atom%, with some sulfur and chlorine elements, 0.3 and 0.1 atom%, attributed to residuals of thionyl chloride from the amidation process (Table 8). Comparing the O-CNF and A-CNF elemental surveys, it is observed that the relative oxygen content decreases from 16.5 to 8.8 atom% and nitrogen increases from 1.0 to 8.8 atom%. Reduction in the oxygen atom is due to the substitution of the carboxylic acid OH with the ethylenediamine which is also in agreement with the increase in the nitrogen content. Hi-res analyses of the carbon, oxygen, and nitrogen peaks (Appendix A) show a reduction in carboxyl species due to amidation which is in agreement with the reduction in C-O from 49.2 to 22.3 atom%. Further information regarding the XPS analyses can be found in Appendix A.

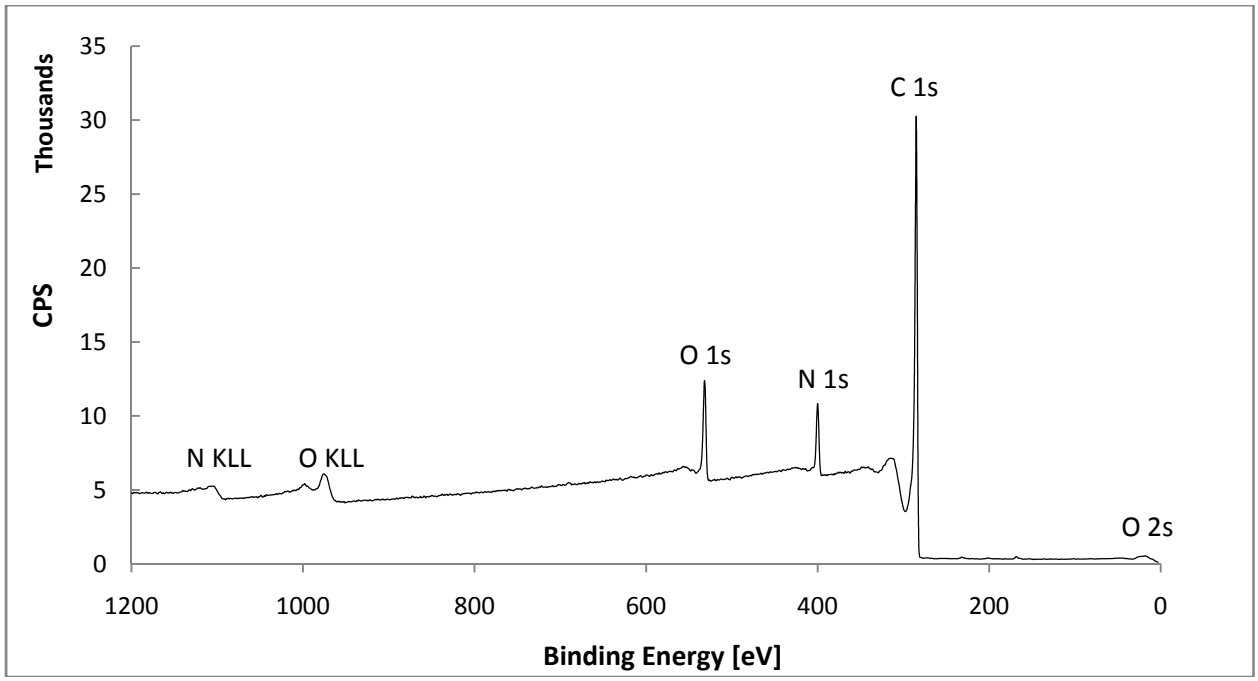

Figure 25. XPS elemental survey of amidized-CNFs.

TABLE 9

RELATIVE COMPOSITION AND PEAK ASSIGNMENT FOR CARBON SPECIES FOR O-CNF AND A-CNF, C 1S REGION

Peak Assignment	O-CNF [Atom %]	A-CNF [Atom %]
C-C, C-H	61.0	53.0
C-O, C-N	24.0	25.0
C=O	5.9	16.0
O-C=O/*N-O=O	8.4	*6.2

TABLE 10

RELATIVE COMPOSITION AND PEAK ASSIGNMENT FOR NITROGEN SPECIES FOR O-CNF AND A-CNF, O 1S REGION

Peak Assignment	O-CNF [Atom %]	A-CNF [Atom %]
Amine, Amide	58	100
Nitrite	42	0

TABLE 11

RELATIVE COMPOSITION AND PEAK ASSIGNMENT FOR OXYGEN SPECIES FOR O-CNF AND A-CNF, O 1S REGION

Peak Assignment	O-CNF [Atom %]	A-CNF [Atom %]
O=C	53.6	77.1
O-C	46.4	22.9

3.3.1.4 Laser Doppler Velocimetry

3.3.1.4.1 Carboxylic Acid-Functionalized Multi-Walled Carbon Nanotubes and Carbon Nanofibers

Electrophoretic mobility values of O-MWCNTs and O-CNFs reveal that these particles are negatively charged in water for the entire pH range studied. EM plots of O-MWCNTs and O-CNFs are shown in Figure 26. A common behavior for both of these is that, for pH values between approximately 2 and 6, the absolute values of the EM increase linearly. This increase in negative charge of the particles leads to higher mobility, which is mainly due to ionization of the carboxylic acid groups ($CNF\text{-}COOH + OH^- \rightarrow CNF\text{-}COO^- + H_2O$) [147]. Higher EM values indicate that the O-MWCNTs/O-CNFs can move faster during EPD, which in turn reduces the deposition time. For pH values above 6, the absolute values of EM stay stable until pH of 10. This indicates that at pH 6, most carboxylic acid groups have already been ionized; therefore, no change in the charge of the particle was attained.

Comparing the EM values of O-MWCNTs and O-CNFs it can be seen that there is a difference of about 1 μm·cm/(V·s) for the entire range of the values studied. This represents about 20% for the high pH range and about 50% for the low pH range. The difference in values may be due O-CNFs having more oxygen-containing groups attached to their surface than O-MWCNTs, as shown by XPS analyses. This is in agreement with the CNFs having more open

walls than MWCNTs; thus, more functional groups can be grafted onto their surface, which results in more negative charges on the surface of the particles.

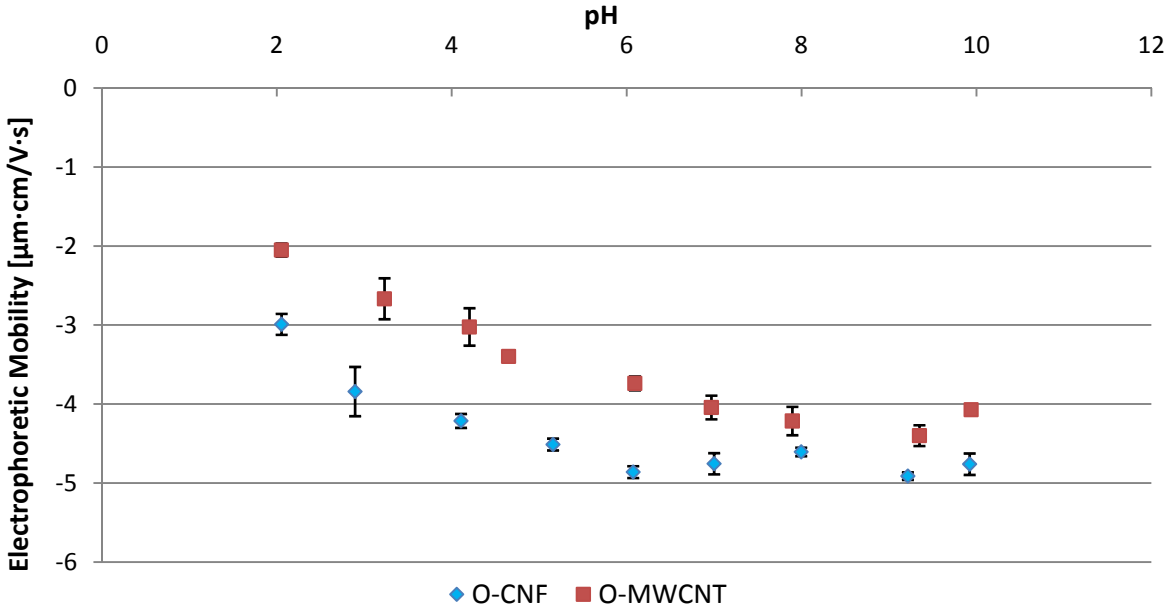

Figure 26. Electrophoretic mobility of O-MWCNTs and O-CNFs as a function of pH. Error bars indicate one standard deviation.

In terms of EPD of O-MWCNTs and O-CNFs, two observations regarding the EM values can be made. The first is that, as mentioned before, the particles are negative for the entire pH range regardless of the pH of the solution. Therefore, upon application of a DC electric field, the particles will always move towards the positive electrode. The second observation is drawn from the stability of the suspension. Although Smoluchowski's theory is strictly valid for evaluating the zeta (ζ) potential of spherical particles, other authors have proposed this theory to estimate the ζ potential of rod-like particles (such as carbon nanotubes) to study the stability of the system in aqueous medium [121, 147]. Assuming that this theory holds for high-aspect-ratio particles, the equation used to calculate the ζ potential is

$$\mu = \frac{\xi \varepsilon \varepsilon_o}{\eta} \qquad (2)$$

where μ is the electrophoretic mobility, ε is the dielectric constant of the liquid, ε_o is the permittivity of the free space (vacuum permittivity), and η is the viscosity of the medium. Using equation 2 to calculate the ζ potential from the EM values plotted in Figure 26, it is found that the lowest absolute values for O-MWCNTs and O-CNFs are -26.16 mV and -38.15 mV, respectively. As a reference value, the limits between stable and non-stable system for spherical particles (particle aggregation) has been established to be a ζ potential of ±30 mV. This indicates that, for the case of O-MWCNTs, the stability of the system can only be obtained above a pH of ~3, which gives a ζ potential of approximately -30 mV. On the other hand, the O-CNFs are stable in aqueous media for the entire pH range studied since the lowest absolute value of the ζ potential is 38.15 at a pH of 2.054.

3.3.1.4.2 Amine-Functionalized Multi-Walled Carbon Nanotubes and Carbon Nanofibers

EM values of amine-functionalized MWCNTs and CNFs at various pH are shown in Figure 27. Also included for comparison are EM values of O-MWCNTs and O-CNFs. The graph shows a strong dependency of EM with respect to the pH values of the solution: A-MWCNTs/A-CNFs are positive at low pH and negative at high pH with an isoelectric point estimated at pH 8.1. This behavior contrasts with that of O-MWCNTs/O-CNFs, where the EM values for the pH range studied are always negative. This could be due to the fact that amines can act as a base depending on the pH of the medium. It is hypothesized that at lower pH (i.e., water + HCl), ionization of the primary amine leads to the formation of cations in water (CNF-$CONHCH_2CH_2NH_2 + H^+ \rightarrow$ CNF-$CONHCH_2CH_2NH_3^+$), while at higher pH (water + NaOH), the amine group leads to the negative charge of the particles in an aqueous medium. These results are essential in determining the polarity of the electric field that has to be applied to the solution in the electrophoresis tank so that the A-MWCNTs/A-CNFs move in the desired

direction. Since the experiments reported were carried out using a solution of pH ~6, the A-MWCNTs/A-CNFs always moved towards the negative electrode (cathode).

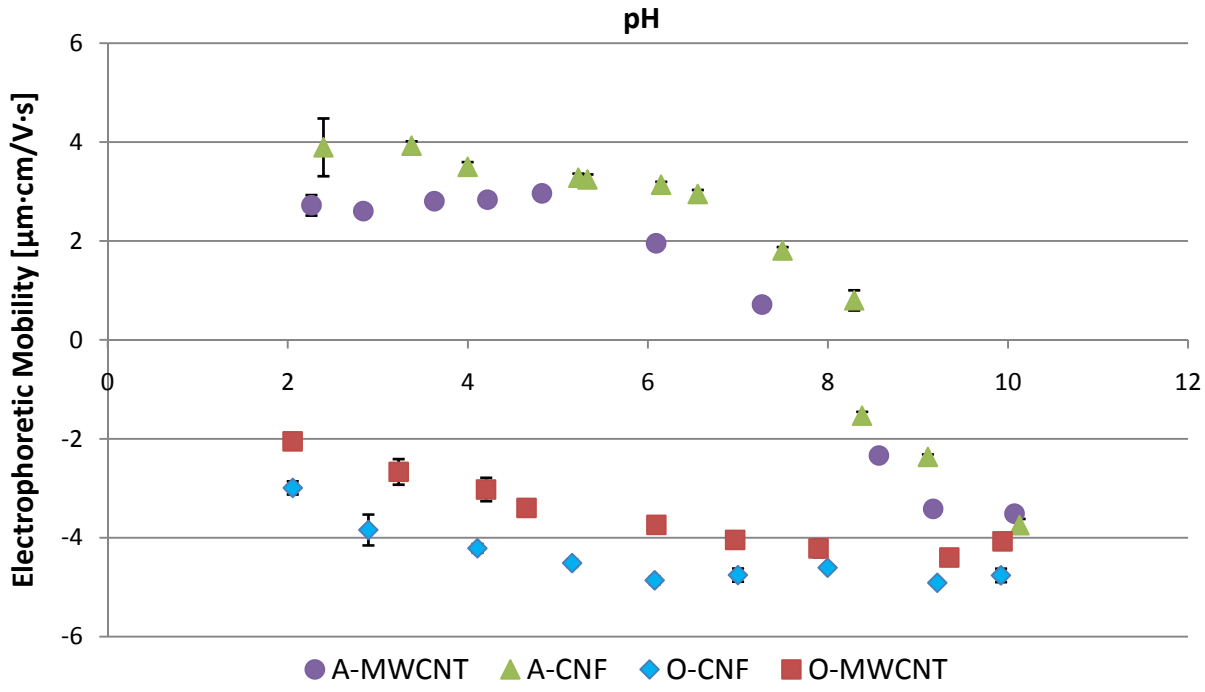

Figure 27. Electrophoretic mobility values of A-MWCNTs and A-CNFs. Error bars indicate one standard deviation.

Comparing the values of A-MWCNTs with A-CNFs, it is observed that latter particles have a higher surface charge. This finding is in agreement with the results obtained for O-MWCNTs and O-CNFs where it was observed that O-CNFs have a higher surface charge. Further corroboration of the relative content of functional groups on the surface of the particles is drawn from the XPS results that show that O-CNFs and A-CNFs have larger amounts of functional groups on the surface than O-MWCNTs and A-MWCNTs, respectively.

In terms of the stability of A-MWCNTs/A-CNFs in aqueous medium, it is noticed that the dispersion of A-MWCNTs is stable only for pH values between 2 and 5.5 and above 9. And for A-CNFs, the particles are stable for pH values between 2 and 7.5 and above 9. In this study,

the pH values for deposition are between 6 and 7. This means that for A-CNFs the system is always stable whereas for A-MWCNTs the system is below the limit of stability.

3.3.2 Electrophoretic Deposition Process

After mixing the functionalized carbon nanoparticles with ultrapure water and inserting the carbon fiber layer with the frame into the electrophoretic tank, several images were taken of the electrophoretic setup. Figure 28 shows two images of the setup before deposition of the nanoparticles. At this initial stage of the process, the aqueous solutions is dark and opaque and light transmission is limited. After EPD, the aqueous solution turns translucent due to the deposition of the particles on the surface of the layers. Figure 29 shows two images of the tank after EPD where this effect can be clearly seen.

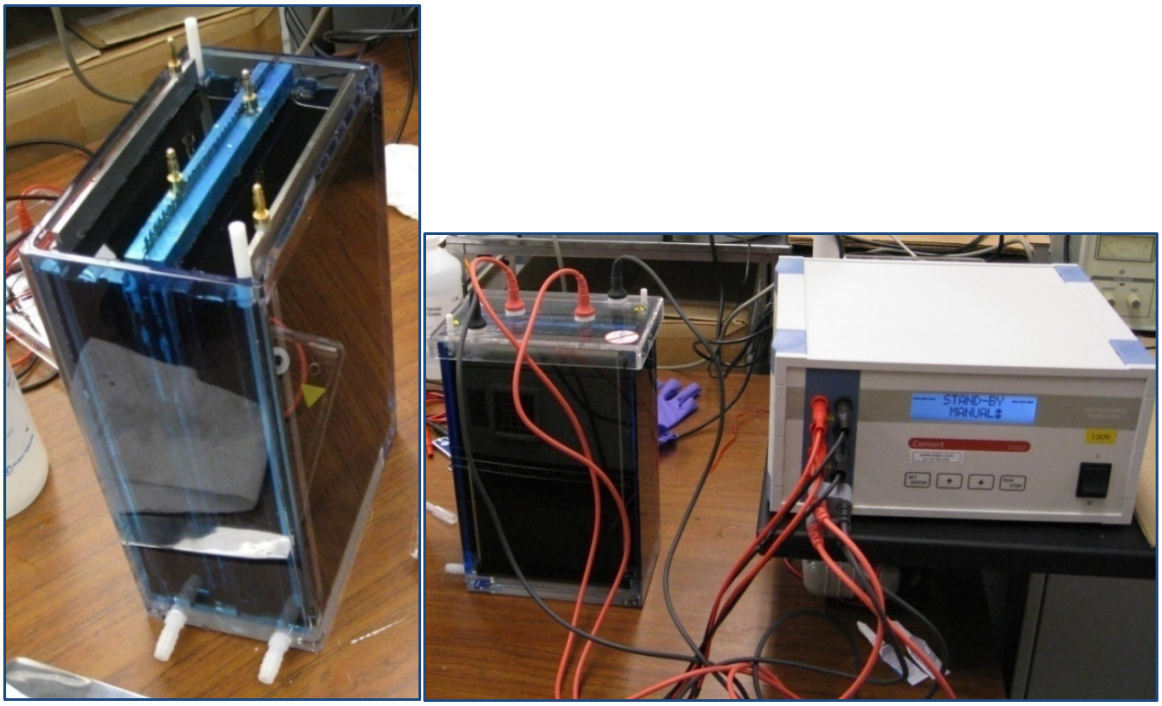

Figure 28. Images of EPD setup before deposition of functionalized carbon nanoparticles.

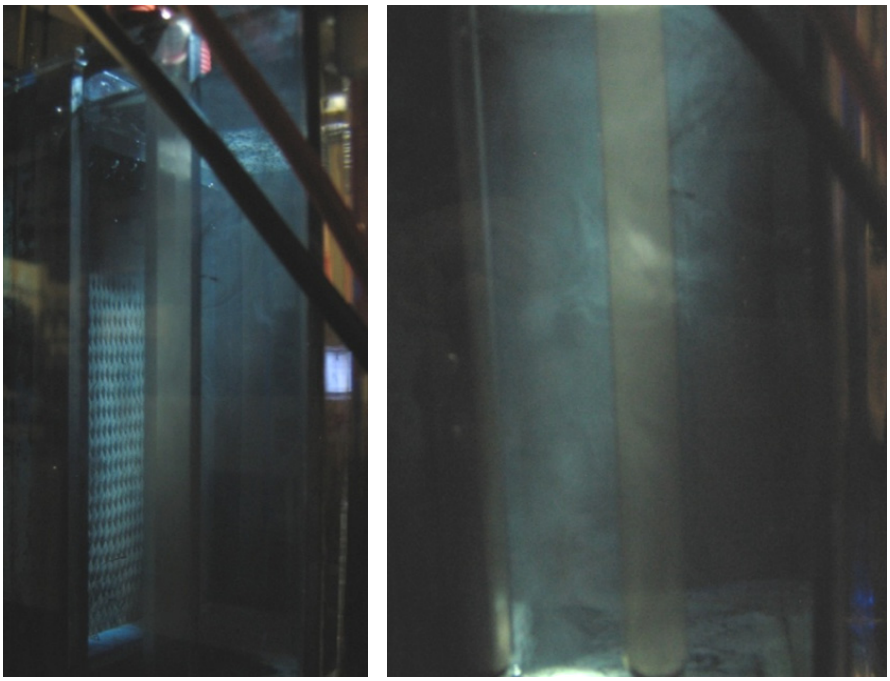

Figure 29. Images of EPD setup after deposition of functionalized carbon nanoparticles. Left: carbon fiber layer inside EPD tank. Right: Aqueous solution.

3.3.3 Characterization of Multiscale-Reinforcement Fabric

3.3.3.1 Deposition and Dispersion of Carbon Nanoparticles

3.3.3.1.1 Multiscale-Reinforcement Fabrics Containing Carboxylic Acid-Functionalized Multi-Walled Carbon Nanotubes and Carbon Nanofibers

Characterization of the carbon fiber layers before and after EPD of O-MWCNTs was performed by observing the deposition of the particles through SEM imaging of the substrates. These images are shown in Figure 30. Two interesting observations can be drawn from observing the MRFs. The first is that the O-MWCNTs were mostly deposited between the carbon fibers and not on top of the substrate. This could be due to redistribution of the O-MWCNTs during the drying step. It is expected that water droplets tend to deposit between fiber tows before evaporating. In this process, due to the surface energy of the water, the droplets attract the O-MWCNTs laying on the surface of the fiber, thus making the nanoparticles move and reposition in-between the fibers. After water has completely evaporated, the O-MWCNT

will then stay between carbon fiber layers with no further movement. The second observation from the images is that, although the O-MWCNTs are mostly positioned between carbon fibers, they are ―for the most part― individually distributed. This exfoliation is important in order to achieve good load distribution when using the O-MWNCNTs carbon fiber layers to reinforce MRPCs subjected to different mechanical loads.

Deposition of O-CNFs was investigated by observing optical microscopy images of carbon fiber layers before and after EPD. From the images shown in Figure 31, it can be observed that O-CNF readily deposited on the surface of the carbon fiber layers and in the intra-tow region. It is important to note that the distribution of O-CNF on the surface of the layers was different than for O-MWCNTs. In the case of O-CNFs, the deposition was not completely uniform and small agglomerates with a radius of about 10–80 μm could be seen on the surface of the layers. This effect can be clearly seen at high optical microscopy magnification (image D from Figure 31) where some of the particles are deposited in the intra-tow region whereas other particles are superficially deposited. On the other hand, as previously observed in Figure 30, O-MWCNTs are more evenly distributed in the intra-tow region. This difference can also be explained by redistribution of the O-CNFs in the drying step. During drying of the MRF layers, the high surface energy of O-CNFs causes the nanoparticles to be pulled by the water droplets and redistributed on the surface of the layer. Due to the size of O-CNFs, some of the particles deposit in the intra-tow region whereas other particles that cannot penetrate the carbon fiber layer can only deposit on the surface. Another observation in EPD of O-CNFs is that since CNFs are larger than MWCNTs, individual O-CNF deposited particles are able to touch several carbon fibers (Figure 32). This type of configuration would lead to fiber bridging when manufacturing

MRPC with this type of layers. This is a desired reinforcing mechanism for the MRPC due to the ability of the nanomaterials to redistribute load to adjacent fibers upon loading of the part.

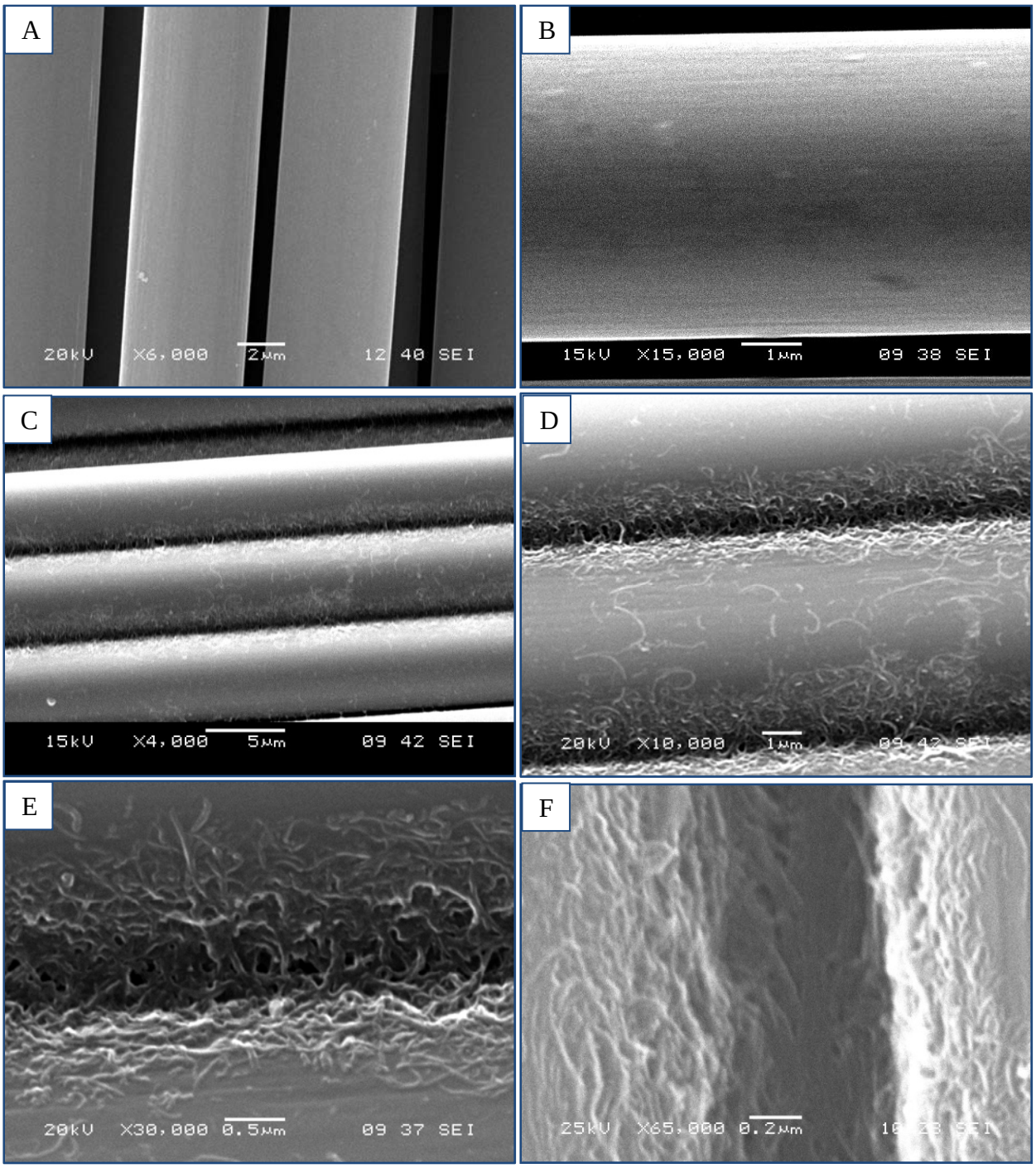

Figure 30. A and B: SEM images of carbon fibers before EPD of O-MWCNTs. C-F: SEM images of carbon fibers after electrophoretic deposition of O-MWCNTs.

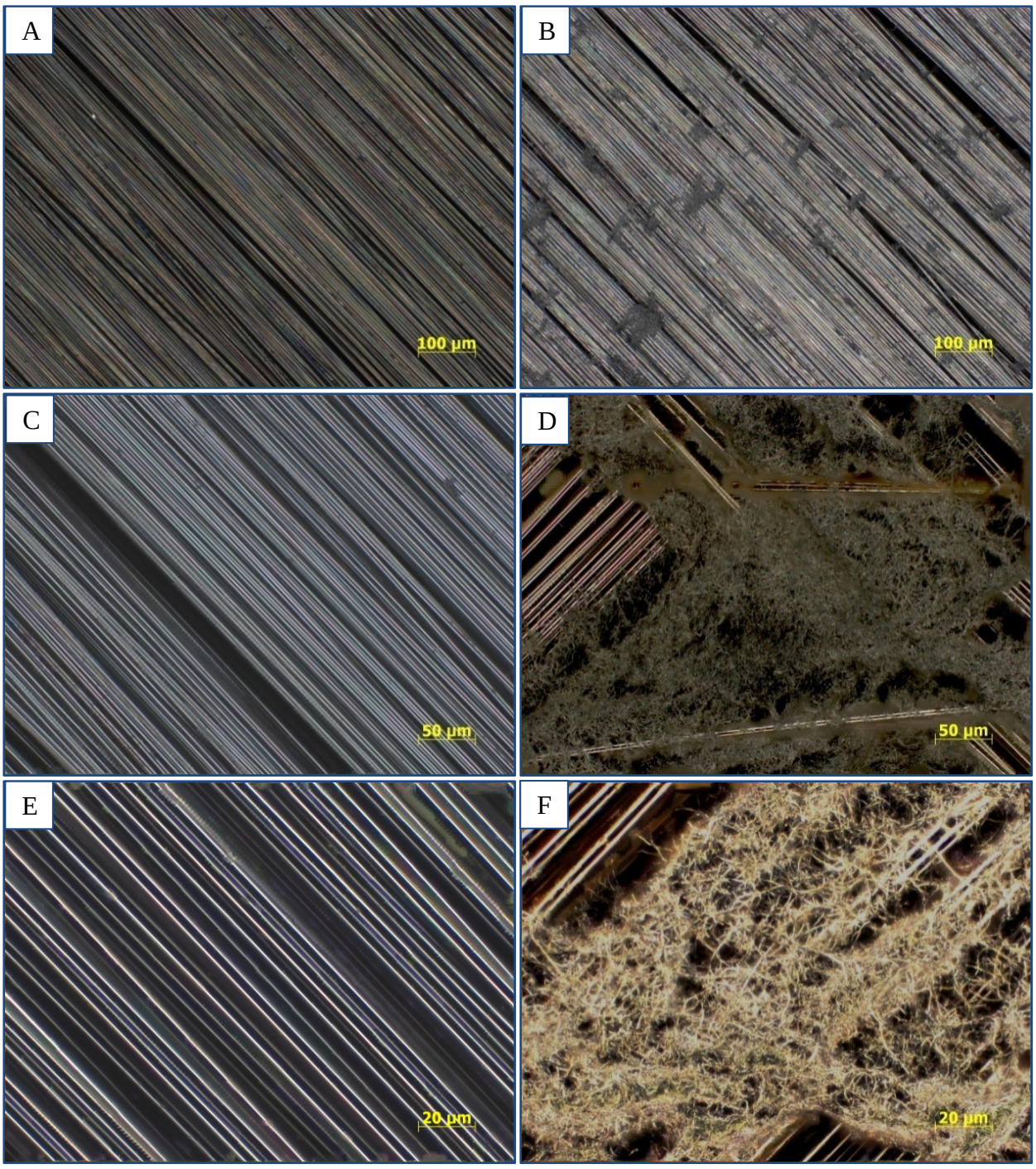

Figure 31. Left column (A, C, and E): Optical images of carbon fiber layers before EPD of O-CNFs. Right column (B, D, and F): Optical images of carbon fiber layers after EPD of O-CNFs.

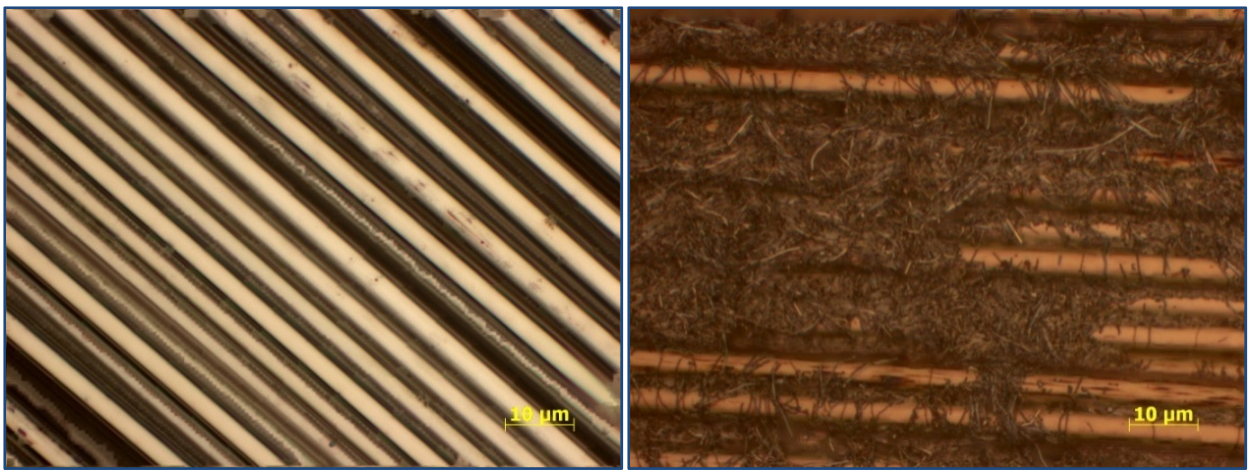

Figure 32. Left: Optical image of a carbon fiber layer before EPD of O-CNFs. Right: Optical image of carbon fiber layer after EPD of O-CNFs.

3.3.3.1.2 Multiscale-Reinforcement Fabrics Containing Amine-functionalized Multi-Walled Carbon Nanotubes and Carbon Nanofibers

EPD of A-MWCNTs onto carbon fiber layers did not result in uniform dispersion or in individual exfoliation of the carbon nanoparticles throughout the layer. As shown in Figure 33, SEM images taken from the A-MWCNT containing carbon fiber layers indicate that the A-MWCNTs agglomerated into clusters of ~20–30 µm in radius and deposited on the surface of the layer. Some other places in the layer showed rope-like agglomeration and deposition of the A-MWCNTs. The clustering and agglomeration effect is caused by the inherent instability of the A-MWCNTs aqueous system due to their high surface area and van der Waals forces. Stability of the colloidal solution of amine-functionalized nanoparticles is an extremely important parameter in EPD. If the nanoparticles suspended in water are not stable, they will start to aggregate and form clusters that would either deposit at the bottom of the tank, or travel and deposit on the surface of the carbon fiber layer. This is a clear indication that EPD is not an effective method to deposit exfoliated A-MWCNTs at pH of approximately 6, which in turn also indicates that rod-like particles are not stable at zeta (ζ) potential values of 24.94 mV (see Figure 27).

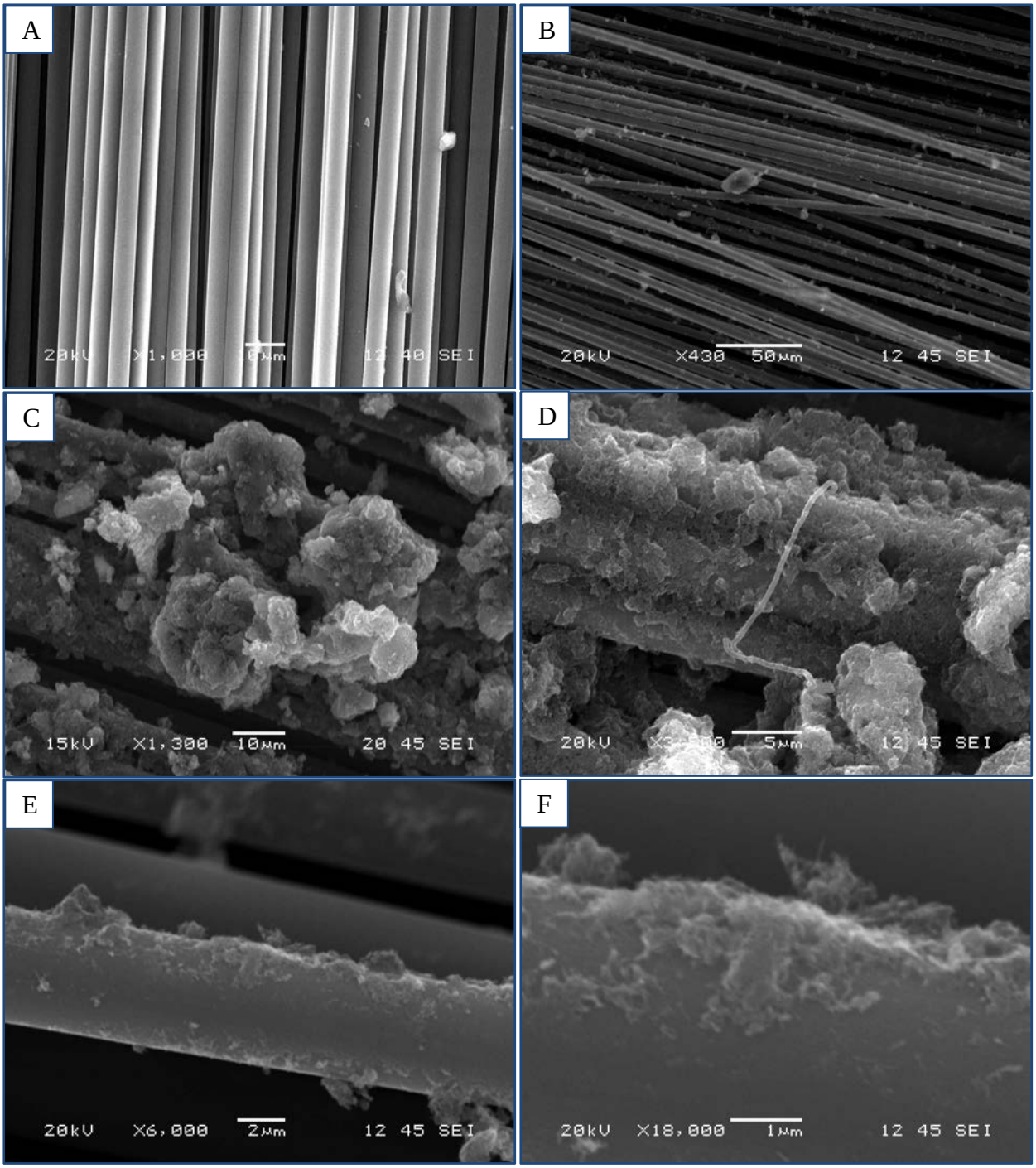

Figure 33. Carbon fiber layers before (A) and after EPD of A-MWCNTs (B-F).

Further efforts were made to stabilize A-MWCNTs in aqueous medium to achieve uniform deposition. To this end, several experiments were performed where different quantities of acid (HCl) were added to the A-MWNT-aqueous solution in order to increase the ζ potential

of the particles. By adding small quantities of acid, the pH of the system decreased which in turn made the system more stable due to an increase in the surface energy of the particles caused by ionization of the functional groups (see Figure 27). By decreasing the pH of the solution, the clusters were reduced in size but not to the point of complete deagglomeration. This effect was captured in SEM images shown in Figure 34, where A-MWCNTs clusters were reduced to half the size of the original clusters (~20–30 µm vs. ~7–15 µm radius) after EPD in a MWCNT-aqueous solution of pH 5. At this pH, the zeta potential is approximately 35 mV, which leads to the idea that in order to obtain a stable solution of rod-like nanoparticles such as A-MWCNT in aqueous medium, the zeta potential has to be higher than $|35|$ mV. Further addition of HCl acid was not pursued since a high concentration of acid in an aqueous medium has detrimental effects on the sizing of the carbon fiber layer.

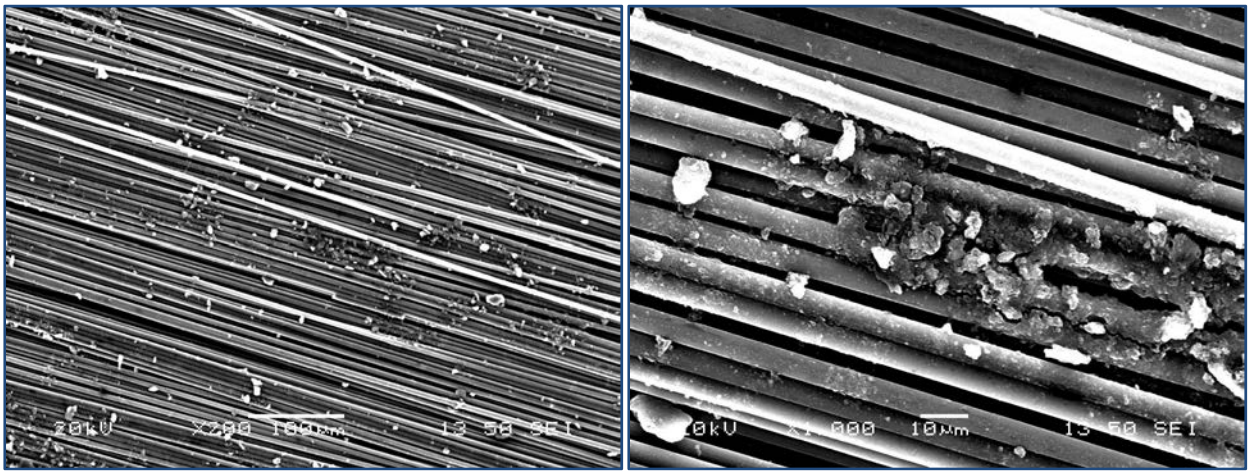

Figure 34. SEM images of carbon fiber layers after EPD of A-MWCNTs dispersed in aqueous medium at pH 5.

In contrast to the case of A-MWCNTs, EPD of A-CNFs onto carbon fiber layers resulted in uniform and individual deposition of the carbon nanoparticles. Also, contrary to the deposition of O-CNFs, deposition of A-CNF resulted in uniform coverage where no significant clusters of particles were observed (Figure 36). This configuration confirms that A-CNF in an aqueous

solution at pH of 6 is stable and that successful deposition can be achieved. Referring to Figure 27 (electrophoretic mobility of functionalized carbon nanoparticles) and referring to the inherent instability of A-MWCNTs at zeta potential of 35 mV, it is suggested that zeta potential stability criterion for rod-like particles such as CNFs and MWCNTs is within ±35–40 mV.

Further insight into the deposition of A-CNFs on the carbon fiber can be gained by observing Figure 36, which shows a set of two images of a single carbon fiber before and after EPD of A-CNFs. It is clearly observed that after EPD, the A-CNFs are not only deposited on the surface of the carbon fiber but also wrapped around it. This wrapping effect has the advantage of increasing the surface area of the fiber, which could lead to higher mechanical properties of the final material by means of mechanical interlocking mechanism. This effect was not previously seen in the deposition of oxidized CNTs in water and also amidized CNTs in DMF on the surface of carbon fiber layers [128, 129]. As in the case of O-CNF, another interesting fact that can be drawn from the optical and SEM images, is the ability of the A-CNFs to deposit in the intra-tow region and eventually join the adjacent fibers to create a fiber bridging configuration. Both SEM images in Figure 37 show a layer with A-CNFs bridging from one fiber to another. It is expected that fiber bridging coupled with high interaction between the A-CNF, sizing of the fiber, and epoxy resin would result in higher mechanical reinforcement in MRPCs manufactured with MRFs containing A-CNFs.

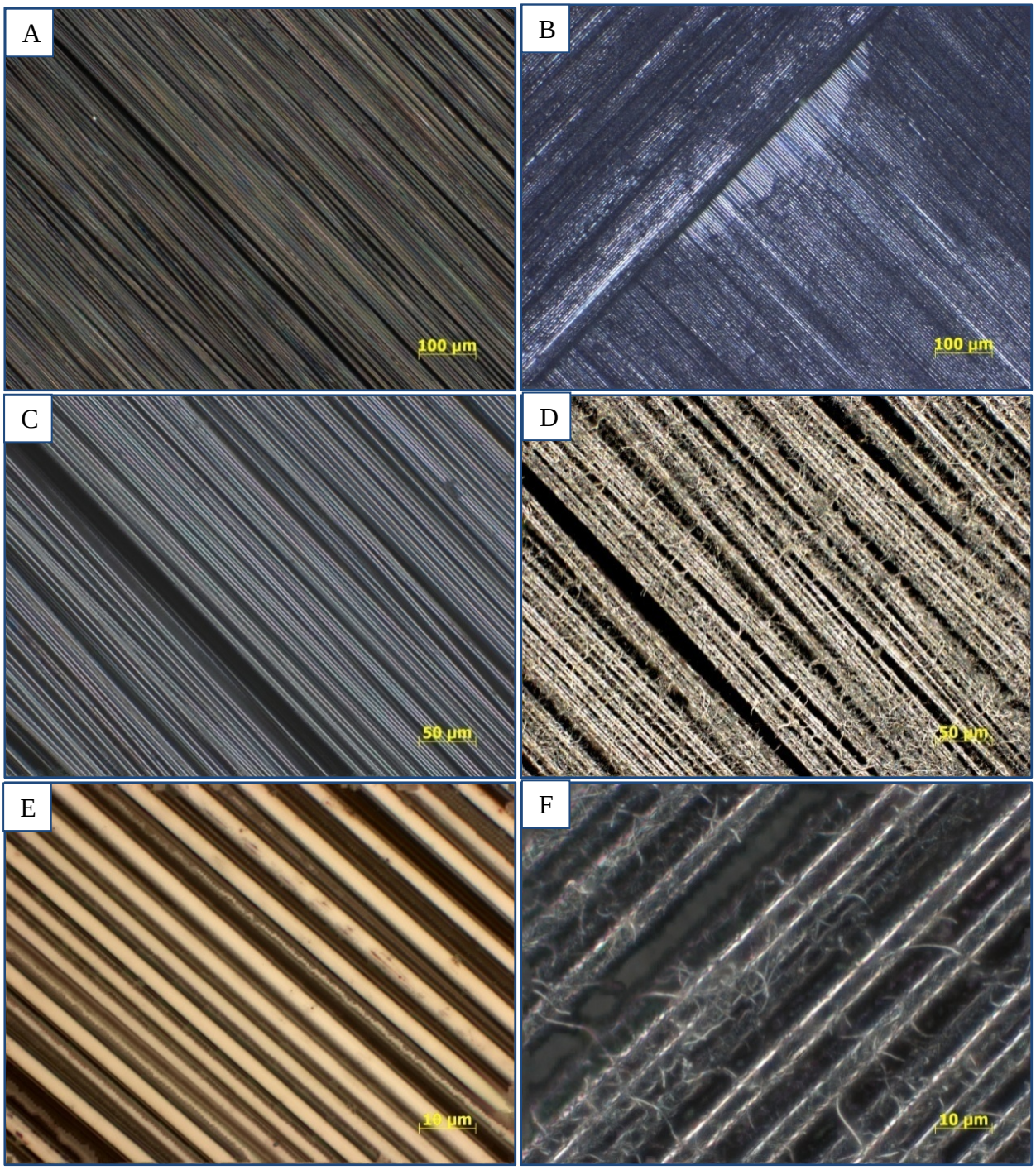

Figure 35. Left column (A, C, and E): Optical images of carbon fiber layers before EPD. Right column (B, D, and F): Optical images of carbon fiber layers after EPD of O-CNFs.

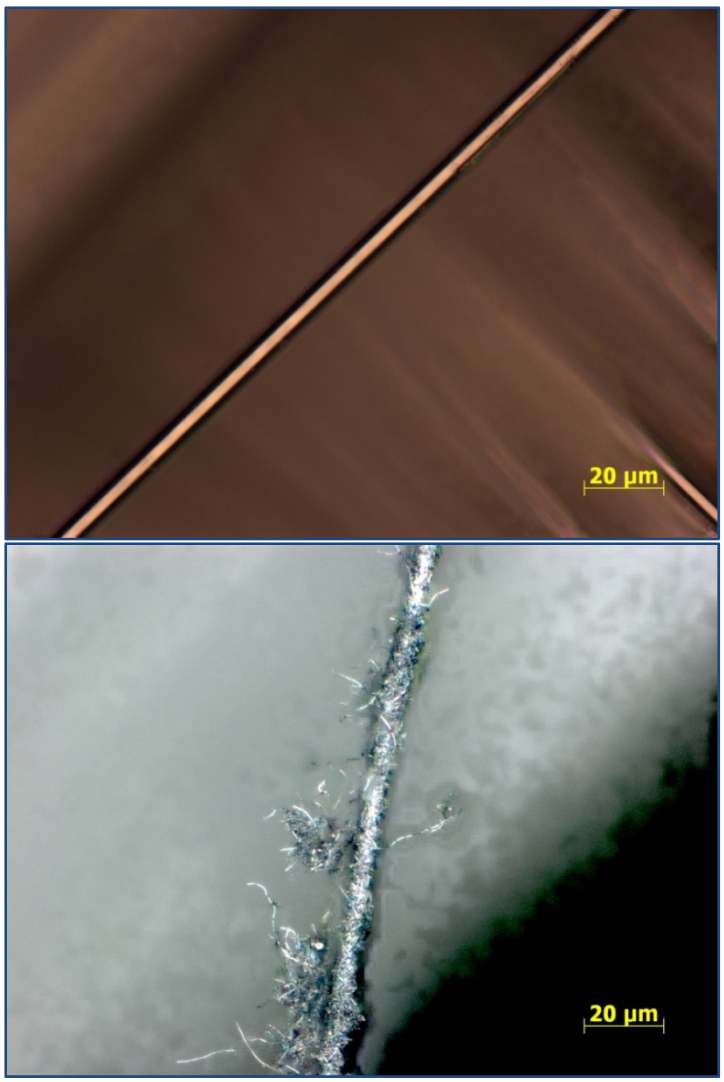

Figure 36. Optical images of carbon fibers before (top) and after (bottom) EPD of A-CNFs.

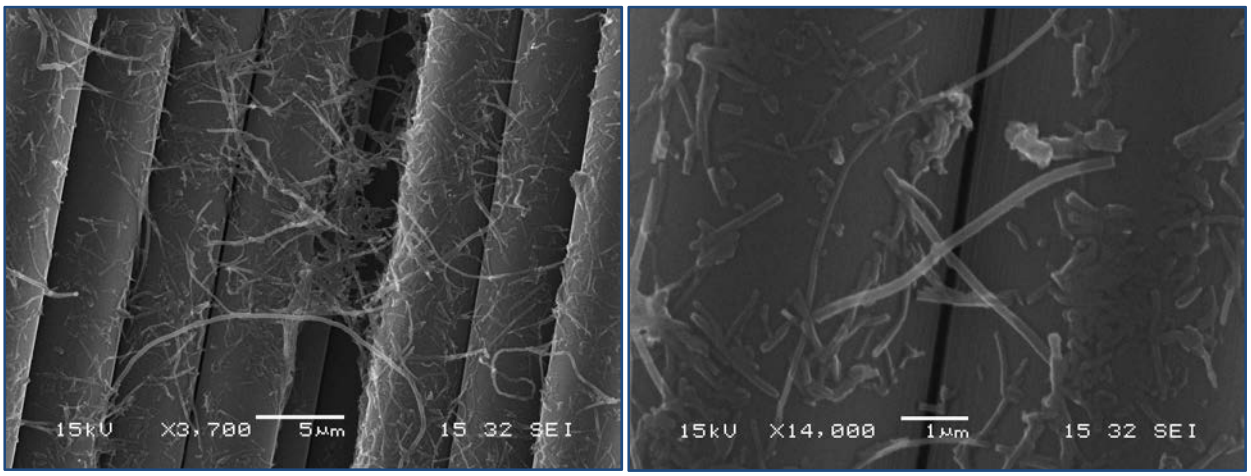

Figure 37. SEM images of carbon fiber layers after EPD of A-CNFs.

3.3.3.2 Quantification of Material Deposition

Light absorbance spectra were obtained for aqueous solutions of different concentrations of carboxylic acid- and amine-functionalized MWCNTs and CNFs to obtain concentration calibration curves. These plots can be found in Appendix B. From the spectra obtained, a linear fit of the concentration as a function of absorbance was plotted at three different wavelengths near the visible range. Note that no absorbance spectra were obtained for A-MWCNTs due to instability of the particles in the aqueous medium. Therefore, no estimation of A-MWCNT deposition onto carbon fiber layers could be obtained for this case.

The calibration curves at three different wavelengths (500 nm, 600 nm, and 700 nm) are shown in Figure 38 for O-MWCNTs, Figure 39 for O-CNF, and Figure 40 for A-CNF. The curve obtained using the 600 nm wavelength data was selected as the reference curve based on the stability of the absorbance at that wavelength and the precision of the linear fit. Then, the equation obtained using the linear regression fit was used to estimate the concentration of the carbon nanoparticles in aqueous media after EPD. It is important to note that light absorption above 1.5 could trigger non-linearity in the concentration vs. absorption plots. However, it is clear that absorption is linear within the range of concentrations studied as proven by the R^2 values calculated from the linear fit curves. From these results, it is determined that the non-linear region was not reached for MWCNTs/CNFs in aqueous media.

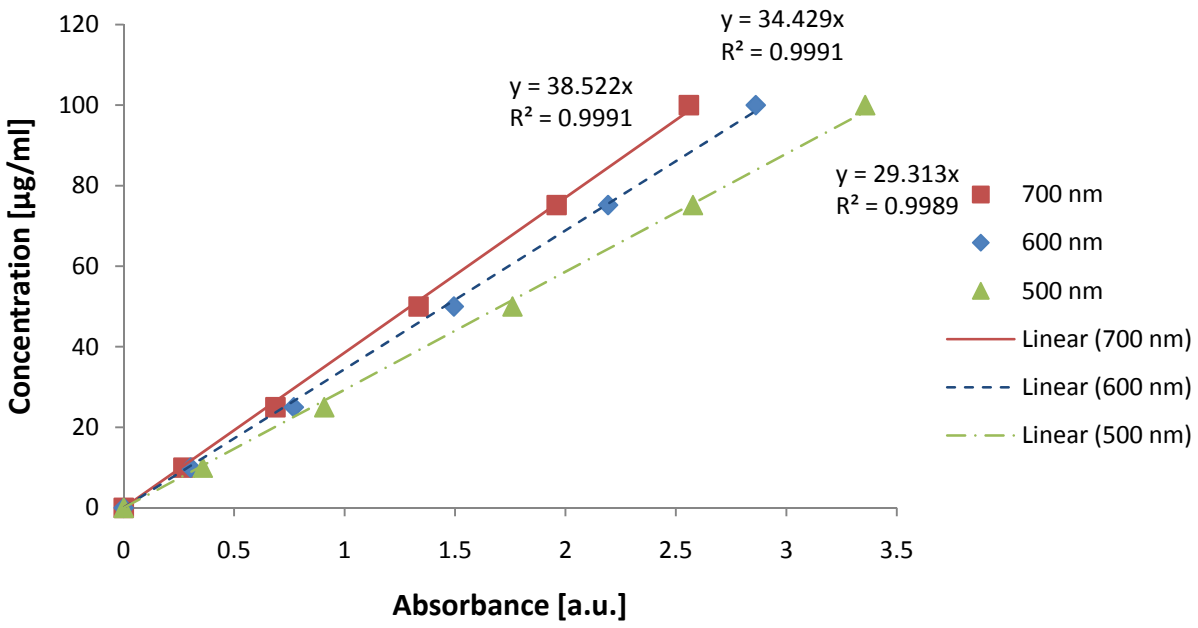

Figure 38. Calibration curves at three different wavelengths as a function of absorbance for carboxylic acid-functionalized MWCNTs.

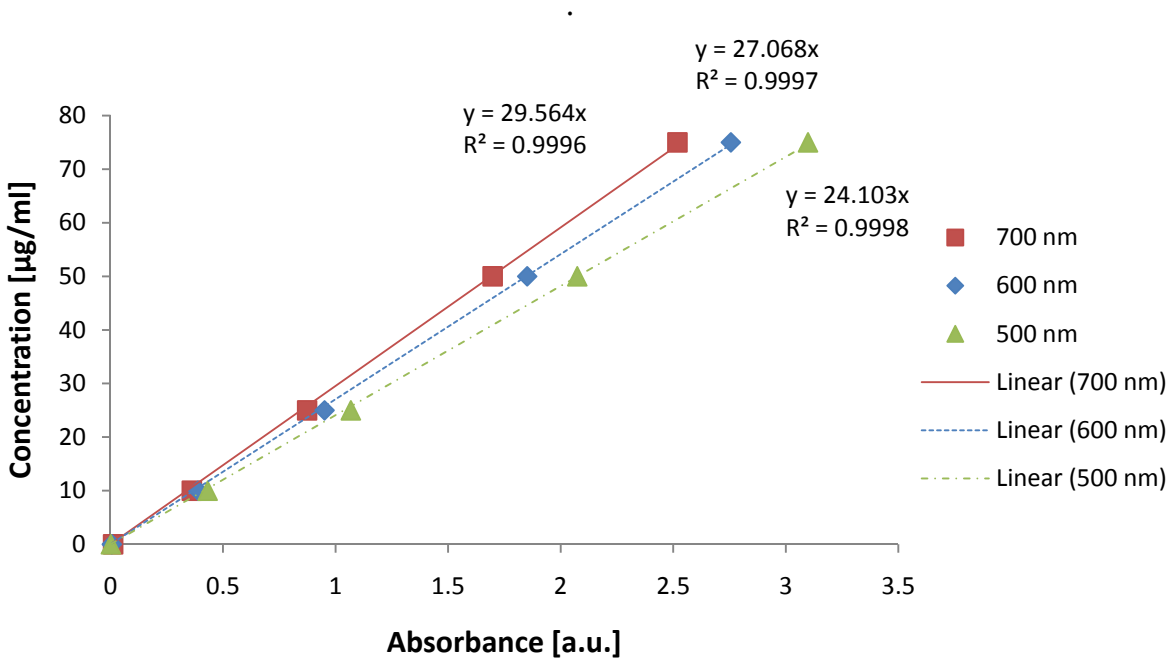

Figure 39.Calibration curves at three different wavelengths as a function of absorbance for carboxylic acid-functionalized CNFs.

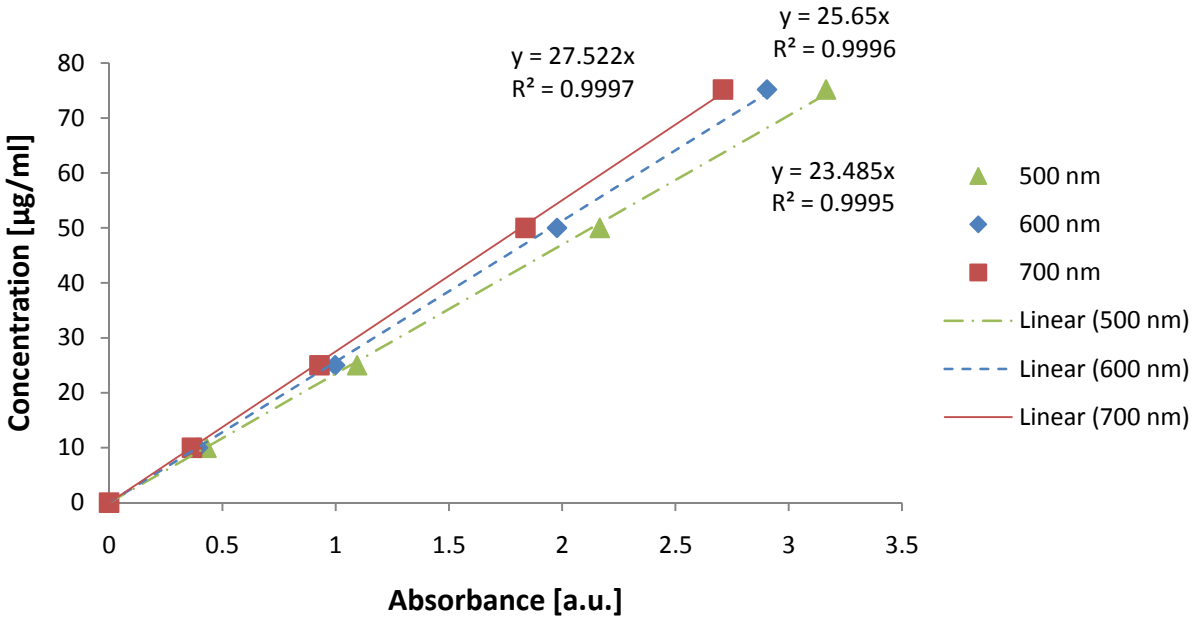

Figure 40. Calibration curves at three different wavelengths as a function of absorbance for amine-functionalized CNFs.

Based on the data collected and using equation 1, the amount of functionalized MWCNTs and CNFs deposited on the surface of carbon fiber layers using the EPD process was estimated. These values are shown in Table 12. Deposition of O-MWCNTs and O-CNFs were estimated to be 24.61 mg/layer and 31.61 mg/layer, respectively. This represents 12.9% and 16.64% of particles deposited with respect to the total amount dissolved in the EPD tank, respectively. The difference in deposition between O-MWCNTs and O-CNFs, approximately 20%, is attributed to the difference in electrophoretic mobility values (Figure 26) of both types of particles that is also around 20% for the pH of ~6. This corroborates the fact that the higher the EM, the higher EPD of particles.

Deposition of A-CNFs was estimated to be 46.93 mg/layer which represents 24.7% of the particles initially dissolved in the aqueous media before EPD. From the images shown in the previous section, it was expected that the A-CNF deposition process promoted higher deposition

than O-MWCNTs and O-CNFs. A-CNFs were seen to be more densely and uniformly deposited than O-CNF (Figure 31). This difference in deposition is attributed to the difference in processing conditions. The A-CNF deposition process consisted of two steps involving longer deposition time, while the deposition of O-CNF consisted of only one step of shorter deposition time.

TABLE 12

QUANTITY OF FUNCTIONALIZED MWCNT AND CNF DEPOSITED ON SURFACE OF CARBON FIBER LAYERS

Particle Type	Quantity Deposited [mg/Layer]	Relative Quantity Deposited [%]
O-MWCNT	24.61	12.9
O-CNF	31.61	16.64
A-MWCNT*	-	-
A-CNF	46.93	24.7

*A-MWCNT deposition onto carbon fiber layers could not be estimated due to the instability of the system.

3.4 Summary and Conclusions

In this chapter, electrophoretic deposition of functionalized multi-walled carbon nanotubes and carbon nanofibers onto carbon fiber layers was investigated. FTIR, TGA, and XPS confirmed the functionalization of the particles with carboxylic acid and amine functional groups. Laser Doppler velocimetry of the particles showed that O-MWCNTs and O-CNFs had a negative charge in aqueous medium for a pH between 2 and 10. Conversely, the A-MWCNTs and A-CNFs exhibited a positive charge at low pH and a negative charge at high pH with the isoelectric point at pH of ~8.1.

SEM images of carbon fiber layers after EPD of O-MWCNTs showed particle deposition in the intra-tow region, whereas O-CNFs deposited in the intra-tow region as well as on the surface. EPD of A-MWCNTs onto carbon fiber layers did not result in uniform dispersion along

the layer. SEM images of the multiscale layers indicated that the A-MWCNT agglomerated into clusters of ~20–30 μm in radius that were deposited on the surface of the layer. This was effect was attributed to the instability of the A-MWCNTs since the nanoparticles are not able to dissolve in aqueous medium due to their low zeta potential values. On the other hand, EPD of A-CNFs onto carbon fiber layers resulted in uniform and individual deposition of the carbon nanoparticles. The configuration of this type of deposition confirmed that A-CNF in aqueous solution at pH of 6 is stable, and that successful deposition could be achieved. From these results it was observed that rod-like particle stability is in the limits of ±35–40 mV. EPD of A-CNF also showed microfiber wrapping which has the advantage of increasing the surface area of the fiber. This was not previously seen when depositing O-MWCNTs or O-CNFs. In addition, optical images showed that individual A-CNF and O-CNF particles were able to deposit and touch several fibers. This leads to fiber bridging, which is a desired reinforcing mechanism in MRPCs.

Quantification of the amount of carbon nanoparticles deposited onto the surface of carbon fiber layers was estimated by determining the concentration of the nanomaterials in water before and after EPD using a light transmission technique. Results showed that O-CNFs deposited in higher quantity than O-MWCNTs due to the difference in electrophoretic mobility. Similarly, A-CNF deposited in higher quantity than the oxidized carbon nanoparticles, which was attributed to the difference in the EPD process.

Based on the aforementioned results, it can be concluded that EPD is an effective and scalable method to deposit O-MWCNTs, O-CNFs, and A-CNFs onto complex substrates such as carbon fiber layers. One limitation of this process is the time and magnitude of the electric field that the carbon fiber layers can be subjected to during the EPD process, since stiffening of the carbon layers was observed for high electric fields and long deposition times. The MRFs made as

described herein can be used to manufacture MRPCs in order to increase selected mechanical properties such as interlaminar shear strength and stiffness as well as compressive strength. Processing and characterization of MRPCs manufactured with MRFs is presented and examined in Chapter 4.

CHAPTER 4

MANUFACTURING AND CHARACTERIZATION OF CARBON NANOPARTICLE/FIBER-REINFORCED POLYMER COMPOSITES

4.1 Introduction

Advanced polymer composites provide excellent in-plane tensile strength-to-weight and stiffness-to-weight ratios, which are dominated by the strength and stiffness of the fibers and the ability of the matrix to transfer load to the fiber. Conversely, advanced polymer composites have poorer out-of-plane and in-plane compressive performance. MWCNTs and CNFs have a unique combination of properties that make them ideal materials for reinforcing resin- and resin/fiber-dependent properties of advanced composites. The usual approaches to incorporating MWCNTs and CNFs into advanced polymer composites pose several manufacturing issues that must be overcome in order to produce parts with higher and consistent properties.

In Chapter 3, a process to synthesize multiscale-reinforcement fabrics by directly depositing functionalized nanoparticles (MWCNTs and CNFs with carboxylic acid or amine functional groups) on the surface of carbon fiber layers through electrophoretic deposition was developed and studied. In this chapter, processing and characterization of the mechanical and electrical properties of MRPCs manufactured with such layers is presented and examined. The mechanical and electrical properties obtained include interlaminar shear strength and stiffness, compressive strength, and through-plane electrical conductivity.

The schematic of the complete MRPC manufacturing process is depicted in Figure 41. In the first stage of the process, MRFs are manufactured as described in Chapter 3. In the second stage of this process, MRFs are stacked and infused with an epoxy-amine resin system to manufacture the final MRPC by vacuum-assisted resin transfer molding (VARTM).

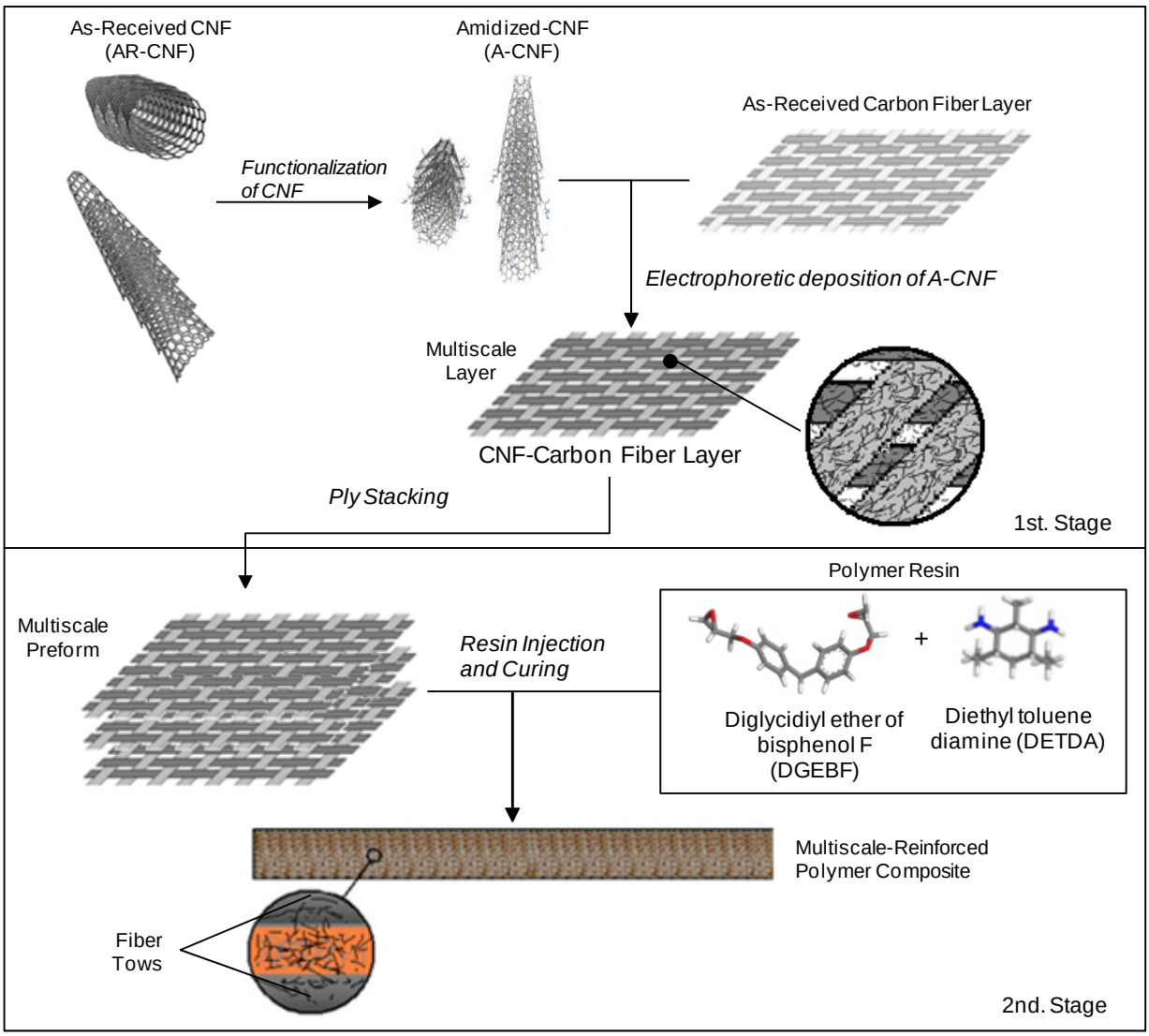

Figure 41. Schematic of manufacturing process of multiscale-reinforced polymer composites.

4.2 Experimental Section

The matrix selected for this study was an epoxy-amine system comprised of diglycidyl ether of bisphenol F (EPON^{TM} 862) and diethyl toluene diamine (EPIKURE^{TM} W) obtained from Hexcel. This system is widely used in aircraft applications and other industries due to its high mechanical properties, excellent adhesion, and chemical resistance. The ratio of epoxy to curing agent used was 100:26.4 by weight, as recommended by the manufacturer. The structures of EPON 862 and EPIKURE W are shown in Figure 42 [148]. Multiscale-reinforcement fabrics

used for this study were manufactured as specified in Chapter 3. All other chemicals were obtained from Fisher Scientific and used as-received.

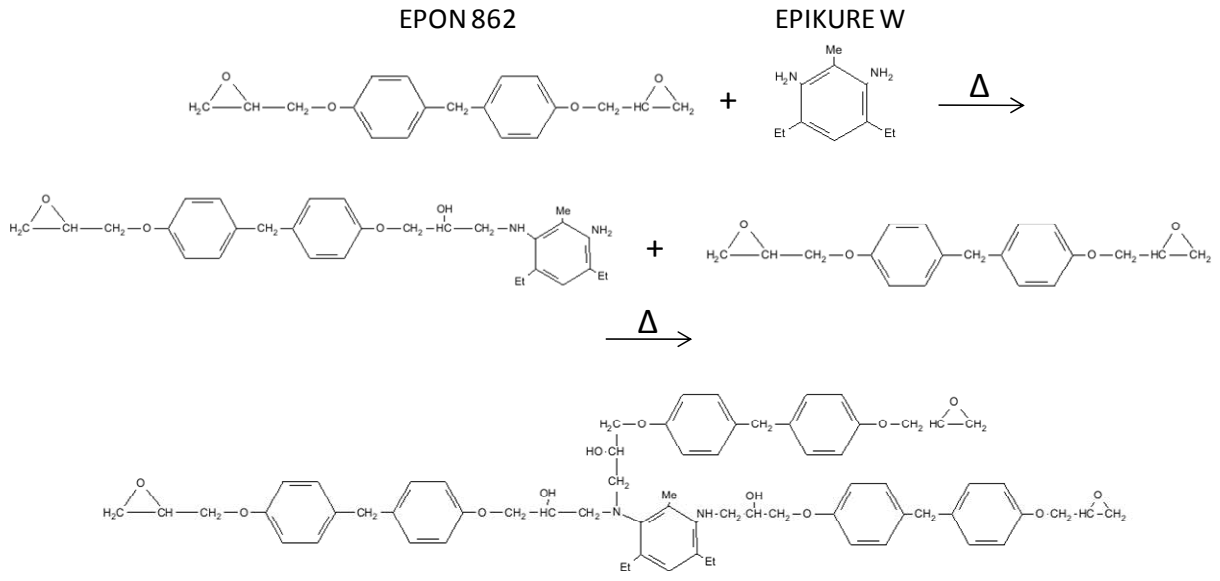

Figure 42. Chemical structures of EPON 862 and EPIKURE W.

4.2.1 Manufacturing of Multiscale-Reinforced Polymer Composites with Multiscale-Reinforcement Fabrics

To study the mechanical and electrical properties of the multiscale-reinforced panels, several flat panels of 25 x 17 cm^2 were manufactured using VARTM utilizing the setup shown in Figure 43. VARTM is a widely-used, cost-effective polymer composite manufacturing technique for fabricating polymer composites. The first panel was standard and made with as-received carbon fibers with no deposited nanoparticles. The second and third panels were made with a preform comprised of MRFs with O-MWCNTs and O-CNFs. Panels four and five were made with preforms containing A-MWCNT and A-CNF, respectively. Description of all panels manufactured are provided in Table 13. All panel preforms were balanced and symmetric and consisted of 16 layers of either as-received carbon fiber layers or MRFs. The stacking sequence of each preform was $[-45,0,+45,90]_{2s}$. After stacking the layers, the preform was infused with the

matrix and then cured according to the manufacturer's recommended cure cycle. This cycle consisted of curing for two hours at 177°C followed by a one hour post cure at the same temperature.

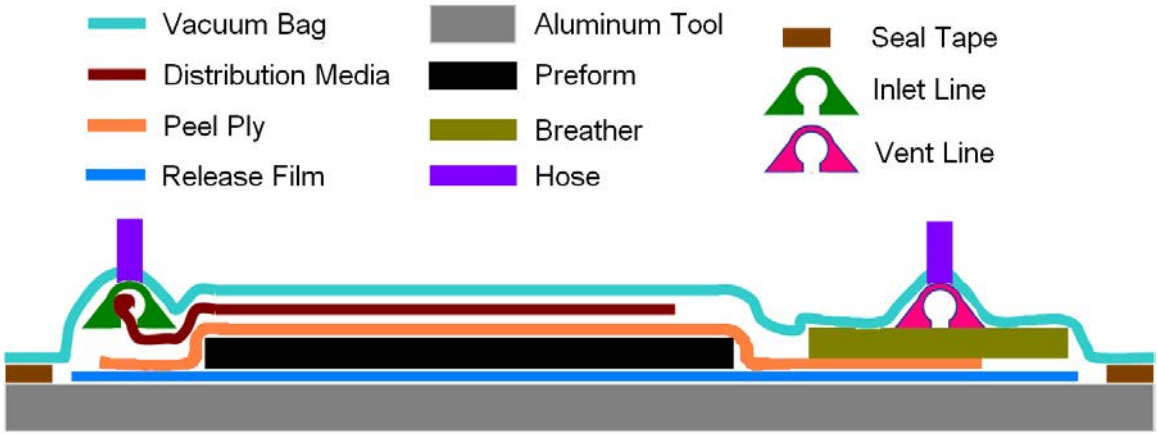

Figure 43.Vacuum-assisted resin transfer molding setup.

TABLE 13

DESCRIPTION OF MULTISCALE-REINFORCED POLYMER COMPOSITE PANELS MANUFACTURED AND CHARACTERIZED

#	Panel Description	Particle Type	Designation
1	Base Panel	N/A	BP
2	O-MWCNT	O-MWCNT	O-MWCNTP
3	O-CNF	O-CNF	O-CNFP
4	A-MWCNT	O-MWCNT	A-MWCNTP
5	A-CNF	A-CNF	A-CNFP

4.2.2 Characterization Methods

All panels were tested for interlaminar shear strength and compressive strength according to ASTM D2344 and Modified ASTM D695 test standards, respectively. Short-beam shear testing is one of the most popular methods for characterizing interlaminar shear strength of composite materials due to simplicity, practicality, and sample size (small amount of material required). Previous publications have suggested that, provided that the resin system is brittle —which is the case of the graphite/epoxy system used in this study—, short-beam shear testing

is a useful tool for determining apparent interlaminar shear strength of composites [149]. A schematic as well as images of the configuration for this test are shown in Figure 44.

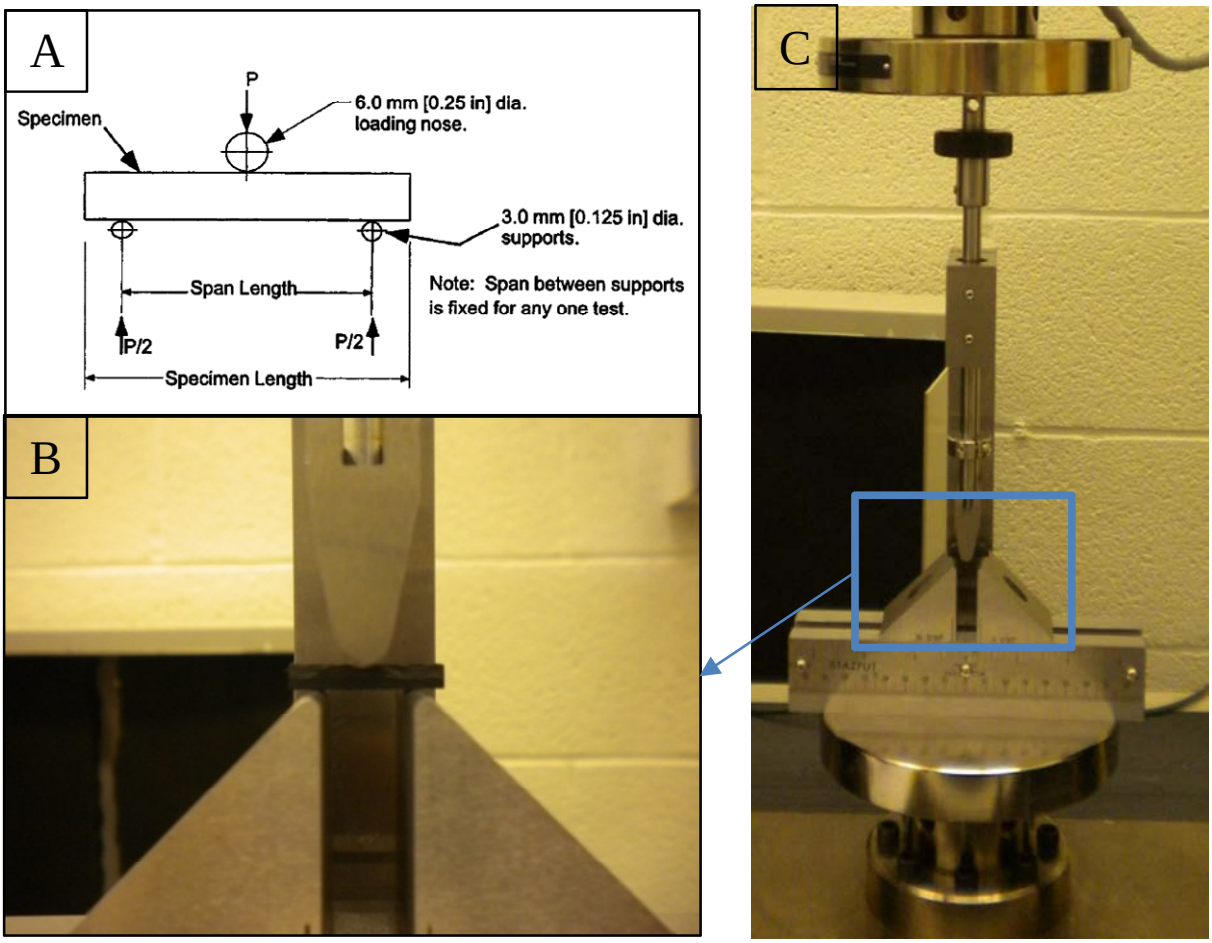

Figure 44. A: Schematic of short-beam shear test configuration [150]. B and C: Images of short-beam shear test configuration.

Due to the dimensions of the specimen, this type of test promotes failure by interlaminar shear. According to classical beam theory, the maximum shear stress occurs at the mid-plane of the specimen. The equation used to calculate the interlaminar shear strength of composites (τ) is

$$\tau = \frac{3P}{4bh} \tag{3}$$

where P is the load, and b and h are the width and the height of the specimen being tested, respectively.

Compressive strength test, as specified in modified ASTM D695, is a method where a tabbed specimen clamped in a support jig is subjected to end compression loading until failure. A valid test is accomplished when the specimen fails in the gage section. Figure 45 depicts this specimen configuration and test setup.

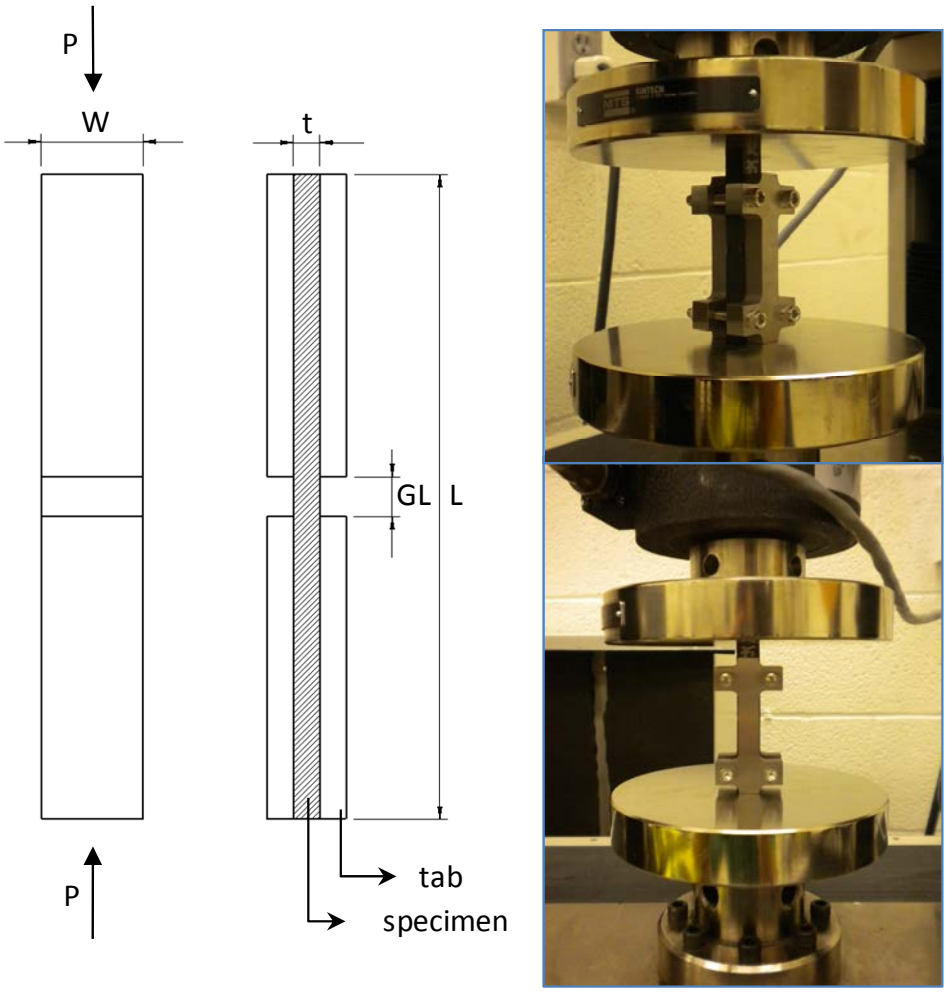

Figure 45. Specimen configuration and test arrangement for compressive strength test.

Through-plane electrical conductivity of the panels was tested following the four-probe method. For these tests, at least three samples were tested and the average value along with the standard deviation corresponding to each set of samples was reported. The dimensions of the samples were 2.54 cm x 2.54 cm. Before measurements were made, the in-plane surfaces of each sample were coated with conductive silver paint to ensure contact between the measuring

electrodes and the sample. To perform the measurements, four-point probe Kelvin clips were connected to the surface of the sample via copper wire. Resistance of the sample was measured, and the final conductivity value was calculated using Ohm's law and the dimensions of the sample.

4.3 Results and Discussion

4.3.1 Multiscale-Reinforced Polymer Composites

Since manufacturing of MRPCs requires injection of resin through the preform prepared with the MRFs, it is important to visualize how the nanoparticles are distributed inside the part after curing. For this purpose, small samples of ~10 mm x 10 mm were chemically etched using nitric acid to the point where the nanoparticles could be visualized but not displaced from the fibers. The etching procedure consisted of immersing the samples into 50 ml of nitric acid followed by heating the system to 50°C for ~60 minutes with occasional stirring.

Images of the etched samples for the base panel and the panels containing O-CNF and A-CNF were captured using optical microscopy at high magnification (Figure 46). From these images, it is interesting to note that the samples containing O-CNFs were dispersed similarly to the MRFs described in Chapter 3 (Figure 31). The distribution was not uniform where the CNF tended to be concentrated in areas of 10-80 μm in radius. The O-CNFs were also seen to touch and reach several carbon fibers, which is indicative of fiber bridging. Contrastingly, the images of the samples containing A-CNF showed that the A-CNFs were individually and uniformly distributed throughout the part, and no clusters of nanoparticles could be seen. Fiber bridging was also observed where several A-CNFs extended over several carbon fibers. These findings show that, although the panels were made through a resin injection molding technique, there was no evidence of CNF washing due to the viscous drag of the resin.

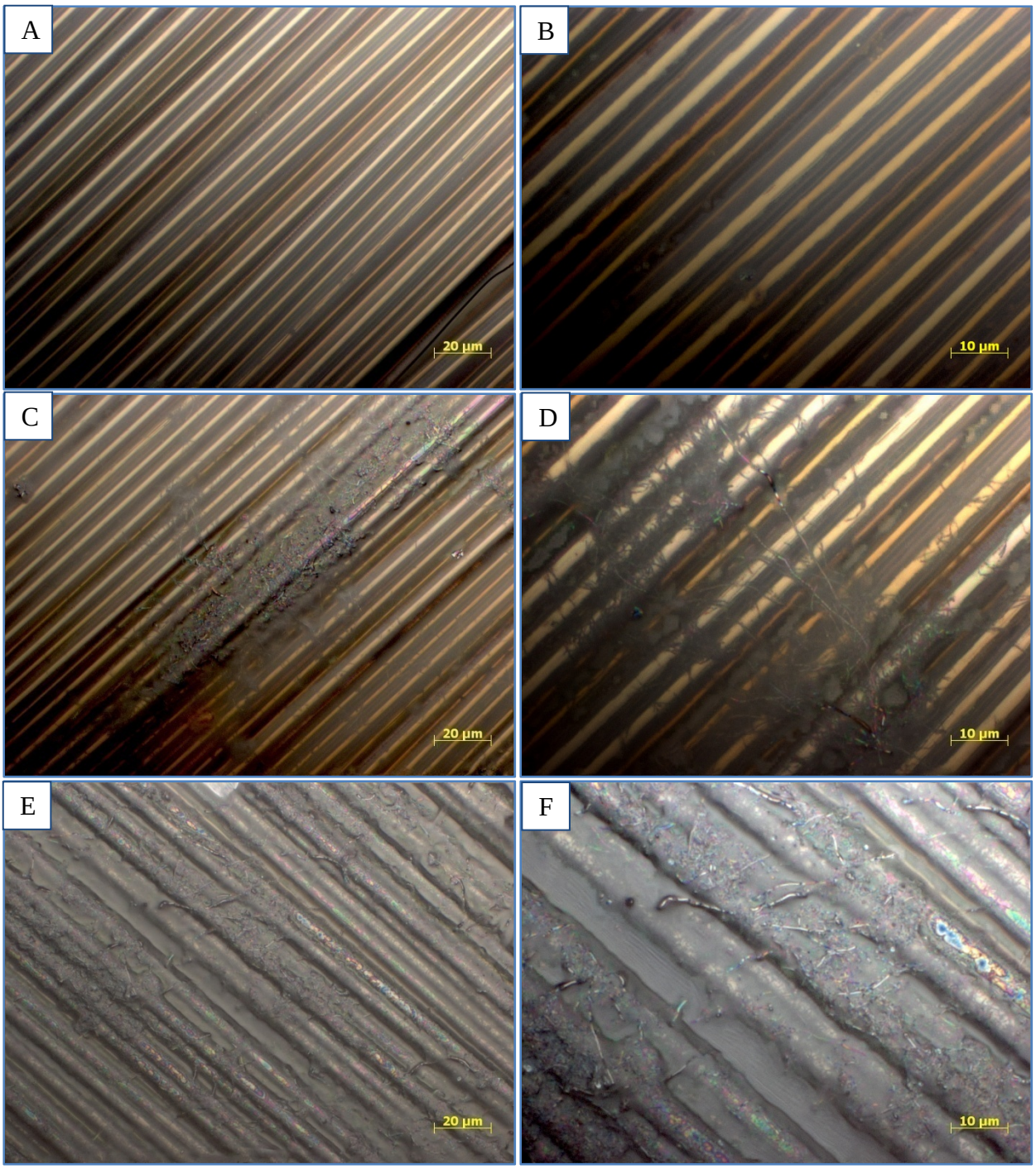

Figure 46. A and B: Top layer of etched sample for composite part with no CNFs inside. C and D: Top layer of etched sample for the MRPC part with O-CNFs inside. E and F: Top layer of etched sample for the MRPC part with A-CNFs inside. Left column images taken at 500x; right column images taken at 1000x.

4.3.2 Mechanical Properties of Multiscale-Reinforced Polymer Composites

4.3.2.1 Interlaminar Shear Strength

The apparent interlaminar shear strength values for the panels manufactured are shown in Figure 47. Results from this test revealed that panels containing O-MWCNT and O-CNF had a higher ILSS than the base panel, with an increase of 6.32% and 9.08%, respectively. Results also revealed that addition of A-MWCNTs and A-CNFs increased the ILSS by 2.76% and 10.01%, respectively. From these tests, it is clear that the addition of any type of functionalized carbon nanoparticle had a positive effect on ILSS, especially for A-CNFs. Note that no relation was found between ILSS and fiber volume fraction, which indicates that nanoparticles have significant influence on this property (Appendix C). In this investigation, an increase of 9%–10% is reported by depositing only 0.5wt.%–1wt% (with respect to the resin) of either MWCNTs or CNFs on the surface of MRFs. This shows that EPD of MWCNTs/CNFs is an effective method to synthesize MRFs capable of increasing the ILSS of MRPC manufactured with such layers.

The standard deviation of each sequence of tests is depicted in the error bars of Figure 47. The standard deviation of the tests conducted indicates that failure mechanisms experience the same combination of stresses. All specimens tested in this work failed by interlaminar shear. (Figure 48 shows a representative specimen of the MRPC containing O-MWCNTs that failed by interlaminar shear.) Coefficient of variation (COV) values show that the ILSS of all panels manufactured are consistent and approximately the same value as the base panel, which is an indication of the reliability of the manufacturing process.

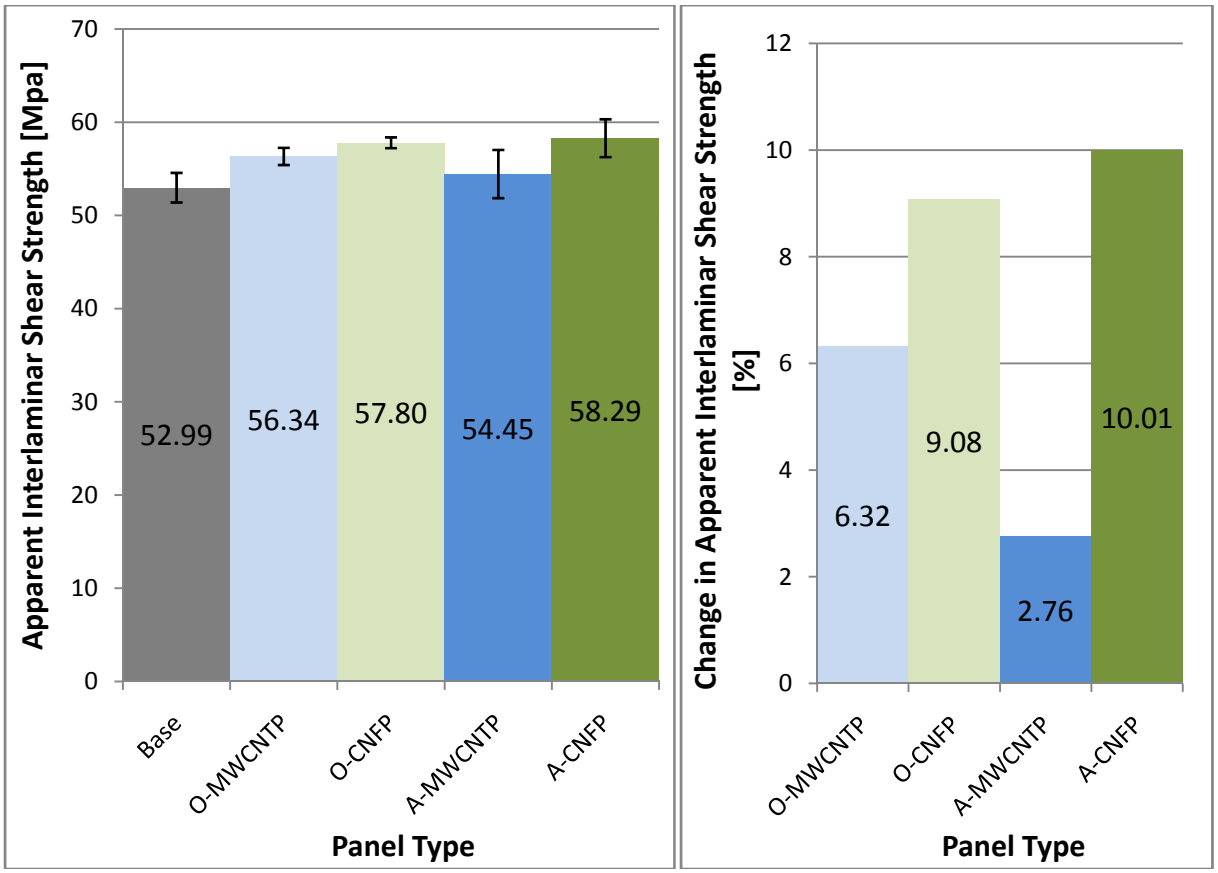

Figure 47. Left: Apparent interlaminar shear strength of nanocomposite panels manufactured. Right: Change in apparent interlaminar shear strength for panels manufactured with respect to base panel. Error bars represent one standard deviation.

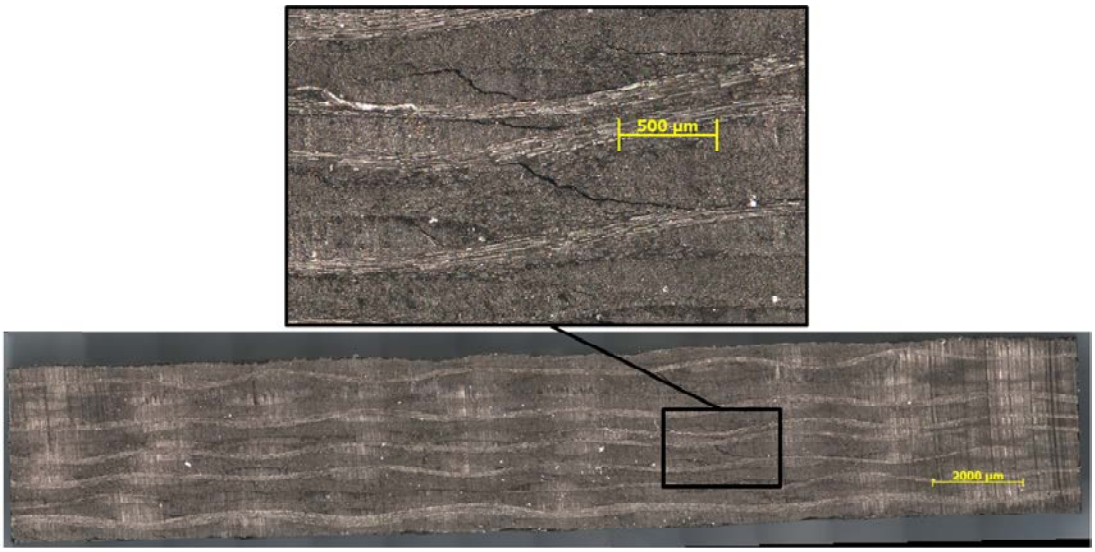

Figure 48. Short-beam shear specimen after testing showing interlaminar shear mode of failure. Specimen corresponds to the panel containing O-MWCNTs.

Investigation into the shear failure of the MRPCs was performed in order to understand the nanoparticles-reinforcement mechanism. For this purpose, the shear stress at the mid-plane of specimens of each panel was plotted against the displacement of the nose normalized with respect to the initial thickness of the sample. These graphs are shown in Figure 49 for specimens containing functionalized MWCNTs and in Figure 50 for specimens containing functionalized CNFs. (For illustrative purposes, the graph only contain plots for representative samples; all other plots have been included in Appendix D.) Both plots show a clear and distinctive behavior of the shear stress vs. displacement between the base panel, the panels containing O-MWCNTs/O-CNFs, and the panels containing A-MWCNT/A-CNFs. It is important to note that it was observed experimentally and also in the shear stress-displacement curves that the failure was sudden and not progressive, which suggests that a sudden drop in load during the test corresponds to increasing deformation at the mid-plane where eventual failure occurred. Comparing the plots containing O-MWCNTs/O-CNFs with respect to the base panel, three observations can be made: (i) increase in the ILSS, (ii) slight increase of shear stiffness of the specimen, and (iii) increase in toughness of the material. On the other hand, for both specimens containing A-MWCNTs and A-CNFs, a significant increase in shear stiffness and decrease in toughness was obtained, as compared to the base panel and the panels containing O-MWCNTs/O-CNFs. The increase in shear stiffness for A-MWCNT/A-CNF is 2.5–3.5 fold with respect to the base and O-MWCNTs/-CNFs panels. These results suggest that amine functionalized carbon nanoparticles interact better with the resin than oxidized carbon nanoparticles. This higher interaction might be due to covalent bonding between the epoxide groups of the resin system and the amine groups grafted to the MWCNTs/CNFs. Also, mechanical interlocking of the A-MWCNTs/A-CNFs with the matrix of the resin system is

expected to occur in both panels due to the fact that ethylenediamine is a longer functional group than the carboxylic acid groups of the O-MWCNTs/O-CNFs.

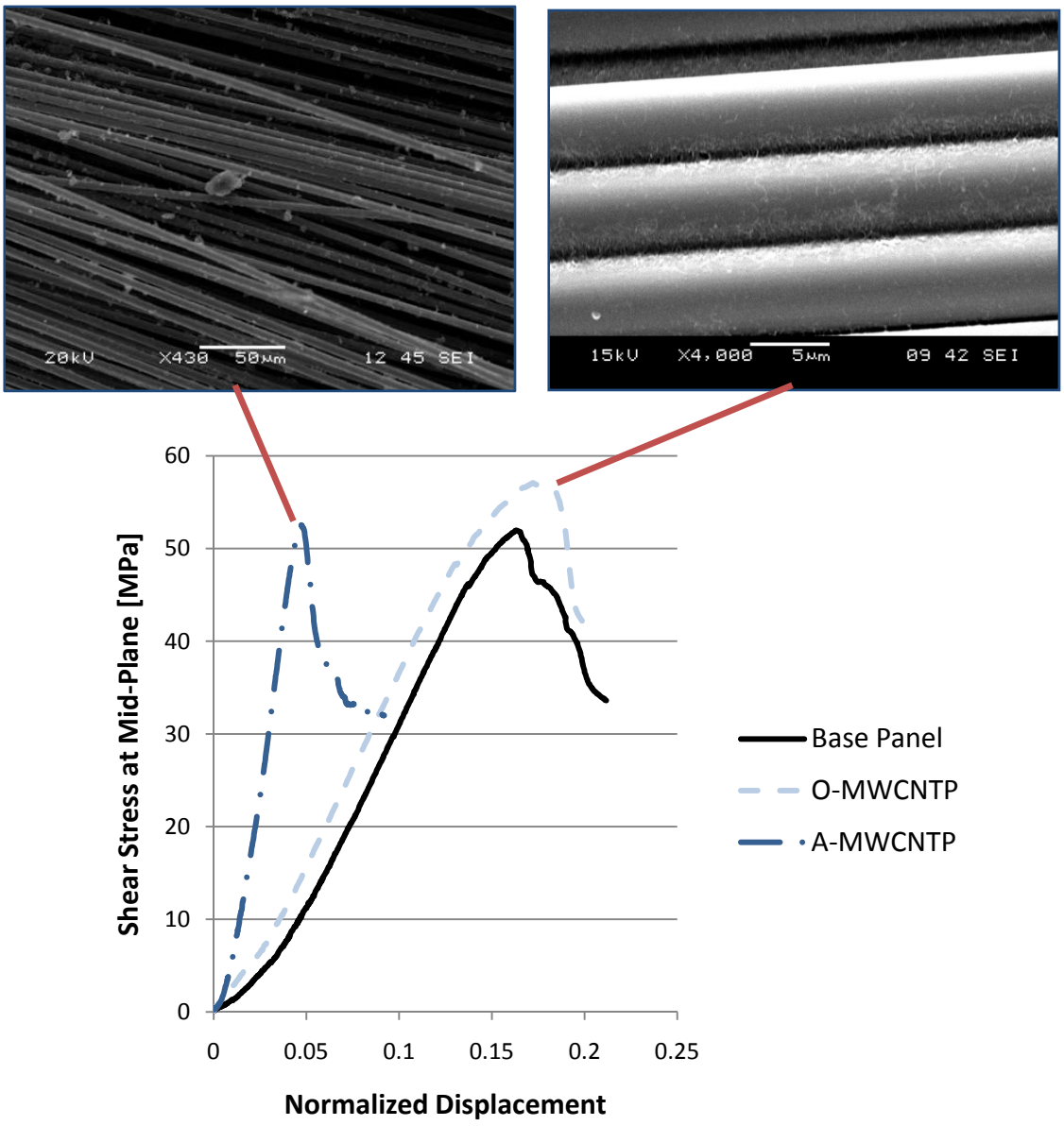

Figure 49. Shear stress at mid-plane for specimens containing functionalized MWCNTs during short-beam shear tests. SEM images correspond to multiscale carbon fiber layers representative of specimens tested.

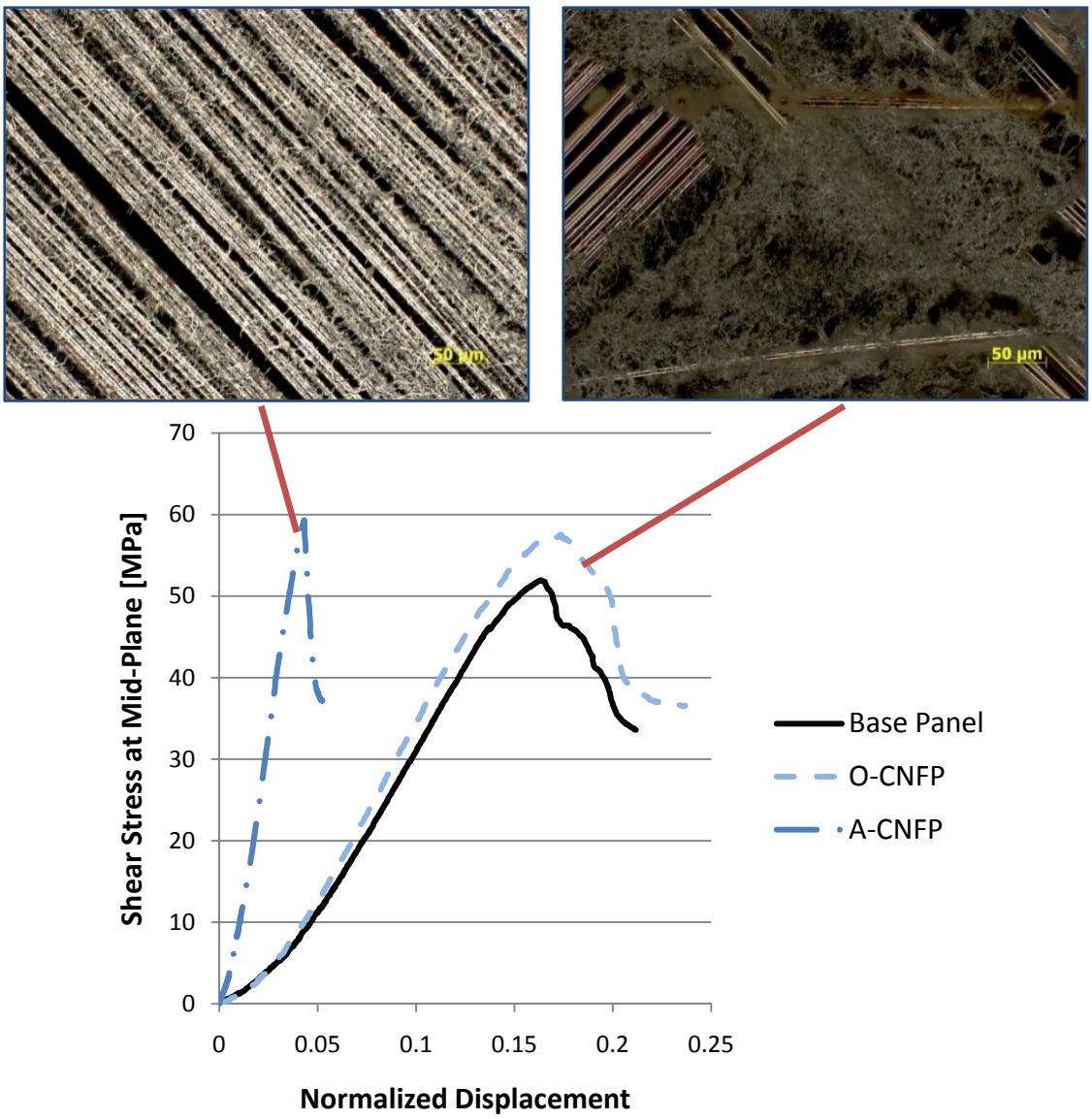

Figure 50. Shear stress at mid-plane for specimens containing functionalized CNFs. Optical microscopy images correspond to multiscale carbon fiber layers representative of specimens tested.

Examination of the fracture surface at high magnification was performed in order to obtain information regarding the reinforcement mechanism. The first observation from the SEM images taken of the fracture surface of the samples containing O-MWCNTs and O-CNFs is that the surface roughness of the fibers closer to the failure crack was higher for all panels containing carbon nanomaterials (Figure 51). Surface roughness of the base panel was very clean whereas

for the panels with oxidized carbon nanomaterials, the surface contains residues of resin and nanoparticles. This surface roughness of the fiber leads to mechanical interlocking of the particles, which in turn could explain the increase in mechanical properties for all samples with nanomaterials. This observation suggests that the failure for the base panel is due to adhesion (detachment of the resin from the fiber), whereas for the panels with CNFs, it is a combination of adhesion and also resin breakage away from the fiber. This is in agreement with a report by Upadhyaya and Tsakiropoulos [151] who suggested that if the surfaces of the fibers are clean of resin after failure, then the failure is dominated by the adhesion of the matrix to the fiber. The authors also suggested that increase in ILSS can be attained if the failure is away from the fiber. The second observation from the SEM images is that the fissure on the fracture surface for the base panel is less pronounced and more spread in the through-thickness direction than for the panels with nanoparticles, where the crack is more defined and pronounced and not seen to be spread through the thickness of the panel.

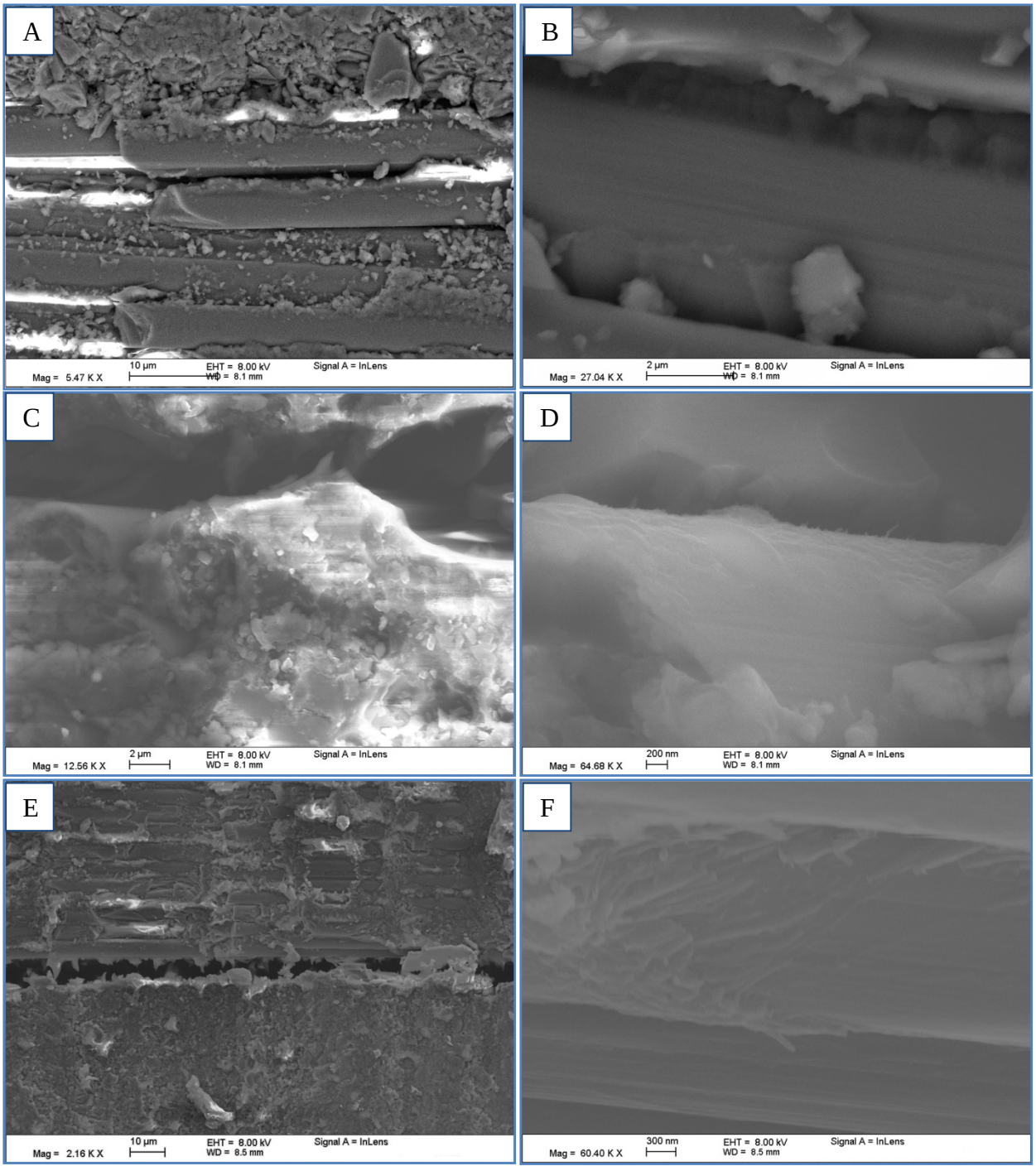

Figure 51. A and B: SEM images of fracture surface of SBS specimens for base panel. C and D: SEM images of fracture surface of SBS specimens for panel containing O-MWCNTs. E and F: SEM images of fracture surface of SBS specimens for panel containing O-CNFs.

Further examination of the fracture surface at higher magnification shows that, upon loading of the sample, O-MWCNTs and O-CNFs tend to slide away from the matrix, whereas A-

CNF has higher interaction with the resin. The O-MWCNTs and O-CNFs are shown to be protruding from the surface of the fiber and matrix, with evidence of sliding and finally detaching from the matrix. Conversely, the A-CNF extends from one fiber to the other without breakage, which is evidence of higher interaction between the A-CNF and the other phases of the MRPC. This effect is seen in Figure 52. These last images support the suggested reinforcing mechanism by fiber bridging within the surface fracture of the specimen. From these results it is also suggested that further increase in the fiber/matrix interface could be obtained by transferring more load to the carbon fiber via direct bonding of the nanomaterials with the microfiber (no sizing) and the matrix system.

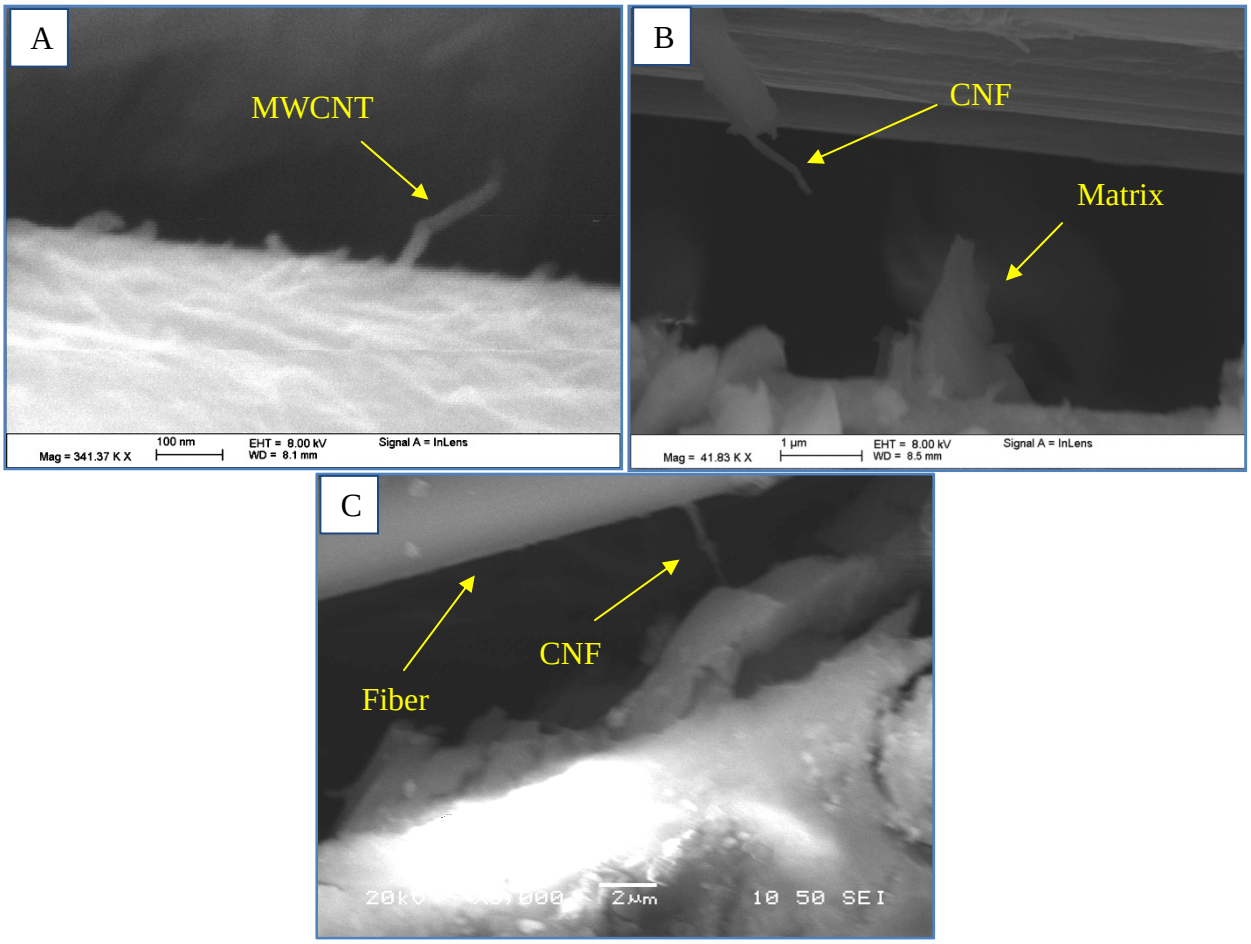

Figure 52. SEM images of fracture surfaces of short-beam shear strength specimens obtained from panel with O-MWCNTs (A), O-CNFs (B), and A-CNFs (C).

Based on the data and images obtained for the MRPCs containing A-MWCNTs and A-CNFs, the reinforcing mechanism is attributed to high interaction of the amine groups with the resin system and mechanical interlocking. In previous reports, it has been shown that amine-functionalized CNTs and CNFs mixed in polymer resins can provide higher reinforcement than pristine nanomaterials due to a significant increase in load transfer [20, 152]. After deposition of the A-MWCNTs/A-CNFs onto the carbon fiber layers and injection of the epoxy-based resin system, the particles are expected to be completely wetted by the resin system and in close contact with the resin and sizing of the carbon fibers. Then, during curing of the nanocomposite, the amine groups grafted on the wall of the carbon nanomaterials could react with the resin and also interlock with the matrix. This type of arrangement is seen in Figure 46 where the A-CNFs are wrapped around several carbon fibers and in contact with adjacent carbon fibers. After curing, this creates a reinforcement network between fibers and layers which leads to fiber bridging in the in-plane as well as out-of-plane direction. As such, when the carbon fiber layers are loaded and try to slide with respect to each other, the movement is restricted by the A-MWCNTs/A-CNFs already in close contact with the matrix and the adjacent carbon fiber layers, enabling load transfer between the phases of the MRPC.

4.3.2.2 Compressive Strength

Compressive strength of the samples containing O-MWCNTs and O-CNFs did not significantly change with respect to the base panel: an increase of 4.38% and 2.69% was obtained for O-MWCNTP and O-CNFP, respectively. On the other hand, an increase of 15.06% and 12.40% in compressive strength was attained for the panels containing MRFs with A-MWCNTs and A-CNFs, respectively (Figure 53). All specimens failed either by shear or delamination of the specimen which validates the data obtained for the tests. These two types of

failure mechanisms are illustrated in Figure 54 for representative samples. Note that, as in the case of ILSS, no relation was found between compressive strength and fiber volume fraction (Appendix C). The increase in compressive strength is attributed to the increase in shear stiffness of samples containing A-MWCNT/A-CNF, which prevents the carbon fibers from buckling prematurely. The increase in shear stiffness was demonstrated in the shear stress vs. displacement curves obtained from ILSS. Evidence of this reinforcement arrangement can also be explained by observing the optical images of A-CNF in the nanocomposite panel (Figure 46). From the images, it can be seen that the nanomaterial is able to extend and touch other fibers, which leads to load transfer between fibers.

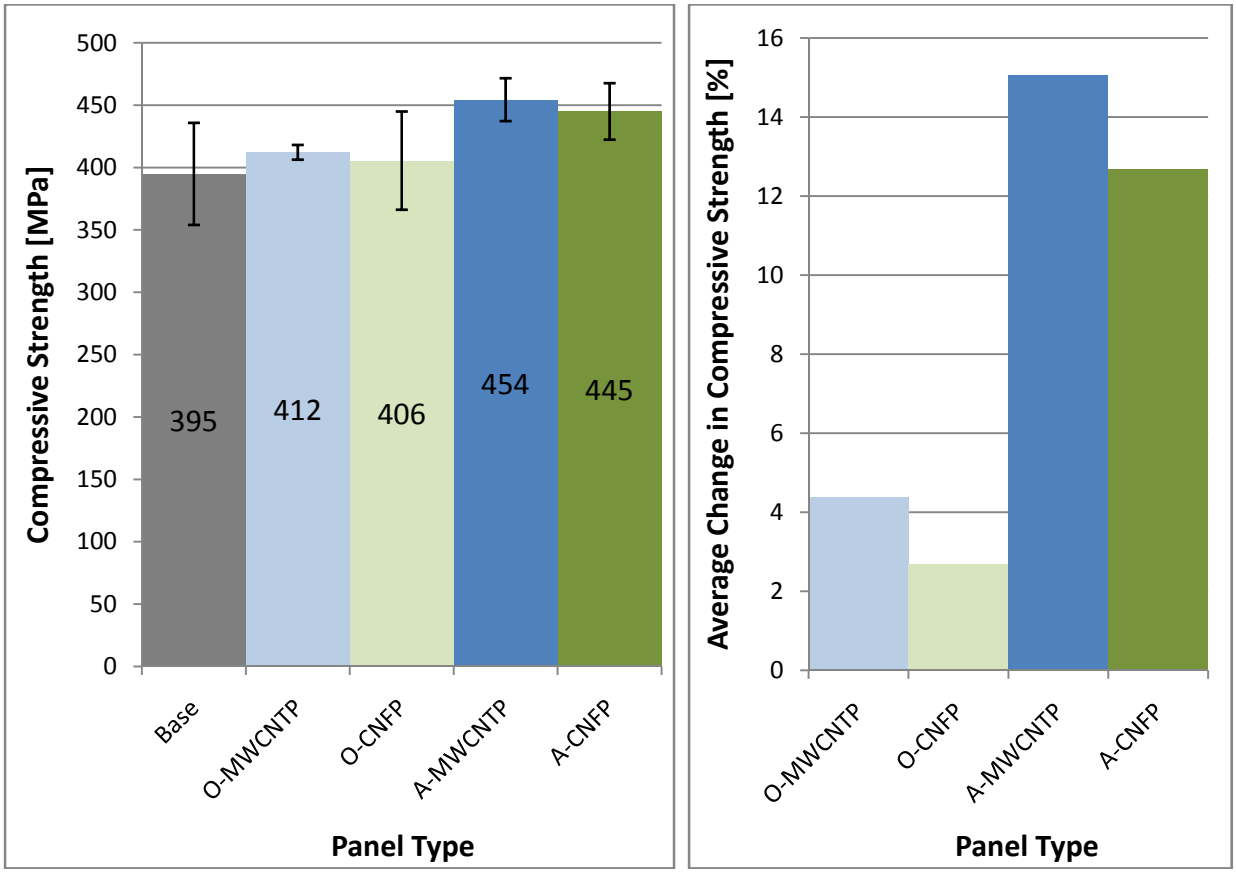

Figure 53. Left: Compressive strength of nanocomposite panels manufactured. Right: Change in compressive strength for panels manufactured with respect to base panel. Error bars represent one standard deviation.

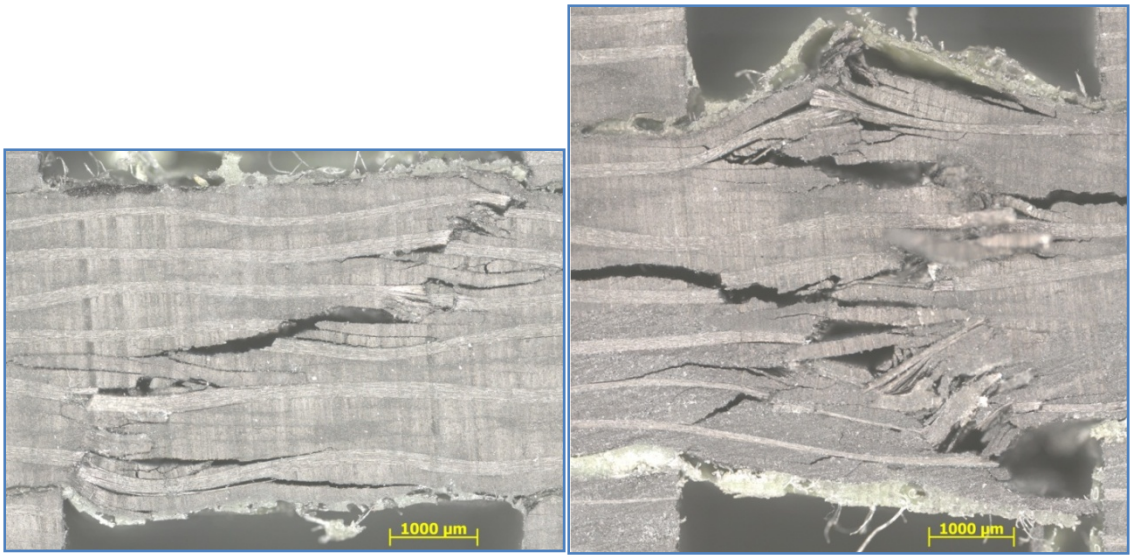

Figure 54. Failure mechanisms for compression strength tests for specimens containing O-MWCNTs. Left: Shear failure. Right: Delamination failure.

It is important to note that the increase in strength for the panel made with A-MWCNT and A-CNF was achieved by adding nanomaterials only to the carbon fiber layers. In a study by Iwahori et al. [19], an increase of 15% in compressive strength was achieved when 5 wt.% of cup-stacked carbon nanofibers was added to the resin. These authors noted manufacturing difficulties regarding the approach taken, including increase in viscosity and void formation. The increase in interlaminar shear strength and compressive strength reported herein were attained by only adding low amount of carbon nanomaterials (~0.5wt.%–1wt.%) without having those manufacturing difficulties in a process that can be scaled to manufacturing of larger parts.

4.3.2.3 Mechanical Properties of Multiscale-Reinforced Composites with Unsized Preforms

In order to investigate the effect of sizing on the process and properties of MRPCs manufactured following the approach described herein, an panel containing unsized carbon fiber layers with A-CNF deposited on their surfaces was manufactured. The reason for choosing A-CNFs is that they provided the highest increase in ILSS and shear stiffness of MRPC.

To remove the sizing, the following methodology was employed. Each layer of the preform was soaked in acetone for 20 minutes and washed. After washing, the layers were dried in an oven at 65°C for 60 minutes. Then, in order to ensure complete removal of the sizing, each layer was heated to 500°C for 30 minutes. After removing the sizing, it was noticed that the layer became significantly more flexible than the layers containing sizing. Deposition of the A-CNF was carried out in the same way as with sized fibers. SEM images before and after EPD of A-CNF onto unsized carbon fiber layers revealed individual and uniform deposition of the nanoparticles as in the case of sized carbon fiber layers (Figure 55).

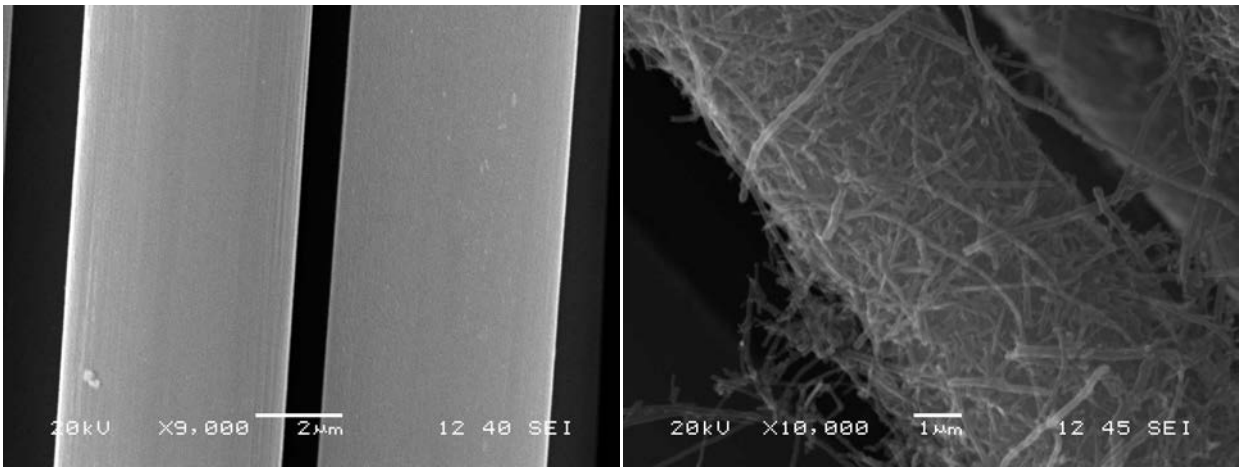

Figure 55. SEM images of carbon fiber layers before and after EPD of A-CNF onto unsized carbon fiber layers.

Results from short-beam shear test showed an increase of 12.43% in ILSS, which is the highest increase for all panels manufactured. In terms of compressive strength, an increase of approximately 11% was attained for this panel. This strength is close to the values obtained for A-CNF with sized fibers. ILSS and compressive strength values for this panel are shown in Figure 56. It is interesting to note that the COV for the base panel as well as the O-CNFP is similar with values circa 10%. Conversely, for the panel made with A-CNF deposition onto sized carbon fibers, it is noted that not only the compressive strength increased but also the COV

decreased by half —5.05% compared to ~10%— (see Figure 53). This finding indicates that panels with A-CNF and sizing have more consistent properties than all other panels. On the other hand, the panel made with A-CNF and no sizing also showed a higher compressive strength than the base panel although the COV remained at around 13%. This effect could be due to degradation of the carbon fibers when they were subjected to removal of sizing. Exposure carbon fibers to thermal cycles in the presence of air increases the oxygen content and also reduce its strength by pitting of the fibers.

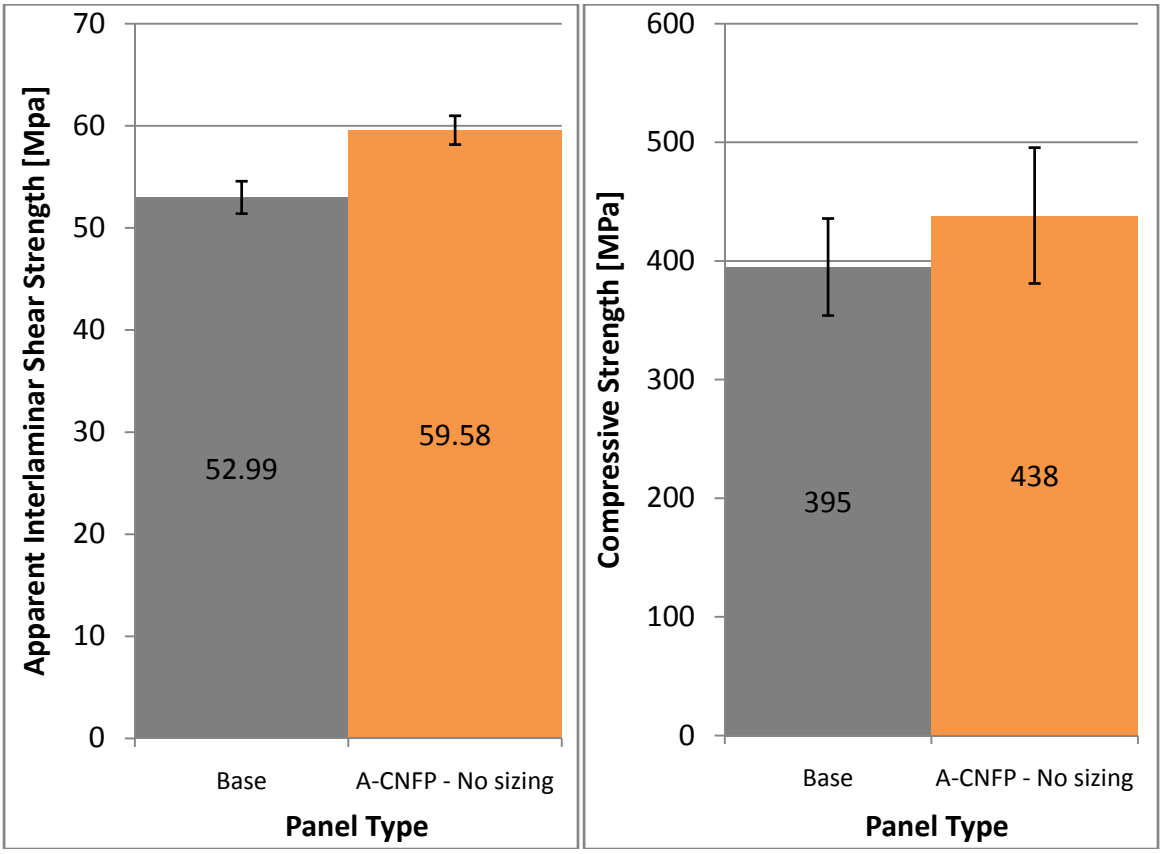

Figure 56. Interlaminar shear strength (left) and compressive strength (right) values for base panel and multiscale-reinforced composites with unsized carbon fiber layers containing A-CNFs. Error bars indicate one standard deviation.

Investigation into the mechanics of deformation of the MRPC was also performed for the unsized panel with A-CNF to understand the reinforcement mechanism. As in the case of sized carbon fiber layers, the shear stress at the mid-plane of the SBS specimens for each panel was

plotted against the displacement of the nose normalized with respect to the initial thickness of the specimen. These plots show that A-CNF in unsized fibers behave in the same manner as A-CNF in sized fibers (Figure 57). (For illustrative purposes, only one representative specimen is shown; plots for all other specimens are shown in Appendix D.) The shear stiffness of the specimen for the unsized carbon fiber layers with A-CNF is similar to the stiffness of the specimens of sized carbon fiber layers with A-CNF. This increase is approximately 4 fold, as compared to the base panel. This indicates that the mechanism of load transfer is similar for sized and unsized MRFs. The fracture surfaces for SBS specimens for both samples show similar roughness as for O-MWCNTs/O-CNFs, which suggest that the increase in strength and failure mechanisms occurs in a similar manner: increase in surface roughness with failure in the matrix and also in the fiber/matrix interface. The fracture surfaces for specimens with A-CNF on sized and unsized carbon fiber layers are shown in Figure 58.

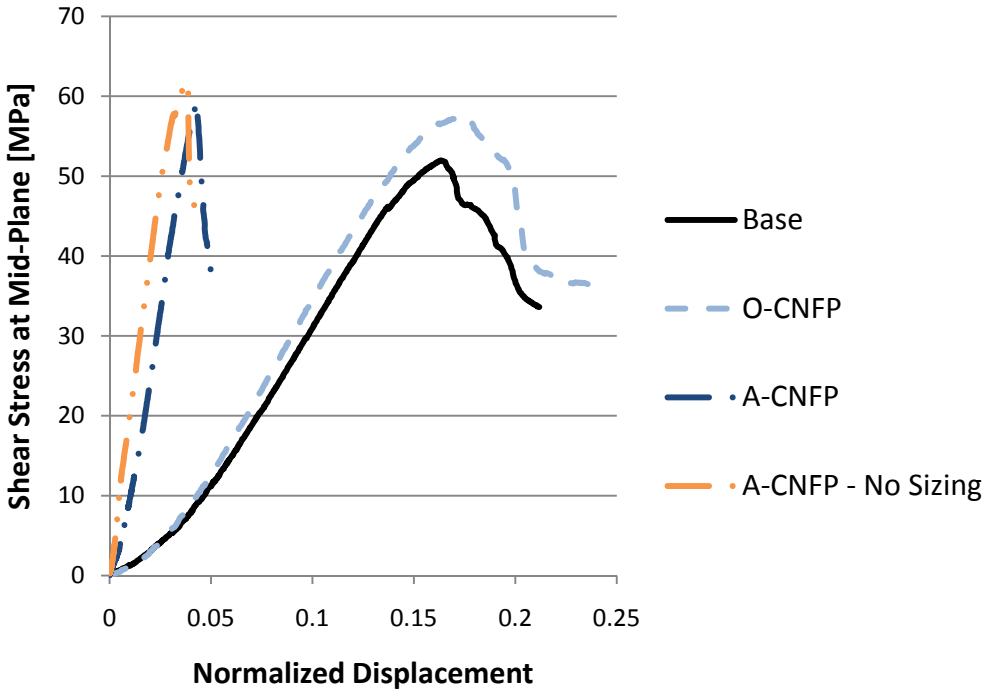

Figure 57. Shear stress at mid-plane for specimens containing unsized carbon fiber layer with A-CNFs.

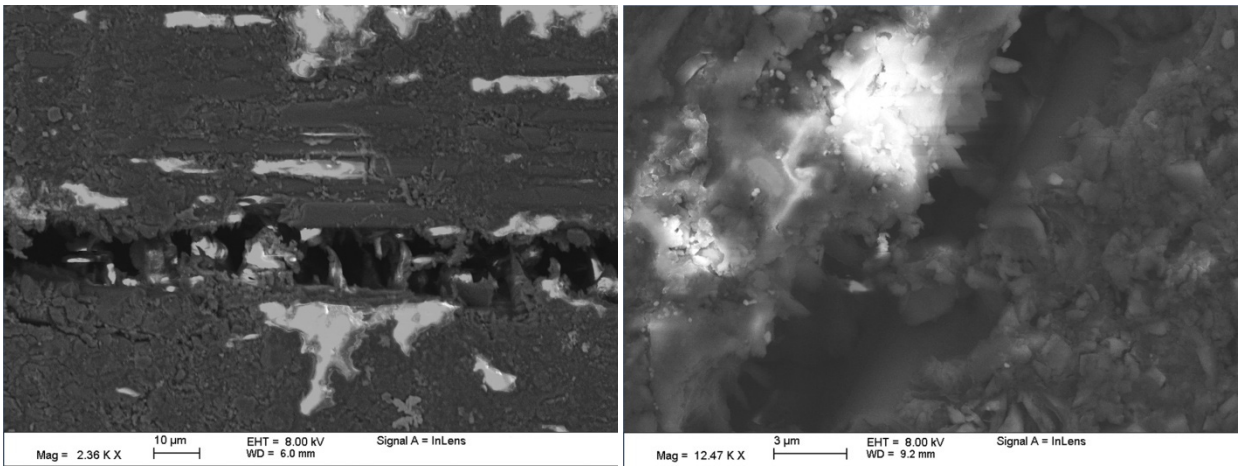

Figure 58. Fracture surfaces of SBS specimens obtained from panels with A-CNF in sized (left) and unsized (right) carbon fibers.

In order to further understand the reinforcement mechanisms of the nanoparticles, examination of the A-CNF/matrix interface was performed using electron microscopy. SEM images at higher magnification show a CNF pulled away from the resin with matrix attached to its surface (Figure 59). This suggests that the A-CNF does not slide from the matrix but instead has high interaction with the matrix and makes the resin break away from its original position upon application of the load. This observation is in agreement with the fact that specimens with A-MWCNTs and A-CNFs have higher shear stiffness than the base panel and the panels with O-MWMCNTs/-CNFs due to the interaction of the A-CNF nanoparticle with the epoxy-based resin system. This finding is contrary to the case of O-MWCNTs and O-CNFs, where it can be seen that the nanoparticles are pulled away from the matrix with no evidence of high interaction between matrix and nanoparticles.

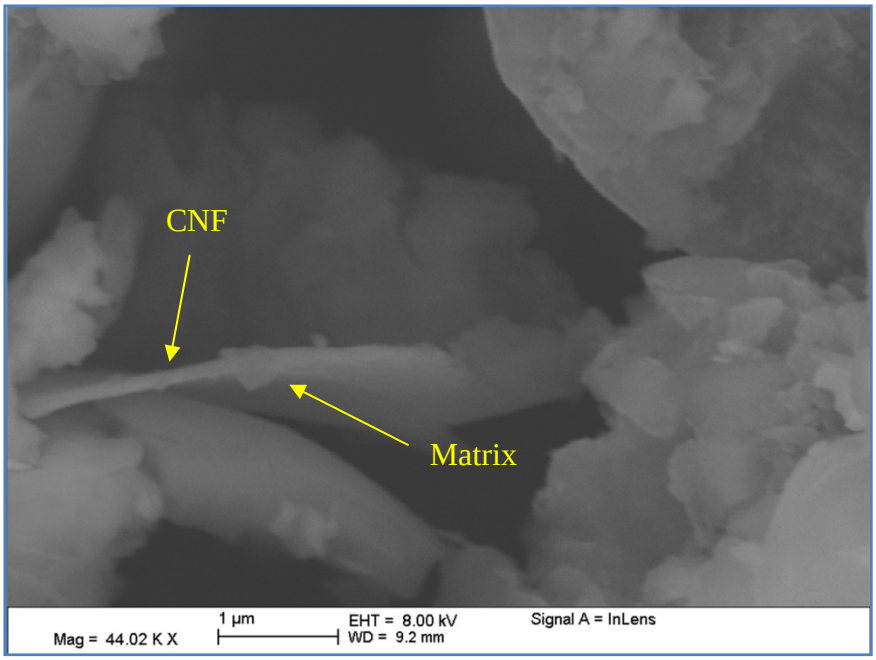

Figure 59. SEM image of fracture surface of SBS specimen obtained from the panel containing A-CNF on unsized carbon fibers.

4.3.3 Electrical Conductivity of Multiscale-Reinforced Polymer Composites

Measured values of through-plane electrical conductivity along with the standard deviation were obtained for all panels and shown in Figure 60. Electrical conductivity of all panels, except for the panel with A-CNF and no sizing, were found to be within the range of previously reported values for carbon nanotube/carbon fiber-reinforced polymer composites [129]. The variation in electrical conductivity of the aforementioned samples with respect to the base panel can be attributed to local changes in fiber volume fraction and also waviness of the carbon fiber layers. This indicates that low amounts of functionalized MWCNTs/CNFs can result in a significant increase in the mechanical properties but not necessarily in electrical properties.

The highest and most significant variation in electrical conductivity was obtained for the panel manufactured with A-CNF and no sizing on the carbon fibers. This panel had an increase in electrical conductivity of about 100%, as compared to the base panel. The electrical conductivity of fiber-reinforced composites depends on the ability of the electrons to travel

through the conductive phase, which in this case is the carbon fibers and the CNFs. It is apparent that the difference in electrical conductivity for the latter panel is due to the reduction in electrical resistance as a result of direct deposition of the A-CNF onto the surface of the carbon fiber (no sizing). Removal of the epoxy-based sizing increased the interaction between the A-CNF and the carbon fiber, thus making the panel less resistant to electron flow. Based on these results, it is envisioned that further increase in electrical conductivity could be gained by increasing the inter-ply and intra-ply bridging with a higher density of conductive nanomaterials.

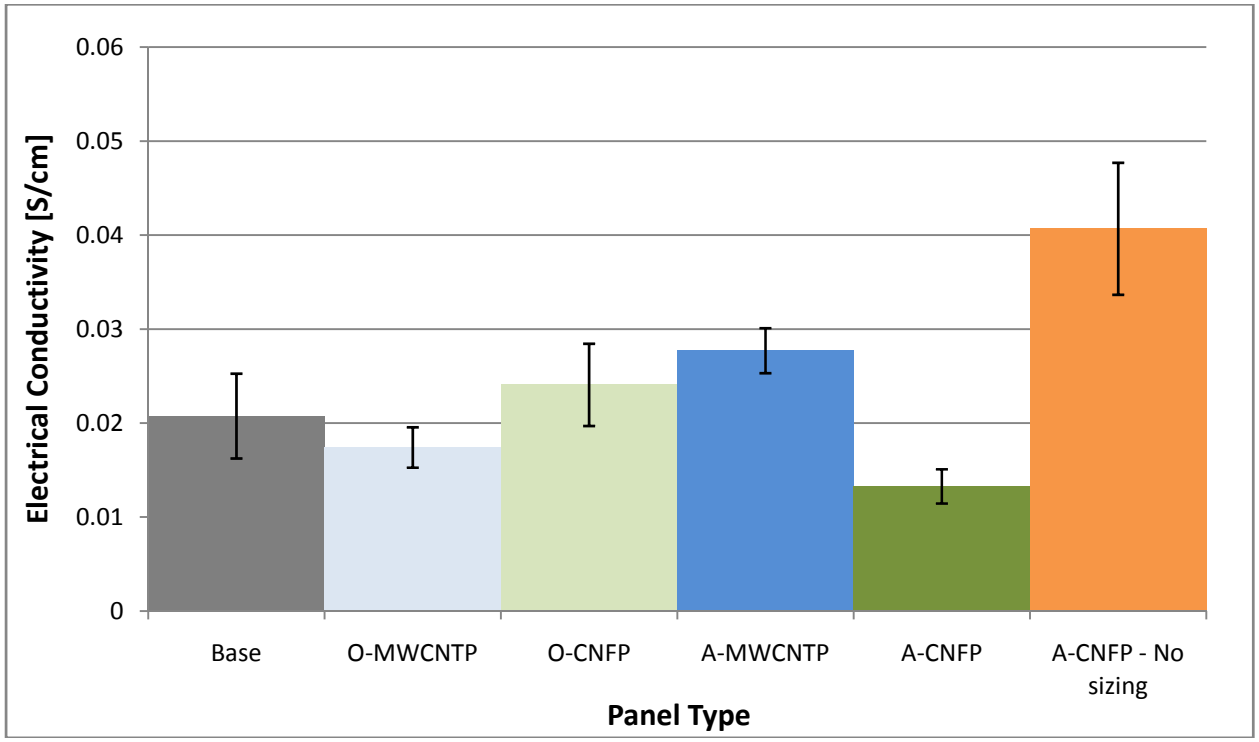

Figure 60. Through-plane electrical conductivity of MRPC panels manufactured measured using four-point probe method. Error bars represent one standard deviation.

4.4 Summary and Conclusions

In this study, multiscale-reinforced polymer composites containing carbon fiber layers with carboxylic acid- and amine-functionalized MWCNTs and CNFs were manufactured and characterized for interlaminar shear strength, shear stiffness, compressive strength, and through-plane electrical conductivity. Optical images of chemically etched samples obtained from the

MRPCs showed some level of agglomeration for O-CNF whereas individual and even distribution inside the part was observed for A-CNFs. Results from short-beam shear (SBS) strength tests showed an increase in ILSS of 6.32% and 9.08% for nanocomposites containing O-MWCNTs and O-CNFs, respectively, and 2.76% and 10.01% for panels containing A-MWCNTs and A-CNFs, respectively. Further investigation into SBS tests showed that MRPCs with carbon fiber layers containing A-MWCNTs/A-CNFs had an increase of 2.5–4x in shear stiffness with respect to the base panel and panels containing O-MWCNTs/O-CNFs. SEM images from the fracture surfaces showed O-MWCNTs and O-CNFs sliding from the matrix, whereas A-CNFs were seen to interact with the fibers and the matrix showing evidence of fiber bridging. These results lead to the conclusion that amine functional groups are able to transfer more load to the nanomaterials than carboxylic acid functional groups. No relation was found between ILSS or compressive strength with fiber volume fraction.

Compressive strength values showed that panels containing O-MWCNTs/O-CNFs did not significantly increase the compressive strength of the panels whereas A-MWCNTs and A-CNFs had an increase in compressive strength of 15.06% and 12.68%, respectively. These results were attributed to the increase in shear stiffness of the samples, which prevents the carbon fibers carrying the load to buckle prematurely. Electrical conductivity tests showed that removing the sizing of the carbon fiber layer and depositing the nanoparticles directly onto the surface of the carbon fibers had a significant impact on the electrical conductivity, increasing this value by 100% as compared to the base panel.

By adding carbon nanomaterials to carbon fiber layers as described in Chapter 3, MRPCs can be manufactured with higher interlaminar shear strength and compressive strength than the base panel. It is important to note that the increase of these properties was attained without

manufacturing difficulties, such as increase in viscosity and void formation in the nanocomposite parts, which are issues previously reported by other authors [19]. The coefficient of variation of the properties reported for the multiscale-reinforced composites were at the same level —in certain cases significantly lower— than that of the base material, leading to the conclusion that manufacturing MRPCs following the process described herein results in parts with consistent properties.

The local reinforcement in the fiber/matrix interface with A-MWCNTs/A-CNFs showed that these particles are able to increase the shear strength and stiffness of the panels. The increase in the mechanical properties was attributed to an increase in load transfer and strength at the fiber/matrix interface due to higher interaction of the amine groups with the resin system and also mechanical interlocking. From these results it is suggested that further increase in fiber/matrix interface strength could be obtained by transferring more load directly to the carbon fiber via bonding of the nanomaterials with the microfiber (no sizing) and the matrix system.

CHAPTER 5

CONCLUSIONS

Carbon nanotubes and carbon nanofibers have an exceptional combination of mechanical, electrical, and physical properties that make them ideal materials to be used as reinforcing nanoparticles for multiscale-reinforced polymer composites (MRPCs). In order to properly incorporate them into advanced composites, several manufacturing difficulties must be overcome. This research was aimed at obtaining fundamental understanding of the processing and properties of MRPCs manufactured following a scalable process. In this work, three major MRPC manufacturing challenges were addressed by developing a methodology to incorporate carbon nanoutubes/carbon nanofibers into advanced composites. This methodology consisted of two stages. In the first stage, multiscale-reinforcement fabrics (MRFs) were fabricated by depositing carboxylic acid- or amine-functionalized CNTs and CNFs on the surface of carbon fiber layers by electrophoretic deposition. In the second stage, the MRFs were stacked and assembled into preforms that were infused with an epoxy-amine resin system by resin injection molding to manufacture the final MRPCs.

By studying the deposition of carbon nanomaterials onto carbon fiber layers as described in this dissertation, it can be concluded that EPD is an effective method to deposit functionalized nanoparticles (O-MWCNTs, O-CNFs, and A-CNFs) onto complex-shaped substrates such as carbon fiber layers. The effectiveness of the deposition of the functionalized MWCNTs and CNFs was correlated to the stability of the particles. Electrophoretic mobility of the particles showed that all particles except A-MWCNTs were stable at pH of 6. From these results, it is suggested that the zeta potential of rod-like particle stability is in the limits of $\left|35 - 40\right|$ mV. The

main limitation of the EPD process is the time and electric field that the carbon fiber layers may undergo without excessive stiffening.

To study the effects of the prescribed method for adding carbon nanoparticles, MRPCs utilizing the resulting MRFs were manufactured and characterized for mechanical and electrical properties. Images from chemically etched samples showed some level of agglomeration for oxidized CNFs, and individual and uniform distribution for amidized CNFs. These results showed a direct correlation between the distribution before and after manufacturing of the MRPCs where no significant nanoparticle filtration or washing was observed. Results from short-beam shear tests indicated an increase in interlaminar shear strength for all MRPC panels manufactured. This was attributed to the increase in surface roughness of the fiber after EPD of the nanoparticles, fiber bridging, and mechanical interlocking. It was also found that the shear stiffness of panels containing A-MWCNTs/A-CNFs increased by 2.5–4x with respect to the base panel and panels with O-MWCNTs/O-CNFs. Investigation into the fracture surface led to the conclusion that amine functional groups are able to transfer more load to nanomaterials than carboxylic acid functional groups. O-MWCNTs and O-CNFs were observed to slide from the matrix whereas amine-functionalized nanoparticles attach to the matrix due to higher interaction with the epoxy-amine resin system. Compressive strength values showed that panels with A-MWCNTs and A-CNFs had a significant increase in compressive strength, whereas panels with O-MWCNTs/O-CNFs did not have significant increase. This was attributed to the increase in shear stiffness of A-MWNCTs/A-CNFs, which prevented the carbon fibers carrying the compressive load to buckle prematurely. Finally, through-plane electrical conductivity tests showed that removing the sizing of the carbon fiber layers and depositing the nanoparticles directly on the surface of the carbon fibers had a significant impact on electrical conductivity,

increasing its value by approximately 100%. Removal of the epoxy-based sizing increased the interaction between the A-CNF and the carbon fiber, thus making the panel less resistant to electron flow.

Through this investigation it was shown that MRPCs can be manufactured with higher interlaminar shear strength and compressive strength than the base panel. It is important to note that these property increases were attained without manufacturing difficulties such as increase in viscosity and void formation. The highest increase in mechanical properties was attributed to an increase in load transfer and strength at the fiber/matrix interface due to high interaction of the amine groups with the resin system and also mechanical interlocking. From these results, it is clear that amine functional groups provide a higher interaction level between the nanoparticles and the epoxy-based resin system than oxygen containing groups. Another benefit of the MRPC process is the consistency of the properties of the resulting parts. This was evidenced by the low coefficient of variation of the sets of specimens tested.

Although CNTs and CNFs have exceptional properties, it is not ascertained whether these properties were completely harnessed even for the amine-functionalized nanoparticles. Fracture surface observations suggested that the failure for the base panel was only due to detachment of the resin from the fiber, whereas for the panels with nanomaterials, it was a combination of this detachment and resin breakage away from the fiber. Although higher properties were attained for the MRPC, it is suggested that further increase in the fiber/matrix interface could be obtained by transferring more load directly to the carbon fibers via covalent bonding of the nanomaterials with the microfiber (no sizing) and the matrix system. In this way, higher levels of interaction can be attained between the nanomaterials and the fibers leading to a higher-strength three-dimensional reinforcement network.

Manufacturing of MRPCs containing MWCNTs and CNFs holds great promise for the future. The realization of MRPCs with optimal properties can only be achieved by overcoming current manufacturing issues and studying the relation between properties and enhancement mechanisms. The findings reported herein can be extended to other fiber-reinforced systems where microfiber/nanoparticle/matrix relationships are fundamental in order to further advance manufacturing of high-performance materials.

LIST OF REFERENCES

LIST OF REFERENCES

[1] Greenhalgh ES, *Failure analysis and fractography of polymer composites*. 2009, Boca Raton, FL: CRC Press LLC. 595.

[2] Kim M, Y-B Park, OI Okoli, and C Zhang, "Processing, characterization, and modeling of carbon nanotube-reinforced multiscale composites." *Composites Science and Technology*, 2009. 69(3-4): pp. 335-342.

[3] Green KJ, DR Dean, UK Vaidya, and E Nyairo, "Multiscale fiber reinforced composites based on a carbon nanofiber/epoxy nanophased polymer matrix: Synthesis, mechanical, and thermomechanical behavior." *Composites Part A: Applied Science and Manufacturing*, 2009. 40(9): pp. 1470-1475.

[4] Qiu J, C Zhang, B Wang, and R Liang, "Carbon nanotube integrated multifunctional multiscale composites." *Nanotechnology*, 2007. 18(27).

[5] Fan Z, K-T Hsiao, and SG Advani, "Experimental investigation of dispersion during flow of multi-walled carbon nanotube/polymer suspension in fibrous porous media." *Carbon*, 2004. 42(4): pp. 871-876.

[6] Sadeghian R, H Kuang-Ting, S Gangireddy, and B Minaie, "Manufacturing carbon nanofibers toughened polyester/glass fiber composites using vacuum assisted resin transfer molding for enhancing the mode-I delamination resistance." *Composites Part A (Applied Science and Manufacturing)*, 2006. 37(10): pp. 1787-95.

[7] Song YS and JR Youn, "Influence of dispersion states of carbon nanotubes on physical properties of epoxy nanocomposites." *Carbon*, 2005. 43(7): pp. 1378-1385.

[8] Spitalsky Z, D Tasis, K Papagelis, and C Galiotis, "Carbon Nanotube-Polymer Composites: Chemistry, Processing, Mechanical and Electrical Properties." *Progress in Polymer Science*. In Press, Accepted Manuscript.

[9] Bal S, "Influence of dispersion states of carbon nanotubes on mechanical and electrical properties of epoxy nanocomposites." *Journal of Scientific and Industrial Research*, 2007. 66(9): pp. 752-6.

[10] Uddin MF and CT Sun, "Improved dispersion and mechanical properties of hybrid nanocomposites." *Composites Science and Technology*. 70(2): pp. 223-230.

[11] Fiedler B, FH Gojny, MHG Wichmann, MCM Nolte, and K Schulte, "Fundamental aspects of nano-reinforced composites." *Composites Science and Technology*, 2006. 66(16): pp. 3115-3125.

[12] Prolongo SG, M Buron, MR Gude, R Chaos-Moran, M Campo, and A Urena, "Effects of dispersion techniques of carbon nanofibers on the thermo-physical properties of epoxy nanocomposites." *Composites Science and Technology*, 2008. 68(13): pp. 2722-2730.

[13] Ajayan PM, LS Schadler, C Giannaris, and A Rubio, "Single-Walled Carbon Nanotube-Polymer Composites: Strength and Weakness." *Advanced Materials*, 2000. 12(10): pp. 750-753.

[14] Gou J, Z Liang, C Zhang, and B Wang, "Computational analysis of effect of single-walled carbon nanotube rope on molecular interaction and load transfer of nanocomposites." *Composites Part B: Engineering*, 2005. 36(6-7): pp. 524-533.

[15] Graff RA, JP Swanson, PW Barone, S Baik, DA Heller, and MS Strano, "Achieving individual-nanotube dispersion at high loading in single-walled carbon nanotube composites." *Advanced Materials*, 2005. 17(8): pp. 980-984.

[16] Ma C, W Zhang, Y Zhu, L Ji, R Zhang, N Koratkar, and J Liang, "Alignment and dispersion of functionalized carbon nanotubes in polymer composites induced by an electric field." *Carbon*, 2008. 46(4): pp. 706-710.

[17] Yan G, MY Liu, J Li, XM Shi, and JK Kim, "Effects of surfactant treatment on mechanical and electrical properties of CNT/epoxy nanocomposites." *Composites Part A (Applied Science and Manufacturing)*, 2008.

[18] Cui S, R Canet, A Derre, M Couzi, and P Delhaes, "Characterization of multiwall carbon nanotubes and influence of surfactant in the nanocomposite processing." *Carbon*, 2003. 41(4): pp. 797-809.

[19] Iwahori Y, S Ishiwata, T Sumizawa, and T Ishikawa, "Mechanical properties improvements in two-phase and three-phase composites using carbon nano-fiber dispersed resin." *Composites Part A: Applied Science and Manufacturing*, 2005. 36(10): pp. 1430-1439.

[20] Wang S, R Liang, B Wang, and C Zhang, "Load-transfer in functionalized carbon nanotubes/polymer composites." *Chemical Physics Letters*, 2008. 457(4-6): pp. 371-375.

[21] Gou J and K Anumakonda. "Molecular dynamics simulations of interactions at the interface between functionalized carbon nanofibers and polymer resins. 2006. Chicago, IL, United States: American Society of Mechanical Engineers, New York, NY 10016-5990, United States.

[22] Shen J, W Huang, L Wu, Y Hu, and M Ye, "Thermo-physical properties of epoxy nanocomposites reinforced with amino-functionalized multi-walled carbon nanotubes." *Composites Part A: Applied Science and Manufacturing*, 2007. 38(5): pp. 1331-1336.

[23] Tan H, LY Jiang, Y Huang, B Liu, and KC Hwang, "The effect of van der Waals-based interface cohesive law on carbon nanotube-reinforced composite materials." *Composites Science and Technology*, 2007. 67(14): pp. 2941-6.

[24] Warrier A, A Godara, O Rochez, L Mezzo, F Luizi, L Gorbatikh, SV Lomov, AW VanVuure, and I Verpoest, "The effect of adding carbon nanotubes to glass/epoxy composites in the fibre sizing and/or the matrix." *Composites Part A: Applied Science and Manufacturing*, 2010. 41(4): pp. 532-538.

[25] Ma P-C, S-Y Mo, B-Z Tang, and J-K Kim, "Dispersion, interfacial interaction and re-agglomeration of functionalized carbon nanotubes in epoxy composites." *Carbon*. In Press, Accepted Manuscript.

[26] Li X and MR Coleman, "Functionalization of carbon nanofibers with diamine and polyimide oligmer." *Carbon*, 2008. 46(8): pp. 1115-1125.

[27] Oberlin A, M Endo, and T Koyama, "Filamentous growth of carbon through benzene decomposition." *Journal of Crystal Growth*, 1976. 32(3): pp. 335-349.

[28] Monthioux M and VL Kuznetsov, "Who should be given the credit for the discovery of carbon nanotubes?" *Carbon*, 2006. 44(9): pp. 1621-1623.

[29] Iijima S, "Helical microtubules of graphitic carbon." *Nature*, 1991. 354(6348): pp. 56-58.

[30] Iijima S and T Ichihashi, "Single-shell carbon nanotubes of 1-nm diameter." *Nature*, 1993. 363(6430): pp. 603-605.

[31] Bethune DS, CH Klang, MS de Vries, G Gorman, R Savoy, J Vazquez, and R Beyers, "Cobalt-catalysed growth of carbon nanotubes with single-atomic-layer walls." *Nature*, 1993. 363(6430): pp. 605-607.

[32] Peng B, M Locascio, P Zapol, S Li, SL Mielke, GC Schatz, and HD Espinosa, "Measurements of near-ultimate strength for multiwalled carbon nanotubes and irradiation-induced crosslinking improvements." *Nat Nano*, 2008. 3(10): pp. 626-631.

[33] Terrones M, "SCIENCE AND TECHNOLOGY OF THE TWENTY-FIRST CENTURY: Synthesis, Properties, and Applications of Carbon Nanotubes." *Annual Review of Materials Research*, 2003. 33(1): pp. 419-501.

[34] Thostenson ET, Z Ren, and T-W Chou, "Advances in the science and technology of carbon nanotubes and their composites: a review." *Composites Science and Technology*, 2001. 61(13): pp. 1899-1912.

[35] Vaccarini L, C Goze, L Henrard, E Hernández, P Bernier, and A Rubio, "Mechanical and electronic properties of carbon and boron-nitride nanotubes." *Carbon*, 2000. 38(11-12): pp. 1681-1690.

[36] Yakobson BI, CJ Brabec, and J Bernholc, "Nanomechanics of Carbon Tubes: Instabilities beyond Linear Response." *Physical Review Letters*, 1996. 76(14): pp. 2511.

[37] Dresselhaus MS, G Dresselhaus, JC Charlier, and E Hernandez, "Electronic, thermal and mechanical properties of carbon nanotubes." *Philosophical Transactions of the Royal Society London, Series A (Mathematical, Physical and Engineering Sciences)*, 2004. 362(1823): pp. 2065-98.

[38] Nardelli MB, BI Yakobson, and J Bernholc, "Brittle and Ductile Behavior in Carbon Nanotubes." *Physical Review Letters*, 1998. 81(21): pp. 4656.

[39] Guzman ME, "Enhancement of Mechanical Properties of a Potting Compound by Addition of Functionalized Single-Walled and Multi-Walled Carbon Nanotubes," in *Mechanical Engineering*. 2010, Wichita State University: Wichita. p. 81.

[40] Journet C, WK Maser, P Bernier, A Loiseau, ML de la Chapelle, S Lefrant, P Deniard, R Lee, and JE Fischer, "Large-scale production of single-walled carbon nanotubes by the electric-arc technique." *Nature*, 1997. 388(6644): pp. 756-758.

[41] Lv X, F Du, Y Ma, Q Wu, and Y Chen, "Synthesis of high quality single-walled carbon nanotubes at large scale by electric arc using metal compounds." *Carbon*, 2005. 43(9): pp. 2020-2022.

[42] Guo T, P Nikolaev, AG Rinzler, D Tomanek, DT Colbert, and RE Smalley, "Self-Assembly of Tubular Fullerenes." *The Journal of Physical Chemistry*, 1995. 99(27): pp. 10694-10697.

[43] Thess A, R Lee, P Nikolaev, H Dai, P Petit, J Robert, C Xu, YH Lee, SG Kim, AG Rinzler, DT Colbert, GE Scuseria, D Tomanek, JE Fischer, and RE Smalley, "Crystalline Ropes of Metallic Carbon Nanotubes." *Science*, 1996. 273(5274): pp. 483-487.

[44] Eklund PC, BK Pradhan, UJ Kim, Q Xiong, JE Fischer, AD Friedman, BC Holloway, K Jordan, and MW Smith, "Large-Scale Production of Single-Walled Carbon Nanotubes Using Ultrafast Pulses from a Free Electron Laser." *Nano Letters*, 2002. 2(6): pp. 561-566.

[45] Nikolaev P, MJ Bronikowski, RK Bradley, F Rohmund, DT Colbert, KA Smith, and RE Smalley, "Gas-phase catalytic growth of single-walled carbon nanotubes from carbon monoxide." *Chemical Physics Letters*, 1999. 313(1-2): pp. 91-97.

[46] Meyyappan M and et al., "Carbon nanotube growth by PECVD: a review." *Plasma Sources Science and Technology*, 2003. 12(2): pp. 205.

[47] Öncel Ç and Y Yürüm, "Carbon Nanotube Synthesis via the Catalytic CVD Method: A Review on the Effect of Reaction Parameters." *Fullerenes, Nanotubes and Carbon Nanostructures*, 2006. 14(1): pp. 17 - 37.

[48] Cheung CL, A Kurtz, H Park, and CM Lieber, "Diameter-Controlled Synthesis of Carbon Nanotubes." *The Journal of Physical Chemistry B*, 2002. 106(10): pp. 2429-2433.

[49] Dervishi E, Z Li, F Watanabe, V Saini, AR Biris, Y Xu, and AS Biris, "High-aspect ratio and horizontally oriented carbon nanotubes synthesized by RF-cCVD." *Diamond and Related Materials*, 2010. 19(1): pp. 67-72.

[50] Hsu WK, JP Hare, M Terrones, HW Kroto, DRM Walton, and PJF Harris, "Condensed-phase nanotubes." *Nature*, 1995. 377(6551): pp. 687-687.

[51] Steiner SA, TF Baumann, BC Bayer, R Blume, MA Worsley, WJ MoberlyChan, EL Shaw, R SchloÌˆgl, AJ Hart, S Hofmann, and BL Wardle, "Nanoscale Zirconia as a Nonmetallic Catalyst for Graphitization of Carbon and Growth of Single- and Multiwall Carbon Nanotubes." *Journal of the American Chemical Society*, 2009.

[52] Endo M, YA Kim, T Hayashi, K Nishimura, T Matusita, K Miyashita, and MS Dresselhaus, "Vapor-grown carbon fibers (VGCFs): Basic properties and their battery applications." *Carbon*, 2001. 39(9): pp. 1287-1297.

[53] Tibbetts GG, MG Devour, and EJ Rodda, "An adsorption-diffusion isotherm and its application to the growth of carbon filaments on iron catalyst particles." *Carbon*, 1987. 25(3): pp. 367-375.

[54] Tibbetts GG, ML Lake, KL Strong, and BP Rice, "A review of the fabrication and properties of vapor-grown carbon nanofiber/polymer composites." *Composites Science and Technology*, 2007. 67(7-8): pp. 1709-1718.

[55] Lake ML and JM Ting, eds. *Vapor grown carbon fiber composites.*, ed. T.D. Burchell. 1999, Pergamon: Amsterdam.

[56] Yokozeki T, Y Iwahori, S Ishiwata, and K Enomoto, "Mechanical properties of CFRP laminates manufactured from unidirectional prepregs using CSCNT-dispersed epoxy." *Composites Part A: Applied Science and Manufacturing*, 2007. 38(10): pp. 2121-2130.

[57] Merkulov V I LDHWYYEG and E Voelkl, "Patterned growth of individual and multiple vertically aligned carbon nanofibers." *Appl. Phys. Lett*, 2000. 76(24): pp. 3555-3557.

[58] Uchida T, DP Anderson, ML Minus, and S Kumar, "Morphology and modulus of vapor grown carbon nano fibers." *Journal of Materials Science*, 2006. 41(18): pp. 5851-5856.

[59] Miyagawa H, MJ Rich, and LT Drzal, "Thermo-physical properties of epoxy nanocomposites reinforced by carbon nanotubes and vapor grown carbon fibers." *Thermochimica Acta*, 2006. 442(1-2): pp. 67-73.

[60] Ozkan T, M Naraghi, and I Chasiotis, "Mechanical properties of vapor grown carbon nanofibers." *Carbon*. 48(1): pp. 239-244.

[61] Jana SC and GA Jimenez, "Electrically conductive polymer nanocomposites of polymethylmethacrylate and carbon nanofibers prepared by chaotic mixing." *Composites Part A (Applied Science and Manufacturing)*, 2007. 38(3): pp. 983-93.

[62] Tibbetts GG, C Kway, JY Howe, and ML Lake, “Heat Treating Carbon Nanofibersfor Optimal Composite Performance,” in *48th International SAMPE Symposium*. 2003, SAMPE. p. 2136-2145.

[63] Thostenson ET, C Li, and T-W Chou, “Nanocomposites in context.” *Composites Science and Technology*, 2005. 65(3-4): pp. 491-516.

[64] Callister WJ, *Materials Science and Engineering An Introduction*. Sixth Edition ed. 2003, New York, NY: John Wiley & Sons.

[65] Gojny FH, MHG Wichmann, B Fiedler, and K Schulte, “Influence of different carbon nanotubes on the mechanical properties of epoxy matrix composites - A comparative study.” *Composites Science and Technology*, 2005. 65(15-16): pp. 2300-2313.

[66] Yang K, M Gu, Y Guo, X Pan, and G Mu, “Effects of carbon nanotube functionalization on the mechanical and thermal properties of epoxy composites.” *Carbon*, 2009. 47(7): pp. 1723-1737.

[67] Truong V-T, KMC Tsang, SJ Keough, and NA St John. “Effect of sonication on the mechanical properties of poly (vinyl alcohol)/carbon nanotube composites. 2007. Adelaide, Australia: SPIE -International Society for Optical Engineering, Bellingham WA, WA 98227-0010, United States.

[68] Qiu J, C Zhang, B Wang, and R Liang. “Multiscale composites reinforced with functionalized nanotubes.” in *SAMPE '07: M and P - From Coast to Coast and Around the World, June 3, 2007 - June 7, 2007*. 2007. Baltimore, MD, United states: Soc. for the Advancement of Material and Process Engineering.

[69] Bal S, “Experimental study of mechanical and electrical properties of carbon nanofiber/ epoxy composites.” *Materials & Design*. In Press, Accepted Manuscript.

[70] Krause B, M Mende, P Pötschke, and G Petzold, “Dispersability and particle size distribution of CNTs in an aqueous surfactant dispersion as a function of ultrasonic treatment time.” *Carbon*. In Press, Accepted Manuscript.

[71] Wang S, R Liang, B Wang, and C Zhang, “Dispersion and thermal conductivity of carbon nanotube composites.” *Carbon*, 2009. 47(1): pp. 53-57.

[72] Gojny FH, MHG Wichmann, U Köpke, B Fiedler, and K Schulte, “Carbon nanotube-reinforced epoxy-composites: enhanced stiffness and fracture toughness at low nanotube content.” *Composites Science and Technology*, 2004. 64(15): pp. 2363-2371.

[73] Hammel E, X Tang, M Trampert, T Schmitt, K Mauthner, A Eder, and P Pötschke, “Carbon nanofibers for composite applications.” *Carbon*, 2004. 42(5-6): pp. 1153-1158.

[74] Rosca ID and SV Hoa, “Highly conductive multiwall carbon nanotube and epoxy composites produced by three-roll milling.” *Carbon*, 2009. 47(8): pp. 1958-1968.

[75] Cheol P, Z Ounaies, KA Watson, RE Crooks, J Smith, Jr., SE Lowther, JW Connell, EJ Siochi, JS Harrison, and TL St Clair, "Dispersion of single wall carbon nanotubes by in situ polymerization under sonication." *Chemical Physics Letters*, 2002. 364(3-4): pp. 303-8.

[76] Zaragoza-Contreras EA, ED Lozano-Rodríguez, M Román-Aguirre, W Antunez-Flores, CA Hernández-Escobar, SG Flores-Gallardo, and A Aguilar-Elguezabal, "Evidence of multi-walled carbon nanotube fragmentation induced by sonication during nanotube encapsulation via bulk-suspension polymerization." *Micron*. 40(5-6): pp. 621-627.

[77] Hernandez-Perez A, F Aviles, A May-Pat, A Valadez-Gonzalez, P Herrera-Franco, and P Bartolo-Perez, "Effective properties of multiwalled carbon nanotube/epoxy composites using two different tubes." *Composites Science and Technology*, 2008. 68(6): pp. 1422-1431.

[78] Lachman N and HD Wagner, "Correlation between interfacial molecular structure and mechanics in CNT/epoxy nano-composites." *Composites Part A: Applied Science and Manufacturing*. In Press, Accepted Manuscript.

[79] Bahr JL and JM Tour, "Covalent Chemistry of Single-Wall Carbon Nanotubes." *Journal of Materials Chemistry*, 2002. 12(7): pp. 1952-1958.

[80] Dyke CA and JM Tour, "Covalent Functionalization of Single-Walled Carbon Nanotubes for Materials Applications." *J. Phys. Chem. A*, 2004. 108(51): pp. 11151-11159.

[81] Yiu-Wing M, X Xiao-Lin, and Z Xing-Ping, "Dispersion and alignment of carbon nanotubes in polymer matrix: A review." *Materials Science & Engineering R: Reports*, 2005. 49(4): pp. 89-112.

[82] Bose S, RA Khare, and P Moldenaers, "Assessing the strengths and weaknesses of various type of pre-treatments of carbon nanotubes on the properties of polymer/carbon nanotubes composites: a critical review." *Polymer*. In Press, Accepted Manuscript.

[83] Marques RRN, BF Machado, JL Faria, and AMT Silva, "Controlled generation of oxygen functionalities on the surface of Single-Walled Carbon Nanotubes by HNO3-hydrothermal oxidation." *Carbon*. In Press, Accepted Manuscript.

[84] Hu H, P Bhowmik, B Zhao, MA Hamon, ME Itkis, and RC Haddon, "Determination of the acidic sites of purified single-walled carbon nanotubes by acid-base titration." *Chemical Physics Letters*, 2001. 345(1-2): pp. 25-28.

[85] Buffa F, GA Abraham, BP Grady, and D Resasco, "Effect of nanotube functionalization on the properties of single-walled carbon nanotube/polyurethane composites." *Journal of Polymer Science, Part B (Polymer Physics)*, 2007. 45(4): pp. 490-501.

[86] Chen C, B Liang, D Lu, A Ogino, X Wang, and M Nagatsu, "Amino group introduction onto multiwall carbon nanotubes by NH3/Ar plasma treatment." *Carbon*. 48(4): pp. 939-948.

[87] Miller SG, JL Bauer, MJ Maryanski, PJ Heimann, JP Barlow, J-M Gosau, and RE Allred, "Characterization of epoxy functionalized graphite nanoparticles and the physical properties of epoxy matrix nanocomposites." *Composites Science and Technology*. In Press, Accepted Manuscript.

[88] Lee JU, J Huh, KH Kim, C Park, and WH Jo, "Aqueous suspension of carbon nanotubes via non-covalent functionalization with oligothiophene-terminated poly(ethylene glycol)." *Carbon*, 2007. 45(5): pp. 1051-1057.

[89] Saini RK, IW Chiang, H Peng, RE Smalley, WE Billups, RH Hauge, and JL Margrave, "Covalent Sidewall Functionalization of Single Wall Carbon Nanotubes." *J. Am. Chem. Soc.*, 2003. 125(12): pp. 3617-3621.

[90] Shen J, Y Hu, C Qin, C Li, and M Ye, "Dispersion behavior of single-walled carbon nanotubes by grafting of amphiphilic block copolymer." *Composites Part A: Applied Science and Manufacturing*, 2008. 39(10): pp. 1679-1683.

[91] Seyhan AT, Z Sun, J Deitzel, M Tanoglu, and D Heider, "Cure kinetics of vapor grown carbon nanofiber (VGCNF) modified epoxy resin suspensions and fracture toughness of their resulting nanocomposites." *Materials Chemistry and Physics*. In Press, Corrected Proof.

[92] Kathi J, K-Y Rhee, and JH Lee, "Effect of chemical functionalization of multi-walled carbon nanotubes with 3-aminopropyltriethoxysilane on mechanical and morphological properties of epoxy nanocomposites." *Composites Part A: Applied Science and Manufacturing*, 2009. 40(6-7): pp. 800-809.

[93] Peng Cheng M, K Jang-Kyo, and T Ben Zhong, "Effects of silane functionalization on the properties of carbon nanotube/epoxy nanocomposites." *Composites Science and Technology*, 2007. 67(14): pp. 2965-72.

[94] Morales G, MI Barrena, JMG de Salazar, C Merino, and D Rodríguez, "Conductive CNF-reinforced hybrid composites by injection moulding." *Composite Structures*. In Press, Accepted Manuscript.

[95] Gojny FH, MHG Wichmann, B Fiedler, W Bauhofer, and K Schulte, "Influence of nano-modification on the mechanical and electrical properties of conventional fibre-reinforced composites." *Composites Part A: Applied Science and Manufacturing*, 2005. 36(11): pp. 1525-1535.

[96] Bai JB, J-L Vignes, T Fournier, and D Michel, "A Novel Method for Preparing Preforms of Porous Alumina and Carbon Nanotubes by CVD." *Advanced Engineering Materials*, 2002. 4(9): pp. 701-703.

[97] Garcia EJ, BL Wardle, A John Hart, and N Yamamoto, "Fabrication and multifunctional properties of a hybrid laminate with aligned carbon nanotubes grown In Situ." *Composites Science and Technology*, 2008. 68(9): pp. 2034-2041.

[98] Qian H, A Bismarck, ES Greenhalgh, and MSP Shaffer, "Carbon nanotube grafted silica fibres: Characterising the interface at the single fibre level." *Composites Science and Technology*. In Press, Accepted Manuscript.

[99] Zhang Q, W Qian, R Xiang, Z Yang, G Luo, Y Wang, and F Wei, "In situ growth of carbon nanotubes on inorganic fibers with different surface properties." *Materials Chemistry and Physics*, 2008. 107(2-3): pp. 317-321.

[100] Thostenson ET, WZ Li, DZ Wang, ZF Ren, and TW Chou, "Carbon nanotube/carbon fiber hybrid multiscale composites." *Journal of Applied Physics*, 2002. 91(9): pp. 6034-6037.

[101] Sager RJ, PJ Klein, DC Lagoudas, Q Zhang, J Liu, L Dai, and JW Baur, "Effect of carbon nanotubes on the interfacial shear strength of T650 carbon fiber in an epoxy matrix." *Composites Science and Technology*, 2009. 69(7-8): pp. 898-904.

[102] Qian H, A Bismarck, ES Greenhalgh, and MSP Shaffer, "Carbon nanotube grafted carbon fibres: a study of wetting and fibre fragmentation." *Composites Part A: Applied Science and Manufacturing*. In Press, Accepted Manuscript.

[103] Qian H, A Bismarck, ES Greenhalgh, G Kalinka, and MSP Shaffer, "Hierarchical Composites Reinforced with Carbon Nanotube Grafted Fibers: The Potential Assessed at the Single Fiber Level." *Chemistry of Materials*, 2008. 20(5): pp. 1862-1869.

[104] Zhang Q, J Liu, R Sager, L Dai, and J Baur, "Hierarchical composites of carbon nanotubes on carbon fiber: Influence of growth condition on fiber tensile properties." *Composites Science and Technology*, 2009. 69(5): pp. 594-601.

[105] Kulkarni M, D Carnahan, K Kulkarni, D Qian, and JL Abot, "Elastic Response of a Carbon Nanotube Fiber Reinforced Polymeric Composite: A Numerical and Experimental Study." *Composites Part B: Engineering*. In Press, Accepted Manuscript.

[106] Kepple KL, GP Sanborn, PA Lacasse, KM Gruenberg, and WJ Ready, "Improved fracture toughness of carbon fiber composite functionalized with multi walled carbon nanotubes." *Carbon*, 2008. 46(15): pp. 2026-2033.

[107] Qiao-Juan G, L He-Jun, W Xiang, F Qian-Gang, W Zhao-wei, and L Ke-Zhi, "In situ catalytic growth of carbon nanotubes on the surface of carbon cloth." *Composites Science and Technology*, 2007. 67(14): pp. 2986-9.

[108] Duan H, J Liang, and Z Xia, "Synthetic hierarchical nanostructures: Growth of carbon nanofibers on microfibers by chemical vapor deposition." *Materials Science and Engineering: B*. In Press, Uncorrected Proof.

[109] Tzeng S-S, K-H Hung, and T-H Ko, "Growth of carbon nanofibers on activated carbon fiber fabrics." *Carbon*, 2006. 44(5): pp. 859-865.

[110] Mathur RB, S Chatterjee, and BP Singh, "Growth of carbon nanotubes on carbon fibre substrates to produce hybrid/phenolic composites with improved mechanical properties." *Composites Science and Technology*, 2008. 68(7-8): pp. 1608-15.

[111] Abot JL, Y Song, MJ Schulz, and VN Shanov, "Novel carbon nanotube array-reinforced laminated composite materials with higher interlaminar elastic properties." *Composites Science and Technology*, 2008. 68(13): pp. 2755-2760.

[112] Arai M, Y Noro, Ki Sugimoto, and M Endo, "Mode I and mode II interlaminar fracture toughness of CFRP laminates toughened by carbon nanofiber interlayer." *Composites Science and Technology*, 2008. 68(2): pp. 516-25.

[113] Garcia EJ, BL Wardle, and A John Hart, "Joining prepreg composite interfaces with aligned carbon nanotubes." *Composites Part A: Applied Science and Manufacturing*, 2008. 39(6): pp. 1065-1070.

[114] Wicks SS, RGd Villoria, and BL Wardle, "Interlaminar and Intralaminar Reinforcement of Composite Laminates with Aligned Carbon Nanotubes." *Composites Science and Technology*. In Press, Accepted Manuscript.

[115] Rojas G, B Maruyama, and E Barrera. "CNT/VGCF reinforced epoxy/cf composites: The role of nanofibers. 2006. Dallas, TX, United states: Soc. for the Advancement of Material and Process Engineering.

[116] Li Y, N Hori, M Arai, N Hu, Y Liu, and H Fukunaga, "Improvement of interlaminar mechanical properties of CFRP laminates using VGCF." *Composites Part A: Applied Science and Manufacturing*. In Press, Accepted Manuscript.

[117] Besra L and M Liu, "A review on fundamentals and applications of electrophoretic deposition (EPD)." *Progress in Materials Science*, 2007. 52(1): pp. 1-61.

[118] Boccaccini AR, J Cho, T Subhani, C Kaya, and F Kaya, "Electrophoretic deposition of carbon nanotube-ceramic nanocomposites." *Journal of the European Ceramic Society*. In Press, Corrected Proof.

[119] Thomas BJC, AR Boccaccini, and MSP Shaffer, "Multi-walled carbon nanotube coatings using Electrophoretic Deposition (EPD)." *Journal of the American Ceramic Society*, 2005. 88(4): pp. 980-982.

[120] Du C, N Pan, and D Heldebrant, "Preparation of carbon nanotubes composite sheet using electrophoretic deposition process." *Journal of Materials Science Letters*, 2002. 21(7): pp. 565-568.

[121] Cho J, K Konopka, K Rozniatowski, E García-Lecina, MSP Shaffer, and AR Boccaccini, "Characterisation of carbon nanotube films deposited by electrophoretic deposition." *Carbon*, 2009. 47(1): pp. 58-67.

[122] Corni I, MP Ryan, and AR Boccaccini, "Electrophoretic deposition: From traditional ceramics to nanotechnology." *Journal of the European Ceramic Society*, 2008. 28(7): pp. 1353-1367.

[123] Du C, D Heldbrant, and N Pan, "Preparation and preliminary property study of carbon nanotubes films by electrophoretic deposition." *Materials Letters*, 2002. 57(2): pp. 434-438.

[124] Yu Jun Y, GJ Zhao, and H Shengshui, "Direct current electrodeposition of carbon nanofibers in DMF." *Electrochemistry Communications*, 2007. 9(11): pp. 2681-5.

[125] Schausten MC, D Meng, R Telle, and AR Boccaccini, "Electrophoretic Deposition of Carbon Nanotubes and Bioactive Glass Particles for Bioactive Composite Coatings." *Ceramics International*. In Press, Accepted Manuscript.

[126] Wu DC, L Shen, JE Low, SY Wong, X Li, WC Tjiu, Y Liu, and CB He, "Multi-walled Carbon Nanotube/polyimide Composite Film Fabricated through Electrophoretic Deposition." *Polymer*. In Press, Accepted Manuscript.

[127] Zhang J, R Zhuang, J Liu, E Mäder, G Heinrich, and S Gao, "Functional Interphases with Multiwalled Carbon Nanotubes in Glass Fibre/Epoxy Composites." *Carbon*. In Press, Accepted Manuscript.

[128] Theodore M, J Fielding, K Green, D Dean, N Horton, A Noble, and S Miller. "Nanostructured coupling agents for multifunctional composites." in *SAMPE '09 Spring Symposium Conference Proceedings, May 18, 2009 - May 21, 2009*. 2009. Baltimore, MD, United states: Soc. for the Advancement of Material and Process Engineering.

[129] Bekyarova E, ET Thostenson, A Yu, H Kim, J Gao, J Tang, HT Hahn, TW Chou, ME Itkis, and RC Haddon, "Multiscale carbon nanotube-carbon fiber reinforcement for advanced epoxy composites." *Langmuir*, 2007. 23(7): pp. 3970-3974.

[130] Du C and N Pan, "Supercapacitors using carbon nanotubes films by electrophoretic deposition." *Journal of Power Sources*, 2006. 160(2 SPEC ISS): pp. 1487-1494.

[131] Van Der Biest O, S Put, G Anne, and J Vleugels, "Electrophoretic deposition for coatings and free standing objects." *Journal of Materials Science*, 2004. 39(3): pp. 779-85.

[132] Zhao H, H Song, Z Li, G Yuan, and Y Jin, "Electrophoretic deposition and field emission properties of patterned carbon nanotubes." *Applied Surface Science*, 2005. 251(1-4): pp. 242-244.

[133] Jin YW, JE Jung, YJ Park, JH Choi, DS Jung, HW Lee, SH Park, NS Lee, JM Kim, TY Ko, SJ Lee, SY Hwang, JH You, Y Ji-Beom, and P Chong-Yun, "Triode-type field emission array using carbon nanotubes and a conducting polymer composite prepared by electrochemical polymerization." *Journal of Applied Physics*, 2002. 92(2): pp. 1065-8.

[134] Gao B, GZ Yue, Q Qiu, Y Cheng, H Shimoda, L Fleming, and O Zhou, “Fabrication and electron field emission properties of carbon nanotube films by electrophoretic deposition.” *Advanced Materials*, 2001. 13(23): pp. 1770-1773.

[135] Yu A, E Bekyarova, ME Itkis, D Fakhrutdinov, R Webster, and RC Haddon, “Application of centrifugation to the large-scale purification of electric arc-produced single-walled carbon nanotubes.” *Journal of the American Chemical Society*, 2006. 128(30): pp. 9902-9908.

[136] Inc. CT. 2005-2009 [cited 2010 04-30-2010]; Available from: http://www.cheaptubes.com/MWNTs.htm#multi_walled_nanotubes-mwnts-20-30nm_specifications.

[137] Zhu J, J Kim, H Peng, JL Margrave, VN Khabashesku, and EV Barrera, “Improving the Dispersion and Integration of Single-Walled Carbon Nanotubes in Epoxy Composites through Functionalization.” Nano Letters, 2003. 3(8): pp. 1107-1113.

[138] Mitchell CA, JL Bahr, S Arepalli, JM Tour, and R Krishnamoorti, “Dispersion of Functionalized Carbon Nanotubes in Polystyrene.” Macromolecules, 2002. 35(23): pp. 8825-8830.

[139] Chiang IW, BE Brinson, RE Smalley, JL Margrave, and RH Hauge, “Purification and Characterization of Single-Wall Carbon Nanotubes.” The Journal of Physical Chemistry B, 2001. 105(6): pp. 1157-1161.

[140] Shen J, W Huang, L Wu, Y Hu, and M Ye, “Study on amino-functionalized multiwalled carbon nanotubes.” Materials Science and Engineering: A, 2007. 464(1-2): pp. 151-156.

[141] Boccaccini AR, J Cho, JA Roether, BJC Thomas, E Jane Minay, and MSP Shaffer, “Electrophoretic deposition of carbon nanotubes.” Carbon, 2006. 44(15): pp. 3149-3160.

[142] Zhu J, H Peng, F Rodriguez-Macias, JL Margrave, VN Khabashesku, AM Imam, K Lozano, and EV Barrera, “Reinforcing epoxy polymer composites through covalent integration of functionalized nanotubes.” Advanced Functional Materials, 2004. 14(7): pp. 643-648.

[143] Wang Y, Z Iqbal, and S Mitra, “Rapidly functionalized, water-dispersed carbon nanotubes at high concentration.” Journal of the American Chemical Society, 2006. 128(1): pp. 95-99.

[144] Pompeo F and DE Resasco, “Water solubilization of single-walled carbon nanotubes by functionalization with glucosamine.” Nano Letters, 2002. 2(4): pp. 369-73.

[145] Stevens JL, AY Huang, H Peng, W Chiang Ivana, VN Khabashesku, and JL Margrave, “Sidewall Amino-Functionalization of Single-Walled Carbon Nanotubes through Fluorination and Subsequent Reactions with Terminal Diamines.” Nano Letters, 2003. 3(3): pp. 331-336.

[146] Figueiredo JL, MFR Pereira, MMA Freitas, and JJM Órfão, “Modification of the surface chemistry of activated carbons.” Carbon, 1999. 37(9): pp. 1379-1389.

[147] Hu H, A Yu, E Kim, B Zhao, ME Itkis, E Bekyarova, and RC Haddon, “Influence of the zeta potential on the dispersability and purification of single-walled carbon nanotubes.” Journal of Physical Chemistry B, 2005. 109(23): pp. 11520-4.

[148] Gou J, B Minaie, B Wang, Z Liang, and C Zhang, “Computational and experimental study of interfacial bonding of single-walled nanotube reinforced composites.” Computational Materials Science, 2004. 31(3-4): pp. 225-236.

[149] Whitney JM and CE Browning, “On short-beam shear tests for composite materials.” Experimental Mechanics, 1985. 25(Copyright 1986, IEE): pp. 294-309.

[150] “Standard Test Method for Short-Beam Shear Strength of Polymer Matrix Composite Materials and Their Laminates.” American Society for Testing Materials, 2000(D 2344/D 2344M-00).

[151] Upadhyaya D and P Tsakiropoulos, “Evaluation of the effect of sizing levels on transverse flexural and shear strengths of carbon/epoxy composites.” Journal of Materials Processing Technology, 1995. 54(1-4): pp. 17-20.

[152] Ahn S-N, H-J Lee, B-J Kim, L-S Tan, and J-B Baek, “Epoxy/amine-functionalized short-length vapor-grown carbon nanofiber composites.” Journal of Polymer Science Part A: Polymer Chemistry, 2008. 46(22): pp. 7473-7482.

APPENDICES

APPENDIX A

X-RAY PHOTOELECTRON SPECTROSCOPY OF FUNCTIONALIZED MULTI-WALLED CARBON NANOTUBES AND CARBON NANOFIBERS

1. Multi-Walled Carbon Nanotubes

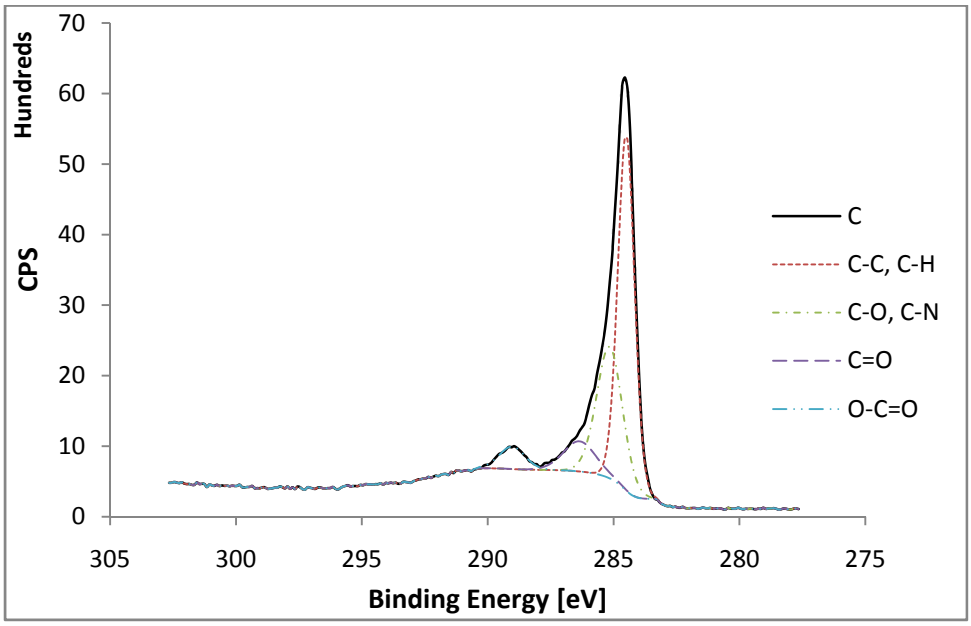

Figure A.1. XPS high-resolution spectrum of O-MWCNTs, C 1s region.

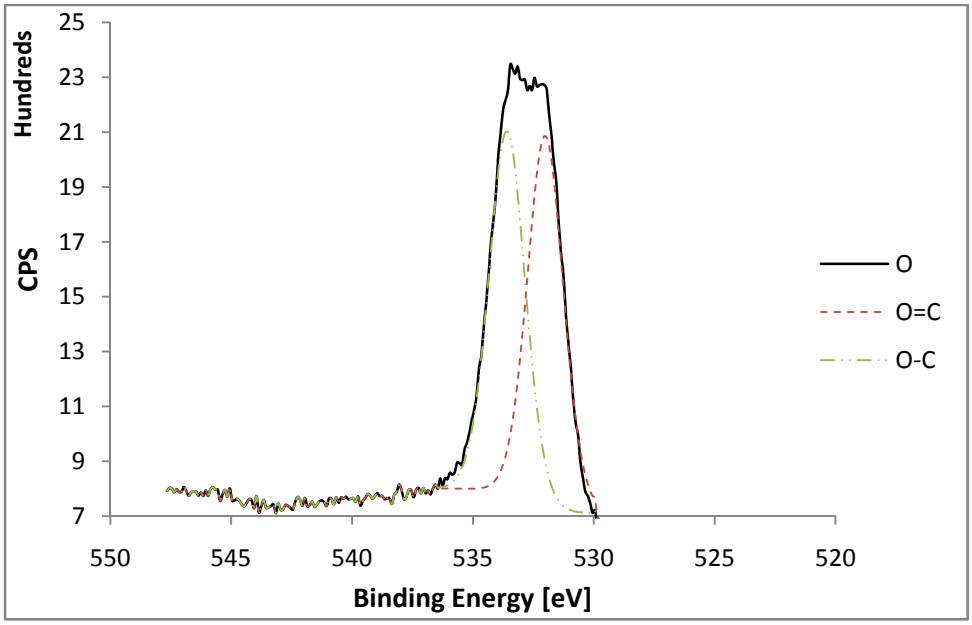

Figure A.2. XPS high-resolution spectrum of O-MWCNTs, O 1s region.

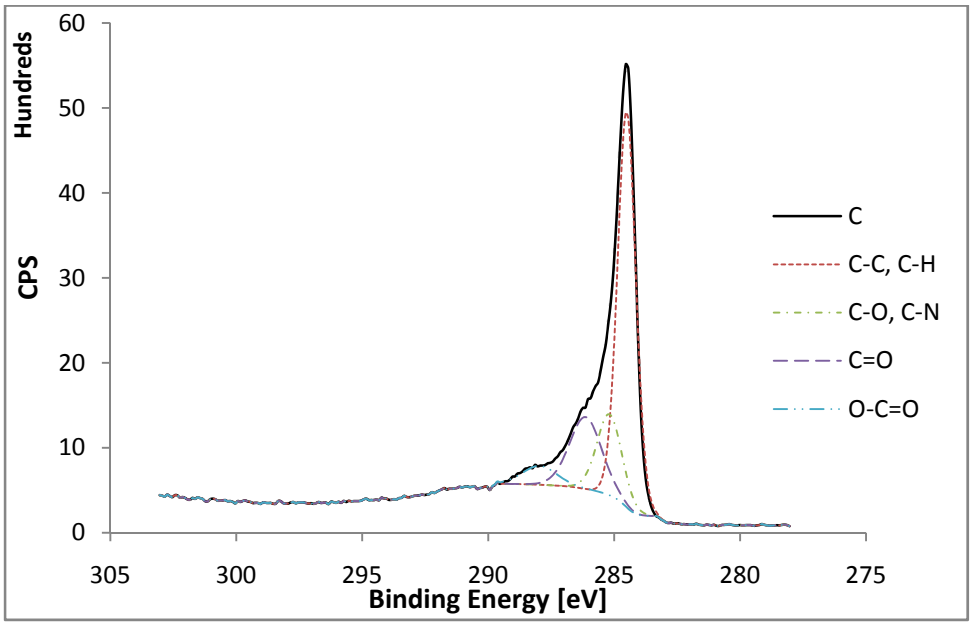

Figure A.3. XPS high-resolution spectrum of A-MWCNTs, C 1s region.

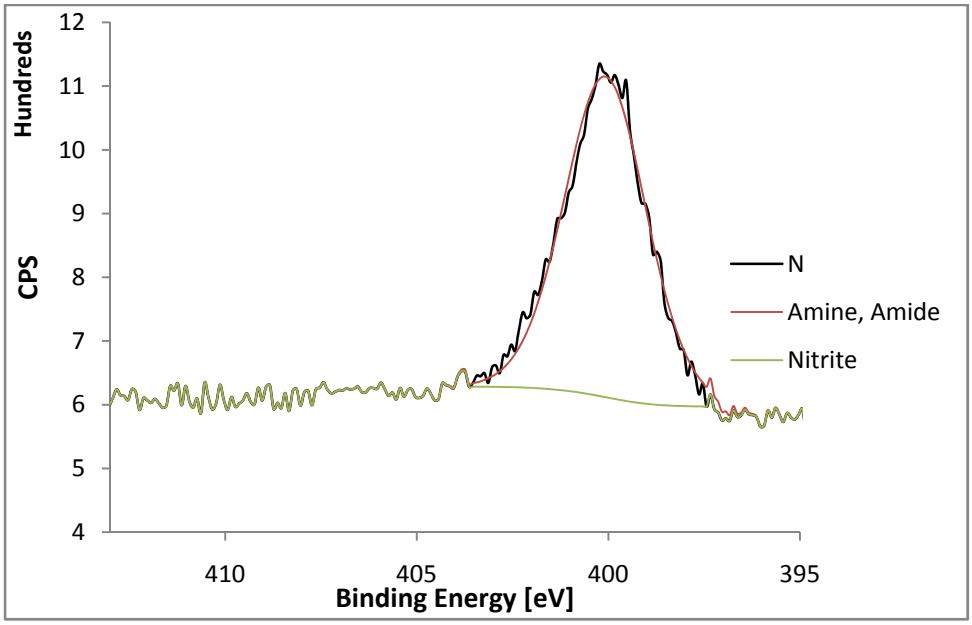

Figure A.4. XPS high-resolution spectrum of A-MWNCTs, N 1s region.

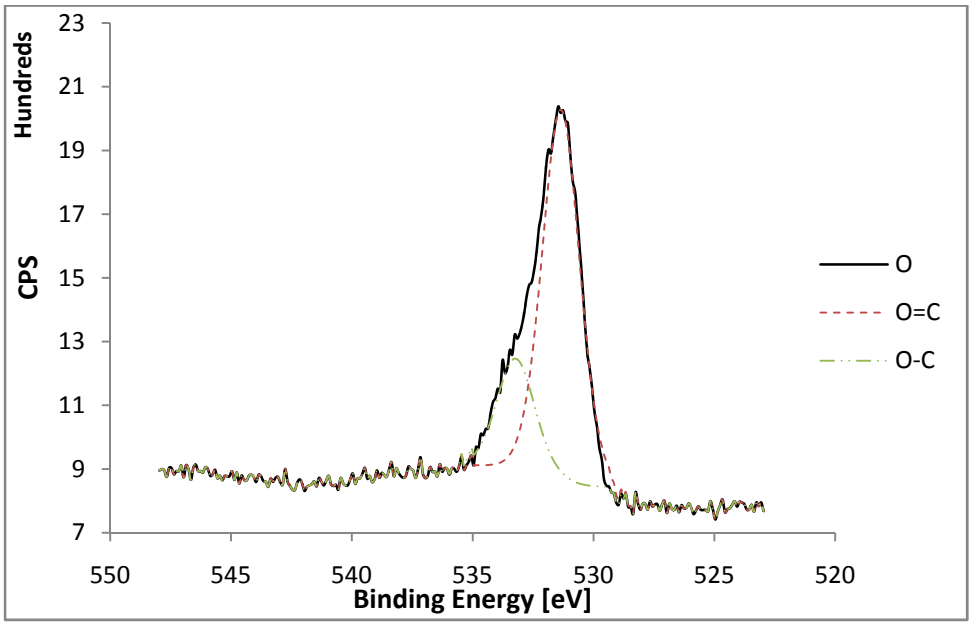

Figure A.5. XPS high-resolution spectrum of A-MWCNTs, O 1s region.

2. Carbon Nanofibers

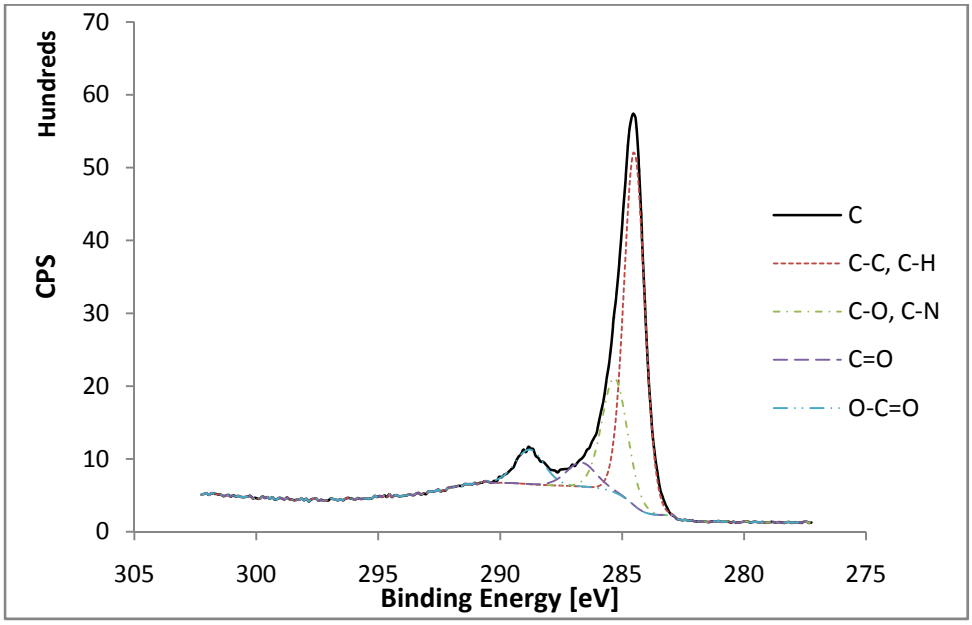

Figure A.6. XPS high-resolution spectrum of O-CNFs, C 1s region.

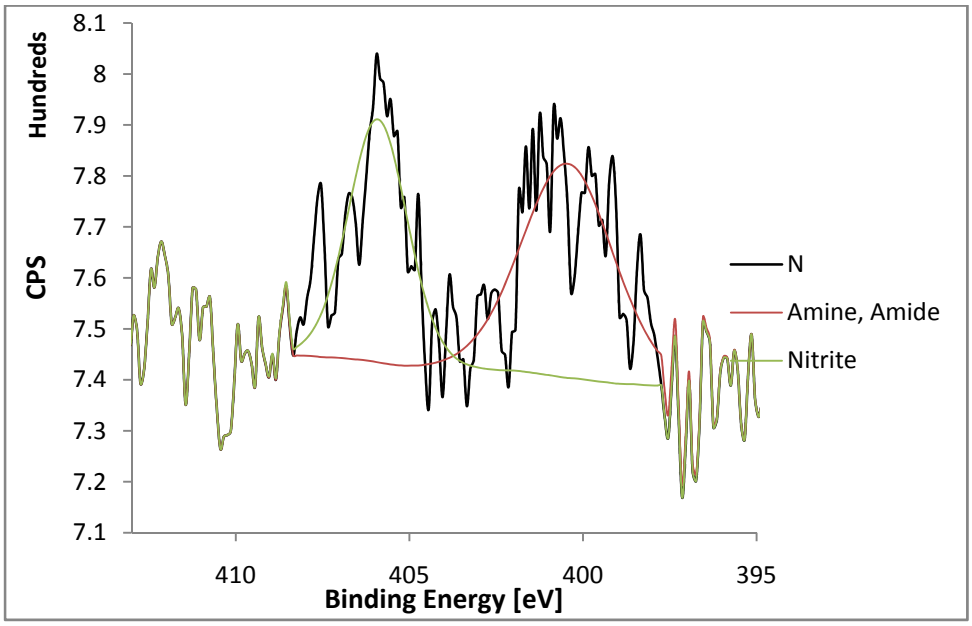

Figure A.7. XPS high-resolution spectrum of O-CNFs, N 1s region.

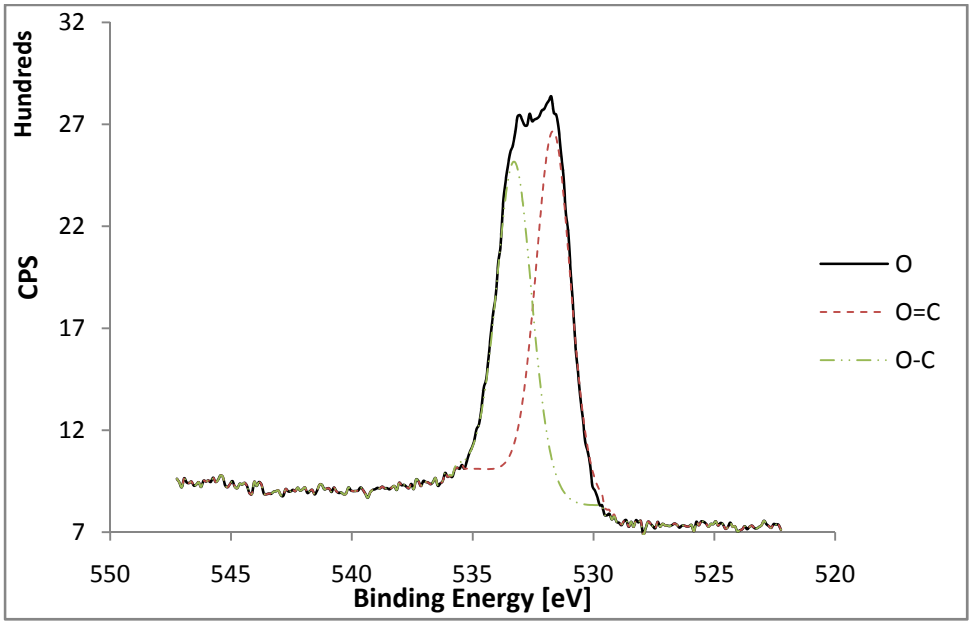

Figure A.8. XPS high-resolution spectrum of O-CNFs, O 1s region.

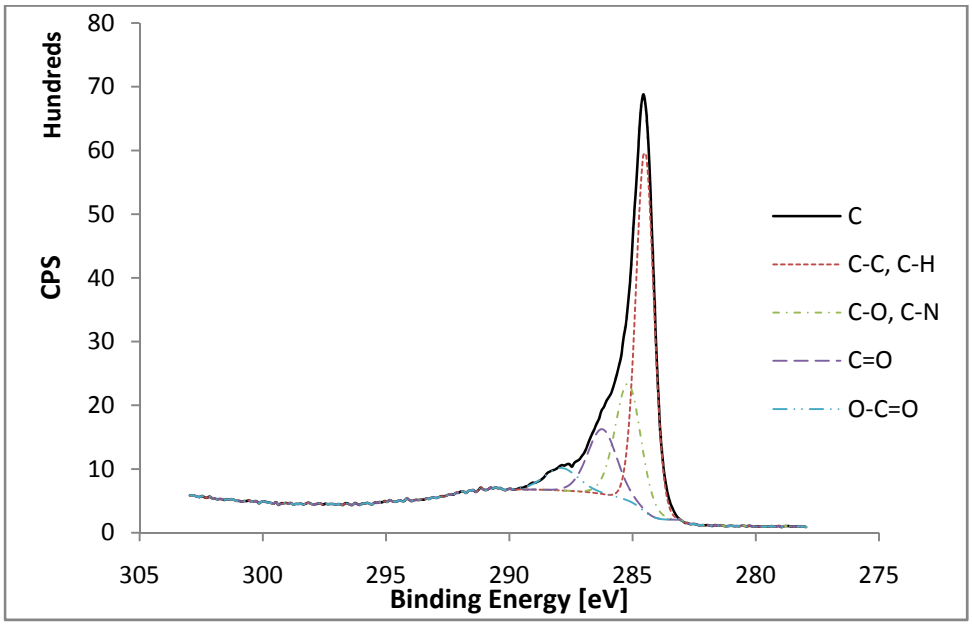

Figure A.9. XPS high-resolution spectrum of A-CNFs, C 1s region.

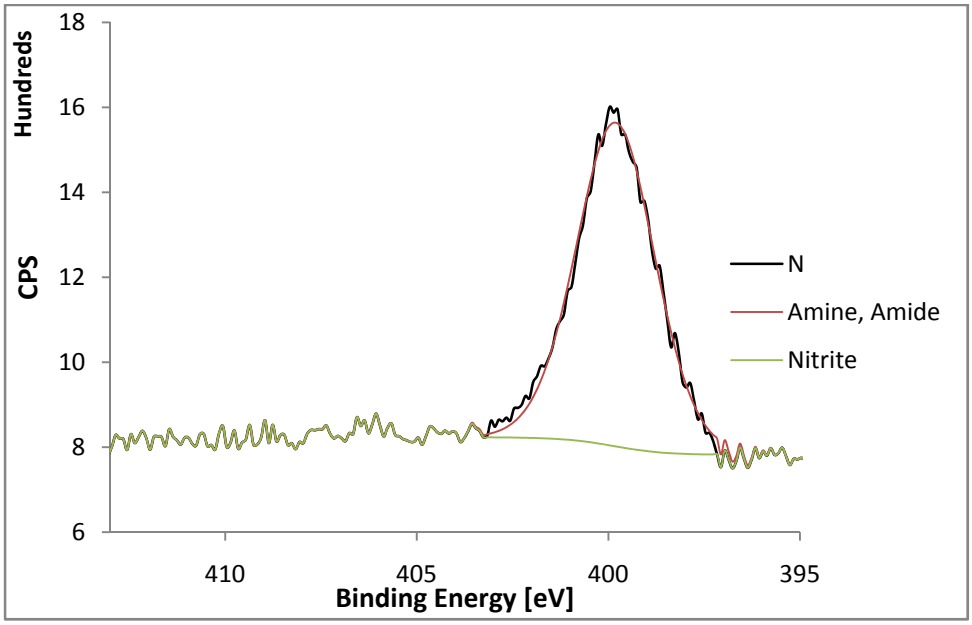

Figure A.10. XPS high-resolution spectrum of A-CNFs, N 1s region.

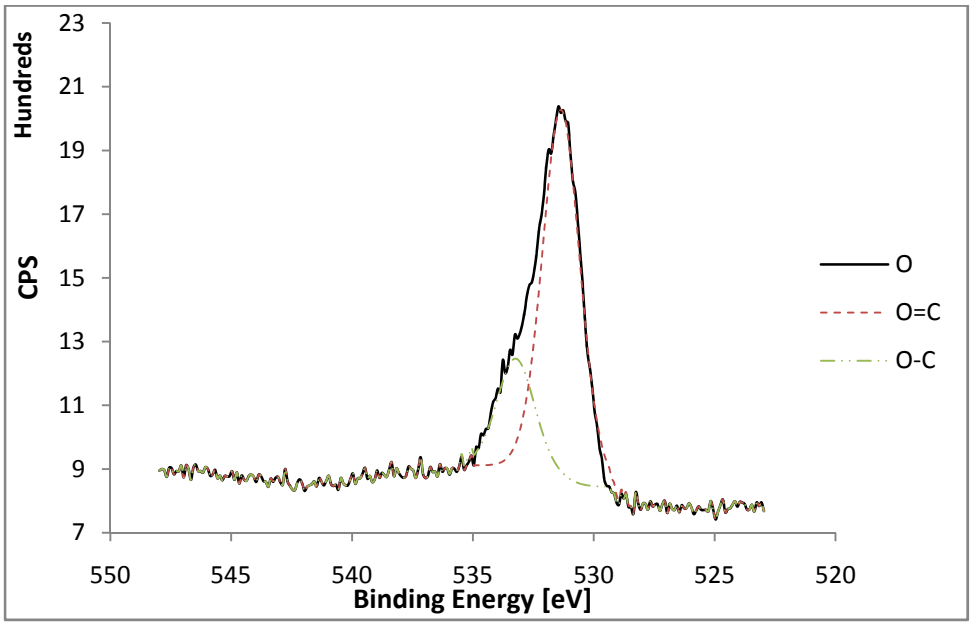

Figure A.11. XPS high-resolution spectrum of A-CNFs, O 1s region.

APPENDIX B

ABSORBANCE SPECTRA FOR FUNCTIONALIZED MULTI-WALLED CARBON NANOTUBES AND CARBON NANOFIBERS

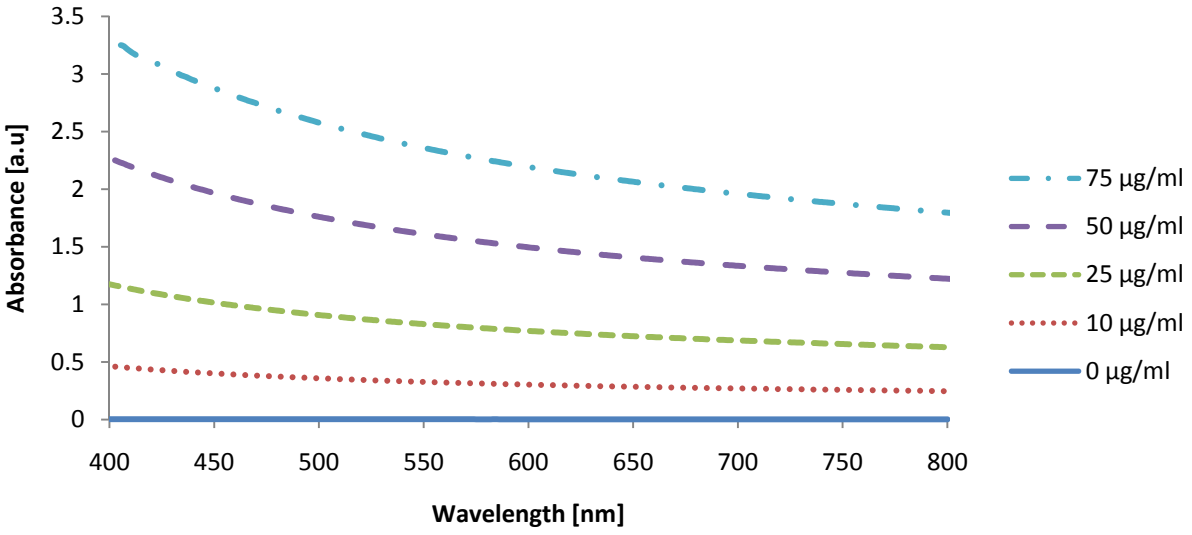

Figure B.1. Absorbance spectra for different concentrations of carboxylic acid-functionalized multi-walled carbon nanotubes in aqueous medium.

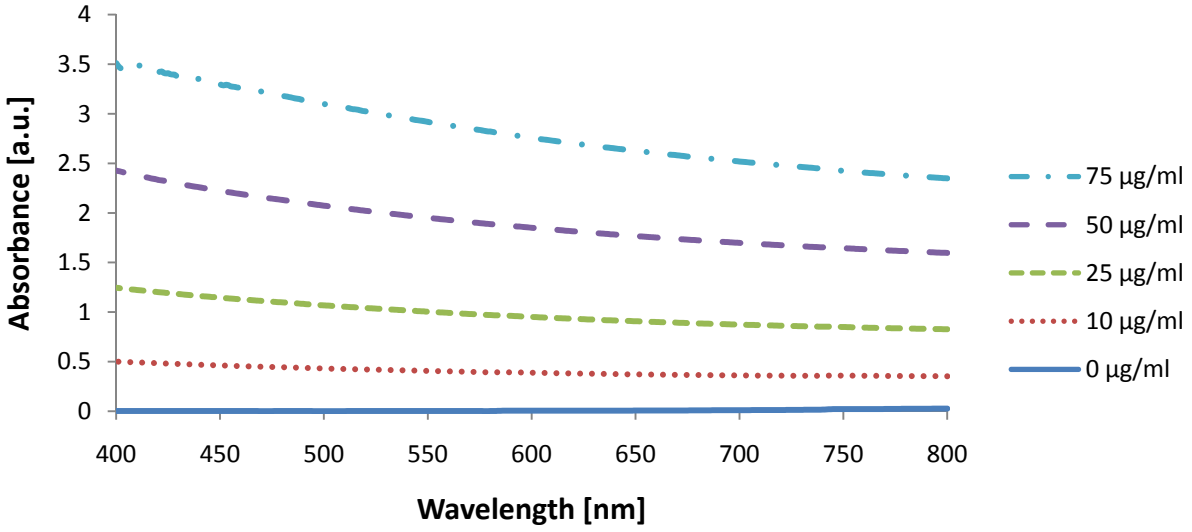

Figure B.2. Absorbance spectra for different concentrations of carboxylic acid-functionalized carbon nanofibers in aqueous medium.

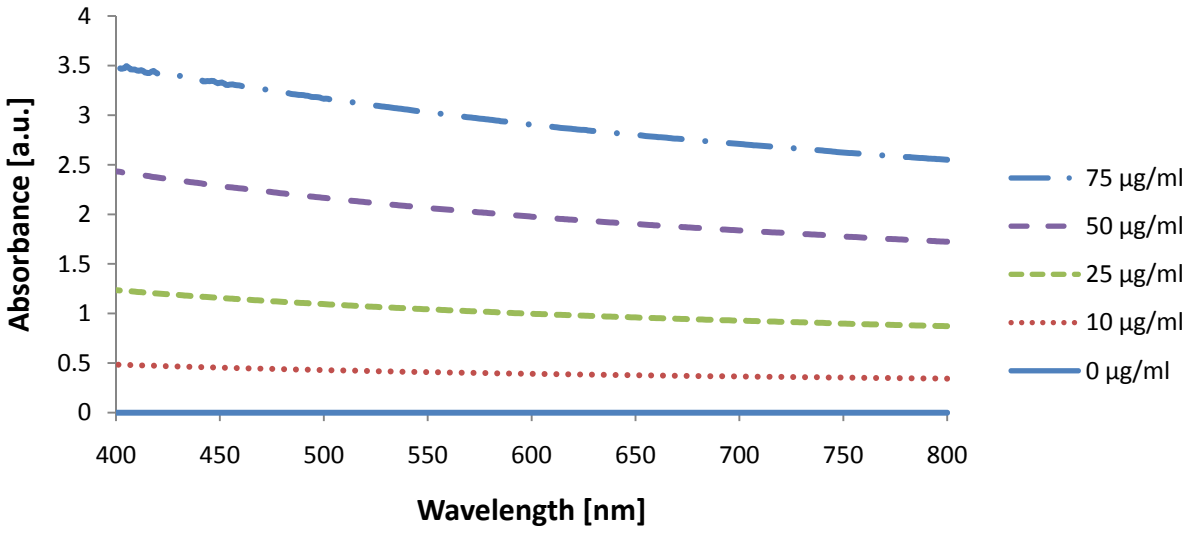

Figure B.3. Absorbance spectra for different concentrations of amine-functionalized carbon nanofibers in aqueous medium.

APPENDIX C

MECHANICAL AND PHYSICAL PROPERTIES OF MULTISCALE-REINFORCED POLYMER COMPOSITES

TABLE C.1.

MECHANICAL, ELECTRICAL, AND PHYSICAL PROPERTIES OF MULTISCALE-REINFORCED COMPOSITES

#	Panel Description	Apparent Interlaminar Shear Strength [MPa]	Compressive Strength [MPa]	Electrical Conductivity [S/cm]	Fiber Volume Fraction [%]
1	Base Panel	52.99	395.93	0.02074	55.16
2	O-MWCNTP	56.34	412.24	0.01740	46.98
3	O-CNFP	57.80	405.55	0.02406	50.09
4	A-MWCNTP	54.45	454.44	0.02770	52.33
5	A-CNFP	58.29	445.01	0.01326	51.75
6	A-CNFP-No Sizing	59.58	438.37	0.04067	55.81

APPENDIX D

SHEAR STRESS AT MID-PLANE VS. NORMALIZED DISPLACEMENT OF LOAD NOSE FOR SHORT-BEAM SHEAR TEST SPECIMENS

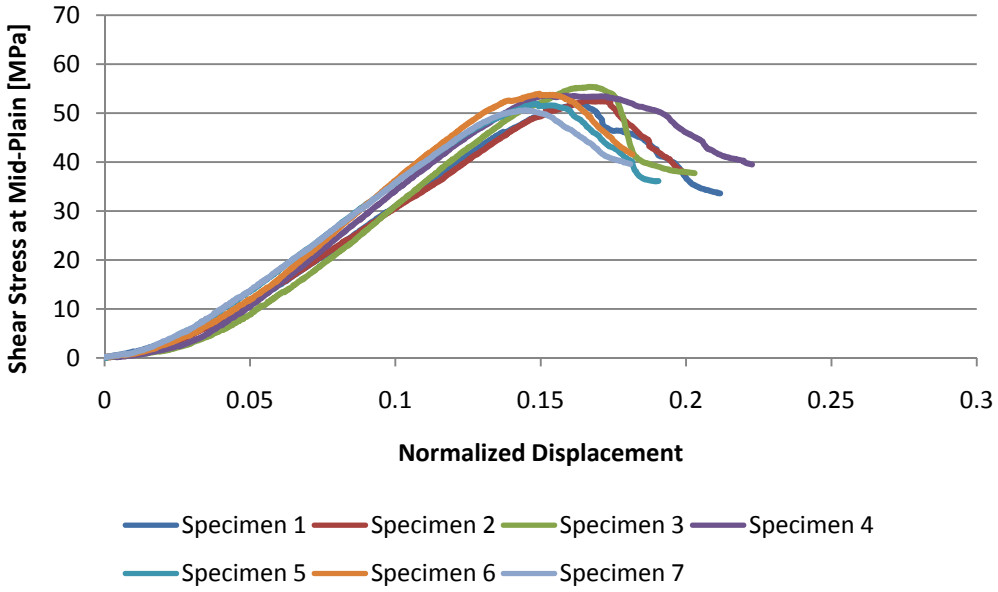

Figure D.1. Shear stress at mid-plane of specimens vs. displacement of load nose normalized with respect to thickness of specimens for base panel.

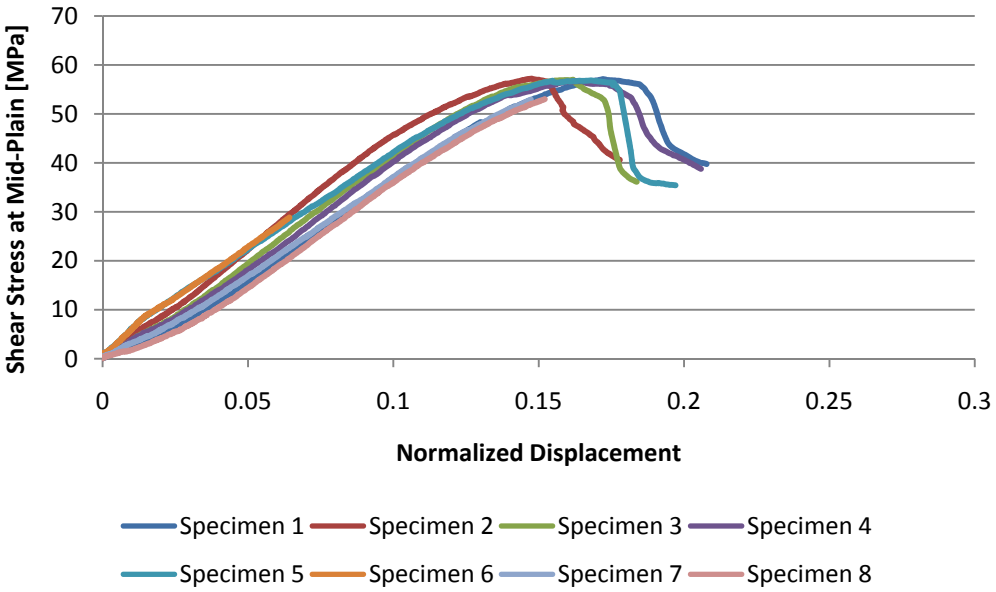

Figure D.2. Shear stress at mid-plane of specimens vs. displacement of load nose normalized with respect to thickness of specimens for panel containing O-MWCNTs.

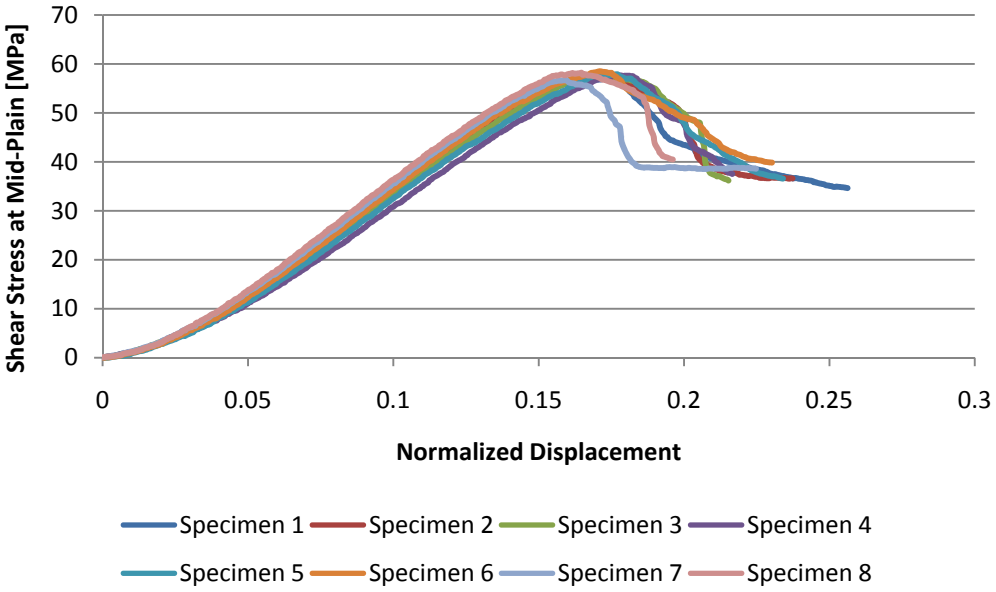

Figure D.3. Shear stress at mid-plane of specimens vs. displacement of load nose normalized with respect to thickness of specimens for panel containing O-CNFs.

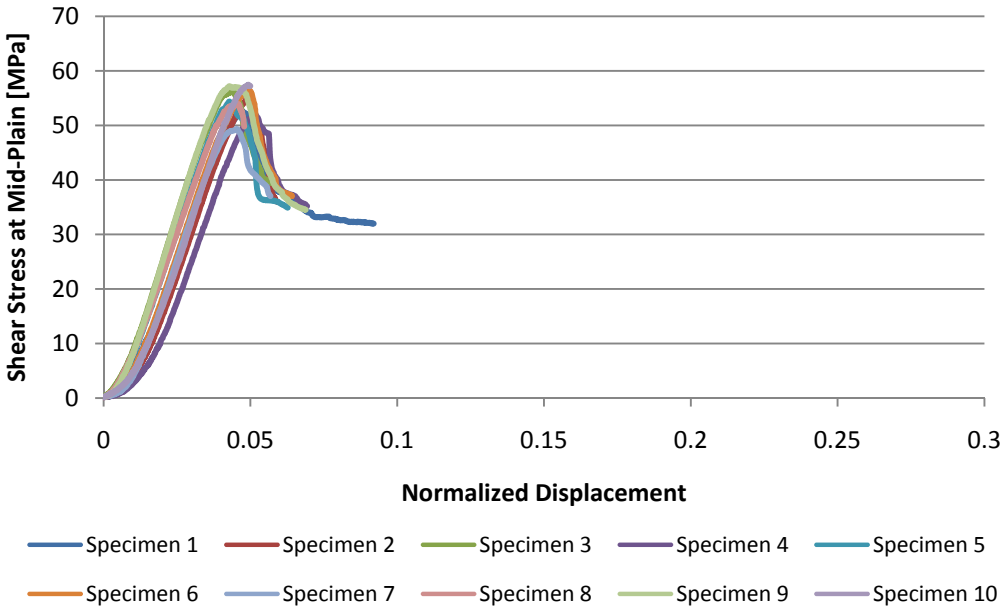

Figure D.4. Shear stress at mid-plane of specimens vs. displacement of load nose normalized with respect to thickness of specimens for panel containing A-MWCNTs.

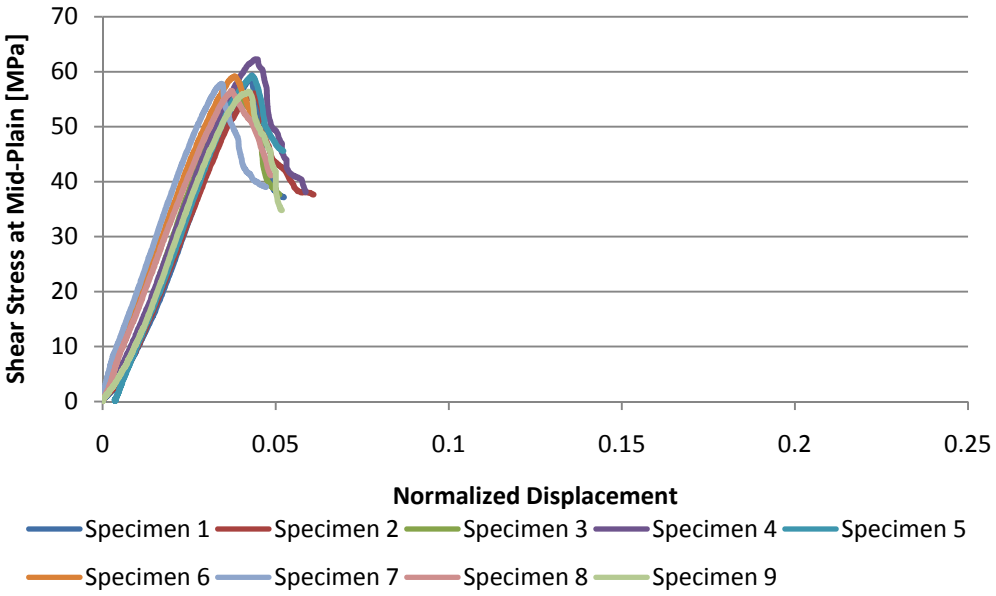

Figure D.5. Shear stress at mid-plane of specimens vs. displacement of load nose normalized with respect to thickness of specimens for panel containing A-CNFs.

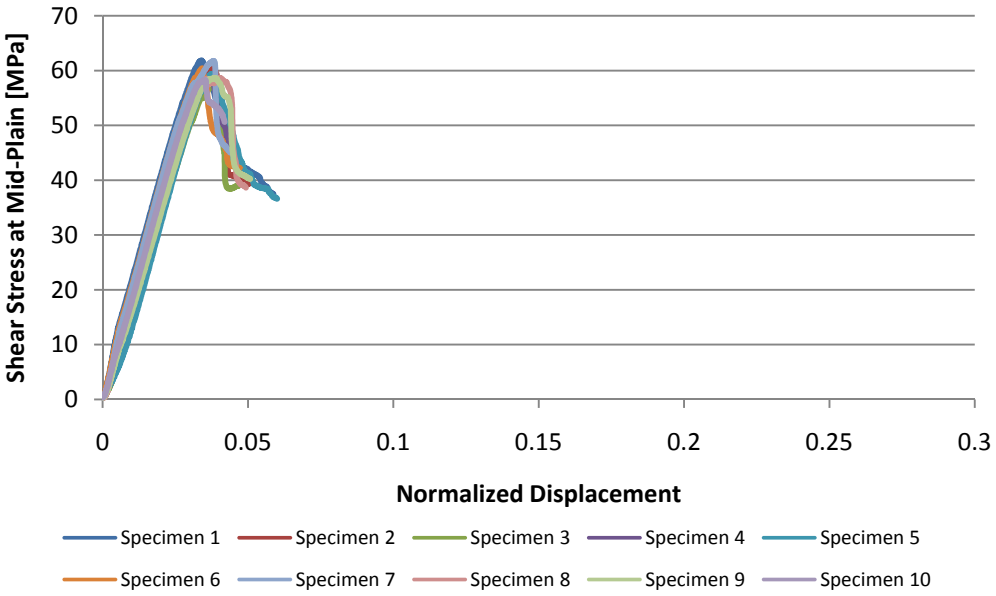

Figure D.6. Shear stress at mid-plane of specimens vs. displacement of load nose normalized with respect to thickness of specimens for panel containing A-CNFs in unsized fibers.